

Rafael Brandão de Rezende Borges

**An Improved WENO Scheme with a New
Steepening Term for Hyperbolic Conservation
Laws**

Rio de Janeiro

Abril de 2014



UFRJ

AN IMPROVED WENO SCHEME WITH A NEW STEEPENING TERM FOR HYPERBOLIC CONSERVATION LAWS

Rafael Brandão de Rezende Borges

Tese de Doutorado apresentada ao Programa de Pós-graduação em Matemática, Instituto de Matemática, da Universidade Federal do Rio de Janeiro, como parte dos requisitos necessários à obtenção do título de Doutor em Matemática.

Orientador: Bruno Alexandre Soares da Costa

Rio de Janeiro

Abril de 2014

B732a Borges, Rafael Brandão de Rezende.
An Improved WENO Scheme with a New Steepening Term for Hyperbolic Conservation Laws/ Rafael Brandão de Rezende Borges. – Rio de Janeiro: UFRJ/ IM, 2014.
xxvi, 99f.: il. (algumas color.); 30 cm.
Orientador: Bruno Alexandre Soares da Costa.
Tese (Doutorado) – Universidade Federal do Rio de Janeiro/ Instituto de Matemática/ Programa de Pós-Graduação em Matemática, 2014.
Referências Bibliográficas: f. 109–112.
1. Esquemas WENO. 2. Indicadores de suavidade. 3. Métodos de alta ordem. 4. Leis de conservação hiperbólicas. I. da Costa, Bruno Alexandre Soares, orient. II. Universidade Federal do Rio de Janeiro, Instituto de Matemática, Programa de Pós-Graduação em Matemática. III. Título.

AN IMPROVED WENO SCHEME WITH A NEW STEEPENING TERM
FOR HYPERBOLIC CONSERVATION LAWS

Rafael Brandão de Rezende Borges

Bruno Alexandre Soares da Costa

Tese de Doutorado apresentada ao Programa de Pós-graduação em Matemática,
Instituto de Matemática, da Universidade Federal do Rio de Janeiro, como parte dos
requisitos necessários à obtenção do título de Doutor em Matemática.

Aprovada por:

Presidente, Prof. Bruno Alexandre Soares da Costa

Prof. Wai Sun Don

Profa. Sandra Mara Cardoso Malta

Prof. Fábio Antônio Tavares Ramos

Prof. Henrique de Melo Versieux

Rio de Janeiro

Abril de 2014

Todo lo que sé, se lo debo al gran maestro Bruno de la Cuesta.

Estas notas são dedicadas ao time do Flamengo (e seu treinador),
Campeão Carioca de 2014 com um gol roubado aos 46 minutos do segundo tempo.

Agradecimentos

Quero agradecer aos meus pais, Enilma e Sigismundo, por todo apoio emocional e financeiro durante todos esses anos de estudo. É enorme a minha gratidão. Sei que não foi fácil, mas tá aí o resultado do esforço. À Carolina por me inspirar a querer ser um homem melhor. Ao Don por tudo que aprendi em Hong Kong, e também à Carol, pelos dois terem me acolhido e aturado por 6 meses. Aos meus amigos e demais parentes, pelo lado bom da vida. A todas as pessoas, presentes ou ausentes, que fizeram parte de minha trajetória até aqui, muito obrigado, de coração.

À minha Alma Mater UFRJ e a todos os professores com quem tive o prazer de conviver e aprender. À CAPES e CNPq, pelo incentivo financeiro desde os tempos da Iniciação. À Hong Kong Baptist University (香港浸會大學) e à cidade de Hong Kong pelas fantásticas experiências vividas. À Ocean University of China (中国海洋大学), em especial aos Profs. Gao Zhen e Xie Shusen e ao Li Peng.

À Tia Deise, sem a qual nada disto seria possível. À secretaria e aos coordenadores da Pós-Graduação, por toda a ajuda e paciência, em especial ao Alan. Ao meu orientador Prof. Bruno Costa; aos membros da banca, Profs. Wai Sun Don, Sandra Malta, Fábio Ramos e Henrique Versieux; aos membros da banca dos meus exames de qualificação, Profs. Flávio Dickstein, Rolci Cicolatti, Dinamérico Pombo Jr. e Milton Lopes Filho; e aos Profs. Monique Carmona, Mario de Oliveira, Milton Ramirez, Paulo Goldfeld, Luiz Carlos Guimarães, Marco Aurélio Cabral e Felipe Acker, obrigado por toda a ajuda, parceria e amizade. Aos amigos e colegas do doutorado, em especial ao Felipe, vulgo Trem; e aos colegas e amigos do laboratório, em especial ao garoto Wesley, valeu pela força e companheirismo.

Finalmente, à Força Maior que rege o Universo e que tanto se esforça para não ser notada, meu agradecimento pela existência.

溫故而知新，可以為師矣。

— 孔夫子

*If a man keeps cherishing his old knowledge,
so as continually to be acquiring new, he may be a teacher of others.*

— Confucius

*Se alguém se mantém revisando seu conhecimento antigo para, assim,
continuamente aprender coisas novas, este alguém está apto a ser um professor.*

— Confúcio

Resumo

Apresentamos um novo esquema WENO que generaliza o esquema WENO-Z com a inclusão de um termo antidissipativo (*sharpening*). Este termo é uma simples função dos indicadores de suavidade já existentes na fórmula do WENO-Z e permite alcançar resultados substancialmente mais precisos em regiões da solução contendo ondas de alta frequência, sem alterar significativamente o custo computacional. Obtemos também uma condição assintótica suficiente para os parâmetros dos pesos, que fazem que o novo esquema WENO alcance a ordem de convergência ótima para soluções suaves, independentemente da existência de pontos críticos. Resultados numéricos usando o novo esquema indicam que ter ordem de convergência total em pontos críticos não é tão relevante para a resolução de esquemas WENO como se pensa atualmente.

Palavras-chave: esquemas WENO, esquemas essencialmente não-oscilatórios, leis de conservação hiperbólicas, indicadores de suavidade, métodos de ordem alta, dissipação numérica.

Abstract

We present a new WENO scheme, which generalizes the WENO-Z scheme by including a sharpening (or *steepening*) term in its formula. This sharpening term is a simple function of the smoothness indicators already present in WENO-Z formula, and it allows the new scheme to achieve substantially sharper results in regions of the solution containing high-frequency waves, with no significant additional computational cost. We also obtain a sufficient asymptotic condition on the parameters of the weights, which makes the new WENO scheme recover optimal accuracy for smooth solutions, regardless of critical points. Numerical results with the new scheme indicate that having full accuracy at critical points is not as relevant to the sharpness of WENO schemes as it is currently thought.

Keywords: WENO schemes, essentially non-oscillatory schemes, hyperbolic conservation laws, smoothness indicators, high-order methods, numerical dissipation.

List of Figures

Figure 1 – Numerical solution of the Riemann problem of Lax by the fifth-order upstream central linear scheme (Central5)	28
Figure 2 – Comparison between a first- and a fifth-order scheme	29
Figure 3 – Numerical solution of the Riemann problem of Lax by the fifth-order WENO-Z scheme	31
Figure 4 – Comparison between classical WENO, WENO-Z, WENO-Z+ and WENO- <i>min</i> in the Shu–Osher shock-entropy test	33
Figure 5 – Comparison between classical WENO, WENO-Z, WENO-Z+ and WENO- <i>min</i> in the Titarev–Toro shock-entropy test	34
Figure 6 – Stencil $\mathcal{S}_{i+\frac{1}{2}}$ and substencils $\mathcal{S}_{i+\frac{1}{2}}^0$, $\mathcal{S}_{i+\frac{1}{2}}^1$ and $\mathcal{S}_{i+\frac{1}{2}}^2$ of a fifth-order WENO scheme	44
Figure 7 – Reference solution of the interacting blast waves problem	52
Figure 8 – Initial condition (and solution) of the GSTE problem	52
Figure 9 – Solution of Lax’s Riemann problem	52
Figure 10 – Solution of Sod’s Riemann problem	54
Figure 11 – Reference solution of shock-entropy wave problem of Shu–Osher	54
Figure 12 – Reference solution of shock-entropy wave problem of Titarev–Toro	54
Figure 13 – Numerical solution of the Gaussian-square-triangle-ellipse linear test by the WENO-C, WENO-M, and WENO-Z schemes	71
Figure 14 – Numerical solution of the shock-entropy problem of Shu–Osher by the WENO-C, WENO-M, and WENO-Z schemes	71
Figure 15 – Numerical solution of the shock-entropy problem of Shu–Osher by the WENO- <i>min</i> , WENO-C, WENO-M and WENO-Z schemes	75
Figure 16 – Numerical solution of the shock-entropy problem of Titarev–Toro by the WENO- <i>min</i> scheme with a small grid	76
Figure 17 – ADR analysis of WENO- <i>min</i> scheme: imaginary part of ϕ	76
Figure 18 – Numerical solution of the shock-entropy problem of Titarev–Toro by the WENO-Z+, WENO-C, WENO-M and WENO-Z schemes with a small grid	77
Figure 19 – Discrete approximations $D^z f$ and $D^{-z} f$ to the derivative of $f(x) = \sin(4\pi x)$	82
Figure 20 – Values of smoothness indicators β and τ for $f(x) = \sin(4\pi x)$	83
Figure 21 – WENO-Z weights ω^z and “anti-Zico” weights ω^{-z} for $f(x) = \sin(4\pi x)$	84
Figure 22 – Reconstruction polynomials $\hat{f}_{i+\frac{1}{2}}^0(x)$, $\hat{f}_{i+\frac{1}{2}}^1(x)$, and $\hat{f}_{i+\frac{1}{2}}^2(x)$ at the stencil $\mathcal{S}_{i+\frac{1}{2}}$	85

Figure 23 – Reconstruction polynomials $\hat{f}_{i-\frac{1}{2}}^0(x)$, $\hat{f}_{i-\frac{1}{2}}^1(x)$, and $\hat{f}_{i-\frac{1}{2}}^2(x)$ at the stencil $\mathcal{S}_{i-\frac{1}{2}}$	85
Figure 24 – Numerical solution of the shock-entropy problem of Titarev–Toro by the WENO-Z+ scheme with different λ	91
Figure 25 – Numerical solution of the shock-entropy problem of Shu–Osher by the WENO-Z+ scheme with different λ	92
Figure 26 – ADR analysis of WENO-Z+ scheme with different λ : imaginary part of ϕ	93
Figure 27 – Numerical solution of the shock-entropy problem of Shu–Osher by the WENO-Z+, WENO-C, WENO-M, and WENO-Z schemes	95
Figure 28 – Numerical solution of the shock-entropy problem of Titarev–Toro by the WENO-Z+, WENO-C, WENO-M, and WENO-Z schemes	95
Figure 29 – Numerical solution of the blast waves problem by the WENO-Z+, WENO-C, WENO-M, and WENO-Z schemes	96
Figure 30 – Numerical solution of the Gaussian-square-triangle-ellipse linear test by the WENO-Z+, WENO-C, WENO-M, and WENO-Z schemes	96
Figure 31 – Numerical solution of the shock-entropy problem of Shu–Osher by the WENO-Z+, WENO-Z, WENO-Z7, and WENO-Z9 schemes	98
Figure 32 – Numerical solution of the shock-entropy problem of Titarev–Toro by the WENO-Z+, WENO-Z, WENO-Z7, and WENO-Z9 schemes	98
Figure 33 – Accuracy tests for the WENO-Z+ scheme with different parameter profiles	104
Figure 34 – Numerical solution of the shock-entropy problem of Titarev–Toro by the WENO-Z+ scheme with different profiles of parameters	105
Figure 35 – Numerical solution of the Gaussian-square-triangle-ellipse linear test by the WENO-Z+ scheme with different profiles of parameters	106

List of Tables

Table 1 – The global optimal order smoothness indicator τ and its leading truncation order $\theta(\tau)_{opt}$ of the $(2r - 1)$ order WENO-Z scheme.	61
Table 2 – Different profiles of WENO-Z+ for accuracy tests	102
Table 3 – Expressions of d_k , $\hat{f}_{i+\frac{1}{2}}^k$, and D_1^k , for order $R = 3$ and varying k	113
Table 4 – Expressions of d_k , $\hat{f}_{i+\frac{1}{2}}^k$, D_1^k , and D_2^k , for order $R = 5$ and varying k	114
Table 5 – Expressions of d_k , $\hat{f}_{i+\frac{1}{2}}^k$, D_1^k , D_2^k , and D_3^k , for order $R = 7$ and varying k	115
Table 6 – Expressions of d_k , $\hat{f}_{i+\frac{1}{2}}^k$, D_1^k , D_2^k , D_3^k , and D_4^k , for order $R = 9$ and varying k	116

List of symbols

\triangleq	Equal by definition, “is defined as.”
$\nabla_i^{\Delta x}$	Undivided backward difference operator. See Definition 4.
$\Delta_i^{\Delta x}, \Delta^{(n)}$	Undivided forward difference operator. See Definition 4.
α, α_k	WENO unnormalized weights. See Section 2.4.3.
α_C	Unnormalized weights of a smooth substencil.
α_D	Unnormalized weights of a discontinuous substencil.
β, β_k	Smoothness indicators of Jiang–Shu. See Section 3.3.
Δx	Grid spacing.
$\delta_i^{\Delta x}, \delta_i$	Undivided central difference operator. See Definition 4.
ε	Sensibility parameter of WENO schemes.
$\Theta(\cdot)$	Standard Bachmann–Landau asymptotic notation. See Definition 2.
$\theta(\cdot)$	“The order of.” See Definition 3.
μ, μ_k	A generic local smoothness indicator.
ν	A generic global smoothness indicator.
$O(\cdot)$	Standard Bachmann–Landau asymptotic notation. See Definition 2.
τ	The original global smoothness indicator of WENO-Z. See Section 3.4.
$\Omega(\cdot)$	Standard Bachmann–Landau asymptotic notation. See Definition 2.
ω, ω_k	WENO normalized weights. See Chapter 2.
ω_C	Normalized weights of a smooth substencil.
ω_D	Normalized weights of a discontinuous substencil.
D_x^W	WENO spatial derivative approximation.
d_k	Ideal weights. See Section 2.2.
f	The flux of a conservation law; the function being availed by WENO schemes.

\hat{f}, \hat{f}_k	Polynomial approximations to h .
h	The numerical flux function. See Eq. (1.6).
i	Grid index.
k	Substencil index.
n_{cp}	Order of a critical point. See Definition 1.
p	Power parameter of WENO schemes.
r	Substencil order, or “suborder”.
R	Stencil order ($R = 2r - 1$).
\mathcal{S}	A stencil.
\mathcal{S}_k	A substencil.

Definitions

Definition 1. If $f(x_c) = f'(x_c) = \dots = f^{(n_{cp})}(x_c) = 0$ but $f^{(n_{cp}+1)}(x_c) \neq 0$, x_c is said to be a *critical point of order n_{cp}* of $f(x)$. If $f'(x_c) \neq 0$, x_c is defined as a critical point of order 0 of $f(x)$.

Definition 2. The standard asymptotic symbols $O(\cdot)$, $\Omega(\cdot)$ and $\Theta(\cdot)$ will be used with their proper meanings:

- $g(\Delta x) = O(\Delta x^n)$ denotes an upper bound to $g(\Delta x)$, that is, $|g(\Delta x)| \leq C\Delta x^n$ for some $C > 0$ as $\Delta x \rightarrow 0$.
- $g(\Delta x) = \Omega(\Delta x^n)$ denotes a lower bound to $g(\Delta x)$, that is, $|g(\Delta x)| \geq C\Delta x^n$ for some $C > 0$ as $\Delta x \rightarrow 0$.
- $g(\Delta x) = \Theta(\Delta x^n)$ denotes the exact order of $g(\Delta x)$, that is, $g(\Delta x) = O(\Delta x^n)$ and $g(\Delta x) = \Omega(\Delta x^n)$ as $\Delta x \rightarrow 0$.

Definition 3. The notation $\theta(g(\Delta x))$ denotes the order of g (as a function of Δx), that is, the power of Δx in the leading term of the asymptotic expansion of $g(\Delta x)$,

$$\theta(g) = n \iff g(\Delta x) = \Theta(\Delta x^n).$$

For instance, if $g(\Delta x) = 5\Delta x^2 + \Delta x^3$, then $\theta(g) = 2$.

Note that $\theta(\cdot)$ has the following properties:

$$\theta(f \cdot g) = \theta(f) + \theta(g), \quad \theta(f/g) = \theta(f) - \theta(g).$$

Also, if $\theta(f) \neq \theta(g)$, or if $\theta(f) = \theta(g)$ but the leading order terms of f and g have the same sign, then

$$\theta(f \pm g) = \min\{\theta(f), \theta(g)\}.$$

Definition 4. For a grid spacing Δx , grid point x_i , and a given function ϕ , we define the following undivided finite difference operators:

$$\begin{aligned} \nabla_i^{\Delta x} \phi &\triangleq \phi(x_i) - \phi(x_i - \Delta x) && \text{(Backward difference)} \\ \delta_i^{\Delta x} \phi &\triangleq \phi(x_i + \Delta x/2) - \phi(x_i - \Delta x/2) && \text{(Central difference)} \\ \Delta_i^{\Delta x} \phi &\triangleq \phi(x_i + \Delta x) - \phi(x_i) && \text{(Forward difference)} \end{aligned}$$

For simplicity, the superscript Δx will often be dropped.

Remark 1. Notice that if $\phi(x_i) = O(\Delta x^n)$ and $\phi(x)$ is sufficiently smooth around x_i , then $\delta_i^{\Delta x} \phi(x) = O(\Delta x^{n+1})$ (the same holds for $\nabla_i^{\Delta x}$ and $\Delta_i^{\Delta x}$).

Contents

	Introduction	27
I	WENO SCHEMES	37
1	FINITE DIFFERENCE SCHEMES FOR HYPERBOLIC CONSER- VATION LAWS	39
1.1	Fixed stencil schemes	40
1.1.1	Time discretization	42
1.1.2	The fifth-order upstream central scheme	42
2	WENO SCHEMES	43
2.1	The fifth-order WENO scheme	44
2.2	Ideal weights and accuracy of WENO schemes	45
2.2.1	The fifth-order case	45
2.2.2	Achieving the optimality condition	46
2.3	Time integration and linear stability	47
2.4	Analysis of WENO schemes	47
2.4.1	The discontinuous/continuous ratio: a relative measure of dissipativity	48
2.4.2	Operation count	48
2.4.3	Unnormalized weights	49
2.5	Testing WENO schemes	50
2.5.1	Stability tests	50
2.5.1.1	Interacting blast waves	50
2.5.1.2	ADR analysis	50
2.5.2	Oscillation tests	51
2.5.2.1	GSTE test	51
2.5.2.2	Riemann problem of Lax	53
2.5.2.3	Riemann problem of Sod	53
2.5.3	Features tests	53
2.5.3.1	Shock-entropy wave test of Shu–Osher	53
2.5.3.2	Shock-entropy wave test of Titarev–Toro	55
2.5.4	Accuracy test	55
3	SMOOTHNESS INDICATORS	57
3.1	A simple smoothness indicator	58
3.2	Forward differences	59

3.3	The smoothness indicator beta of Jiang–Shu	59
3.4	The global smoothness indicator tau	60
4	CLASSICAL WEIGHT SCHEMES	63
4.1	Classical weight formula	63
4.1.1	ENO property	63
4.1.2	Operation count	64
4.2	The original WENO scheme	64
4.3	The classical WENO scheme (WENO-C)	64
4.4	The mapped WENO scheme (WENO-M)	65
4.4.1	Operation count	65
5	ZICO WEIGHT SCHEMES	67
5.1	Zico weight formula	67
5.1.1	ENO property	68
5.1.2	Discontinuous/continuous ratio	68
5.1.3	Operation count	68
5.2	The Zico WENO scheme (WENO-Z)	69
5.3	A comparison between classical and Zico weight schemes	69
5.4	Other schemes	70
II	A NEW WENO SCHEME	73
6	TOWARDS A NEW WENO SCHEME	75
7	THE EXPERIMENTAL WENO-MIN SCHEME	79
7.1	The <i>min</i> weight formula	79
7.1.1	ENO property	79
7.1.2	Discontinuous/continuous ratio	80
7.1.3	Operation count	80
7.2	The WENO-min scheme	80
7.2.1	Stability analysis	81
8	A NEW IMPROVED WENO SCHEME	87
8.1	Designing a new weight formula	87
8.1.1	ENO property	88
8.1.2	Discontinuous/continuous ratio	88
8.1.3	Operation count	89
8.2	The new WENO-Z+ scheme	90
8.2.1	The parameter lambda	90

8.2.2	Comparison with other WENO schemes	94
8.2.3	Comparison with WENO-Z of different orders	97
9	ACCURACY OF THE WENO-Z+ SCHEME	99
9.1	Properties of beta	99
9.2	The accuracy constraint	100
9.3	The fifth-order WENO-Z+ scheme	102
9.4	Accuracy tests	102
9.5	“Accuracy at critical points” versus “sharpness”	103
9.6	Accuracy and spurious oscillations	105
	 Conclusions	 107
	 BIBLIOGRAPHY	 109
	 APPENDIX A – CONSTANTS AND EXPRESSIONS USED BY WENO SCHEMES FROM ORDER 3 TO 9	 113
A.1	Order 3	113
A.2	Order 5	113
A.3	Order 7	114
A.4	Order 9	114
	 APPENDIX B – PROPERTIES OF THE SMOOTHNESS INDI- CATOR BETA	 117
	 APPENDIX C – PROPERTIES OF THE ANTI-ZICO WEIGHTS	 123
	 Index	 125

Introduction

Weak solutions of a system of hyperbolic conservation laws

$$\begin{cases} \frac{\partial \mathbf{u}(\mathbf{x}, t)}{\partial t} + \nabla \cdot \mathbf{f}(\mathbf{u}(\mathbf{x}, t)) = 0 \\ \mathbf{u}(\mathbf{x}, 0) = \mathbf{u}_0(\mathbf{x}) \end{cases} \quad (1)$$

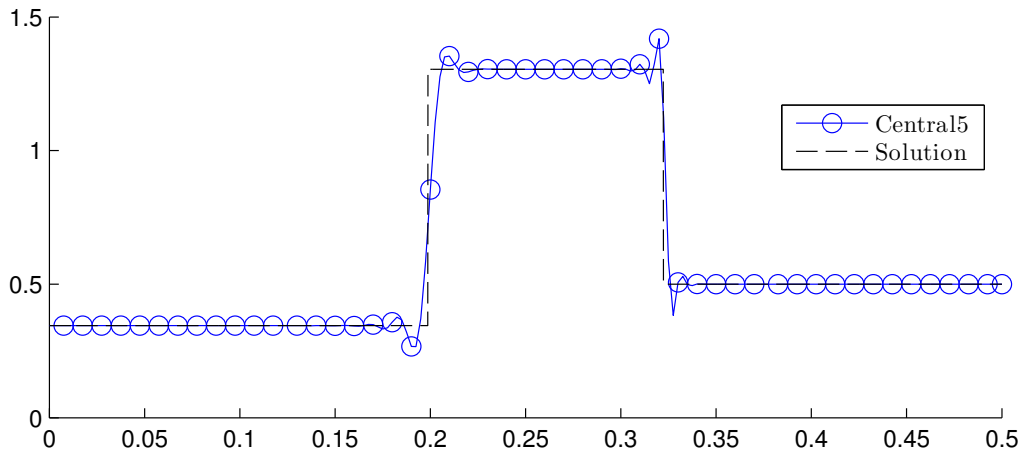
may develop discontinuities even when the initial condition $\mathbf{u}_0(\mathbf{x})$ is smooth [1, 2, 3, 4]. Such discontinuities pose both analytical and numerical difficulties, namely:

Correct shock speed. The location and speed of jump discontinuities in genuine weak solutions of (1) must satisfy the Rankine–Hugoniot conditions, which relates the shock speed with the values of the solution at both sides of the jump [2, 3, 4]. Not every numerical scheme produces solutions which converge to a genuine weak solution of the problem: the shock speeds of resulting solutions may be wrong ([2, Chap. 12] has a good example). In order to guarantee that all converging solutions converge to a genuine weak solution (Lax–Wendroff theorem), the numerical scheme must satisfy a discrete version of the conservation law. In other words, the scheme must be *conservative*.

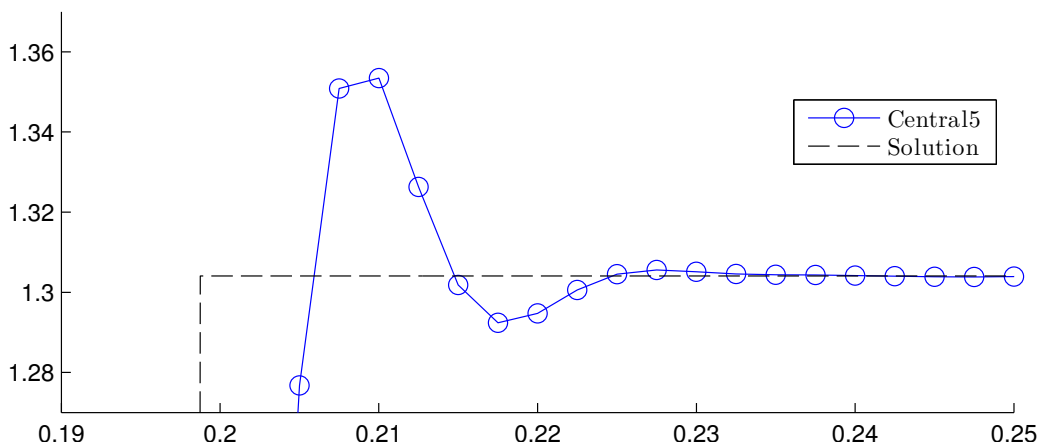
Entropy solution. The problem (1) may have infinite weak solutions. Usually, only one of them is physically relevant, viz. the limit solution of a modified Eq. (1) with an additional viscosity term which vanishes in the limit. At least in the scalar case with convex and smooth f , there exists a unique such solution, which is also the only weak solution which satisfies some form of entropy condition [1, 4]. For this reason, it is called the *entropy solution*. There are conservative numerical schemes whose solutions converge to a genuine weak solution of (1) which nevertheless is not the physically relevant entropy solution ([2, Eq. (12.50)] is a nice example). In order to assure convergence to the entropy solution, the scheme should satisfy a discrete version of the entropy condition similar to the one which occurs in the proof of Lax–Wendroff theorem [2].

Gibbs-like phenomenon. Even when the solutions of a numerical scheme converge to the correct, entropy solution, they may present spurious oscillations near jump discontinuities, which are similar to the Gibbs phenomenon of Fourier series [5, 6]. Godunov’s theorem [2, 7] implies that linear schemes with accuracy order greater than 1 are bound to generate oscillations, in general. These oscillations are not only qualitatively wrong, but they do not decrease in size when the grid is refined, they may be amplified as time goes on in the case of nonlinear conservation laws, and they often lead to numerical instabilities [5]. Figure 1 exemplifies this: the solution of the Riemann problem of Lax (Section 2.5) by the fifth-order upstream central linear scheme (Central5) noticeably oscillates near the two jump discontinuities.

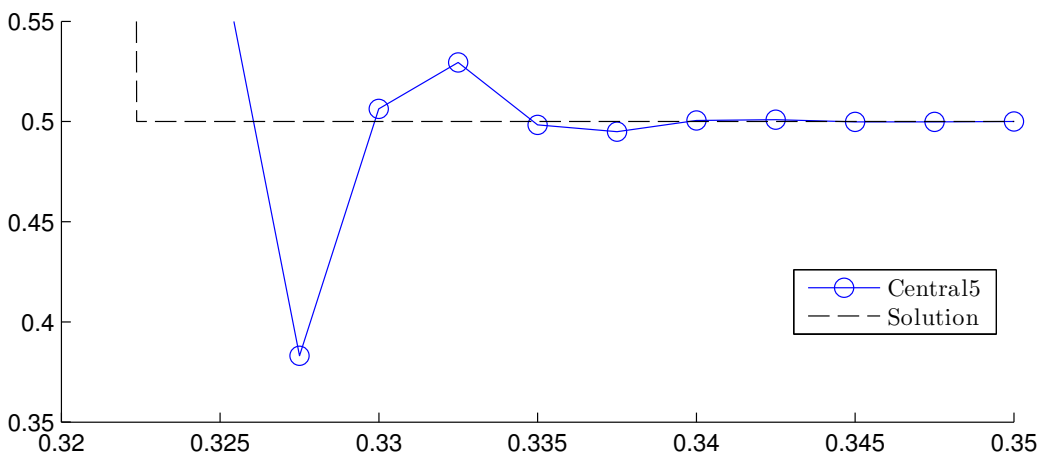
Figure 1 – Numerical solution of the Riemann problem of Lax by the fifth-order upstream central linear scheme (Central5)



(a) Zoom in the relevant region



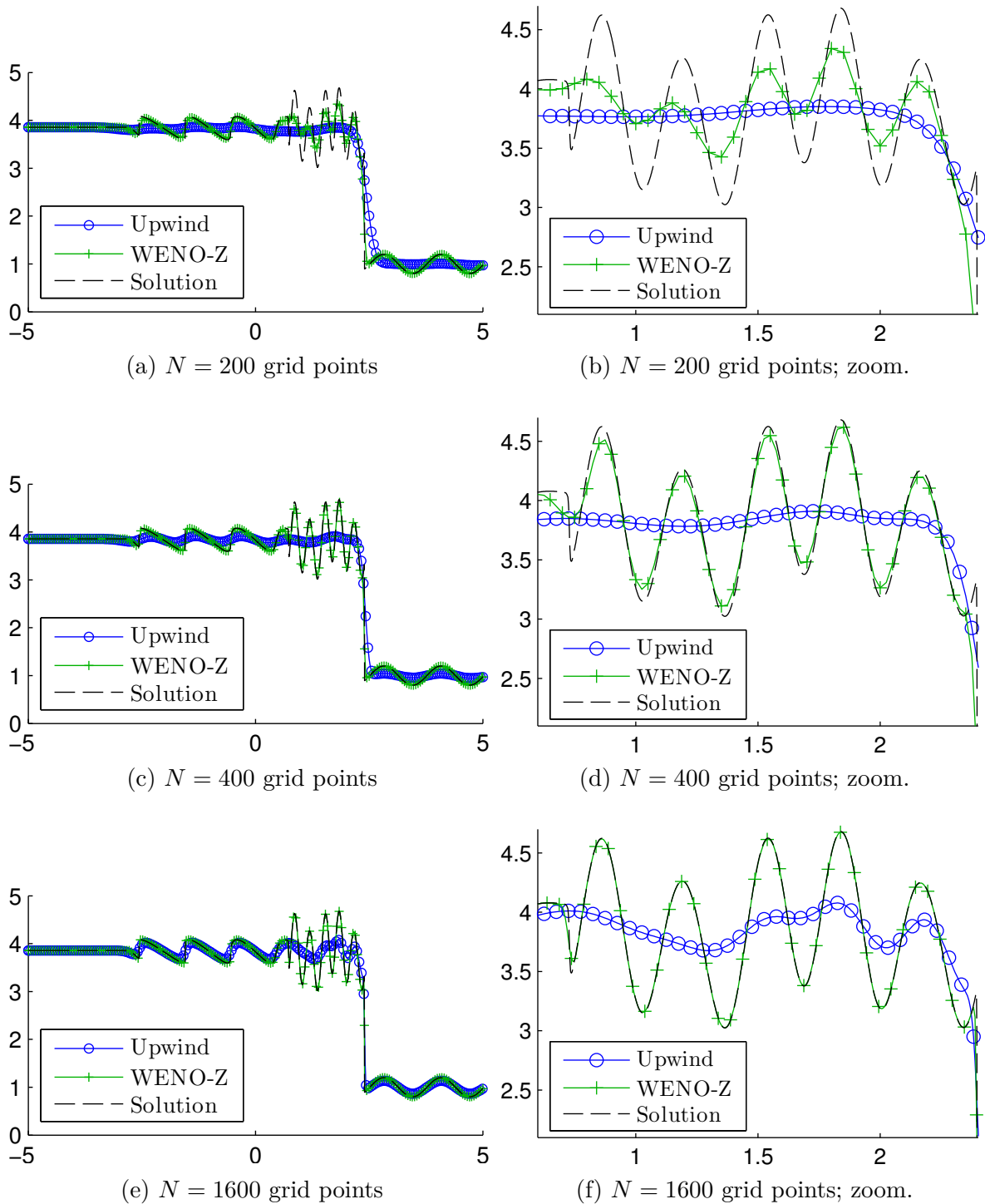
(b) Zoom in the contact discontinuity



(c) Zoom in the right shock

The figures show the density of the solution at $t = 0.13$. $N = 800$ points were used. CFL = 0.5.

Figure 2 – Comparison between a first- and a fifth-order scheme



The figures show the density of the solution of the shock-entropy problem of Shu-Osher at $t = 1.8$. $CFL = 0.5$.

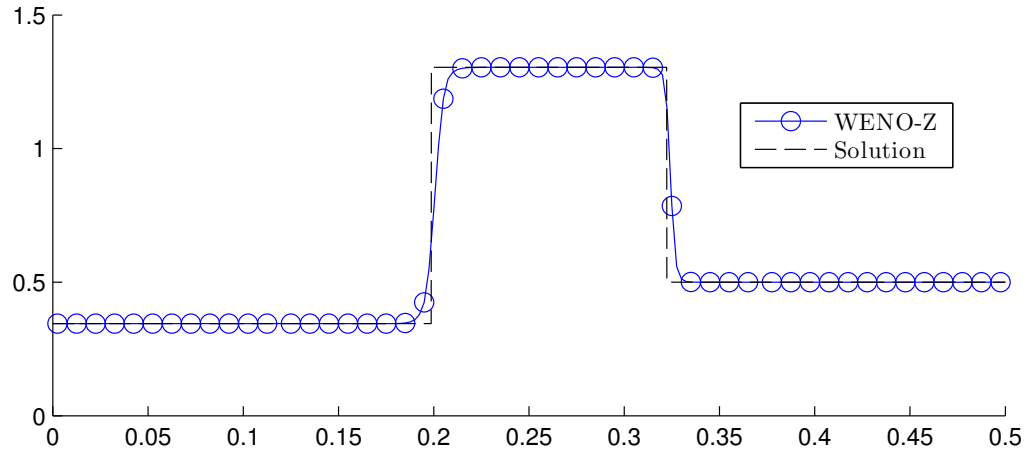
A natural way to avoid all of these problems would be to use the linear, first-order upwind scheme. However, first-order schemes are perhaps too dissipative — it takes a considerable higher number of grid points in order to resolve fine smooth structures of the solution in comparison to higher-order methods. Take, for instance, the archetypical Shu–Osher shock-turbulence test (Section 2.5), a problem whose solution contains both shocks and a high-frequency waves region. Figure 2 shows that WENO-Z, a fifth-order scheme, already resolves most of the fine structures of the solution with $N = 400$ grid points, while the upwind scheme does not resolve them even with $N = 1600$. This exemplifies a feature of high-order methods: in problems involving both shocks and smooth structures, it is more computationally efficient to use them than first-order methods [5, 8], even more so in 2D and 3D [9].

Since Godunov’s theorem imposes a limitation on the order of *linear* schemes, high-order schemes for hyperbolic conservation laws must employ some kind of nonlinear approach. Examples of nonlinear approaches for reducing spurious oscillations are 1) adding an artificial viscosity term which assumes larger values near the discontinuities, and 2) applying a flux limiter in order to achieve the TVD property [5, 2, and references therein]. The TVD, MUSCL, and PPM schemes use these strategies. However, the parameter controlling the size of the artificial viscosity term of the first approach is highly problem-dependent; and, in the second approach, the flux limiters of TVD schemes necessarily makes the scheme degenerate to first-order near critical points, and sometimes they drastically alter the shape of the solutions.

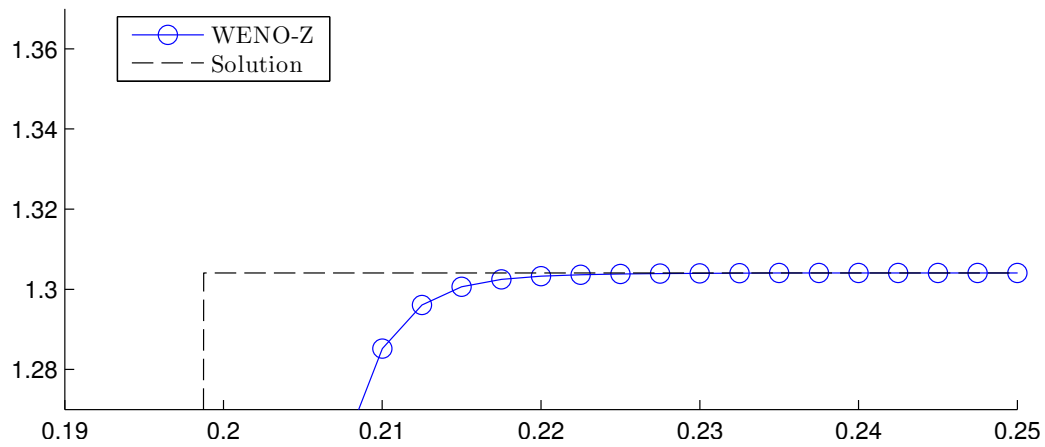
A third approach was introduced by the ENO (essentially non-oscillatory) scheme in [10, 11], and later improved and adapted to finite differences in [12, 13]. It consists in dynamically choosing, out of a stencil \mathcal{S} of $2r - 1$ points, the substencil \mathcal{S}_k of r points in which the function is smoothest. In this way, if the solution is discontinuous in \mathcal{S} but not in a given substencil \mathcal{S}_k , the scheme avoids interpolating across discontinuities of the solution, which is the cause of the spurious oscillations. The resulting solution is *essentially non-oscillatory*, that is, the size of the oscillations are $O(\Delta x^q)$, for some $q \geq 1$ [5].

The WENO (weighted ENO) scheme improves on ENO’s approach by always using the information contained in the whole stencil \mathcal{S} instead of picking the “smoothest” r points substencil \mathcal{S}_k . The way WENO operates will be detailed in the introductory Part I of this thesis (particularly Chapters 1 and 2); but, in general lines, it assigns a nonlinear weight ω_k to the polynomial interpolations in each substencil \mathcal{S}_k , $k = 0, \dots, r - 1$, making the final approximation a convex combination of the local approximations. This is done in such a way that $\omega_k \sim 0$ when \mathcal{S}_k contains a discontinuity, effectively emulating ENO’s strategy of avoiding interpolations across discontinuities. Moreover, when \mathcal{S} is smooth (that is, when the solution is smooth in \mathcal{S}), the ω_k are designed to recover the $(2r - 1)$ th-order of accuracy, which is the maximum allowed by a $2r - 1$ points stencil (in contrast to

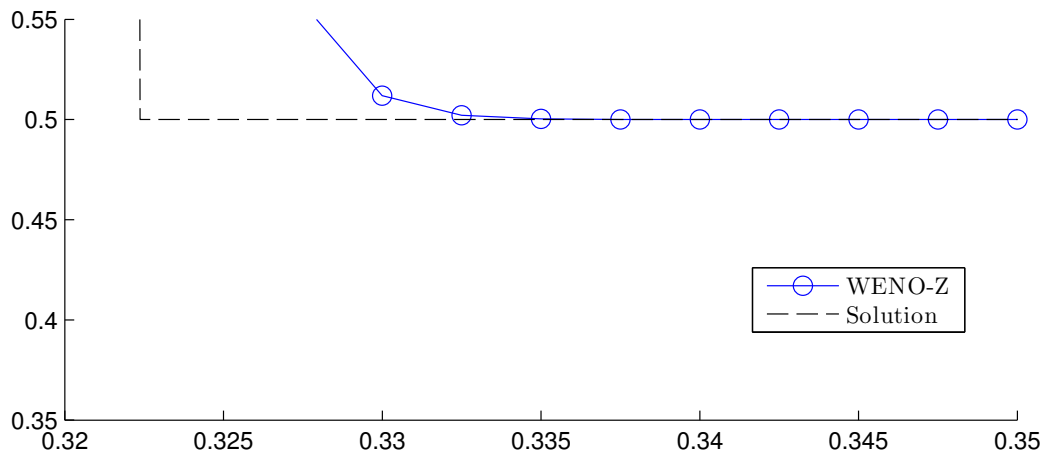
Figure 3 – Numerical solution of the Riemann problem of Lax by the fifth-order WENO-Z scheme



(a) Zoom in the relevant region



(b) Zoom in the contact discontinuity



(c) Zoom in the right shock

The figures show the density of the solution at $t = 0.13$. $N = 800$ points were used. CFL = 0.5.

ENO's r th-order in the same $2r - 1$ points stencil). Figure 3 shows the numerical solution of Riemann problem of Lax, this time by the fifth-order WENO-Z scheme. Notice how this scheme resolves the jump discontinuities with no apparent oscillation near them.

The classical WENO weights, which were the first weight formula to be developed, were introduced in [14] and later improved to its final form in [15], where the weights are defined as:

$$\alpha_k \triangleq \frac{d_k}{(\beta_k + \varepsilon)^p}, \quad \omega_k \triangleq \frac{\alpha_k}{\sum_{j=0}^{r-1} \alpha_j}, \quad k = 0, \dots, r - 1. \quad (2)$$

Here, d_k are constants called *ideal weights* (they are discussed in Section 2.2), β_k are *smoothness indicators* (Chapter 3), whose value is a function of the smoothness of the solution in \mathcal{S}_k (the smoother the solution, the smaller the value), p is the *power parameter* and ε is the *sensitivity parameter*, which was originally introduced in the formula for avoiding a division by zero. As all these values are non-negative, Eq. (2) gives $\omega_k \geq 0$, $\sum_{k=0}^{r-1} \omega_k = 1$. Because of the properties of β_k , it is immediate that ω_k is larger in the substencils where the solution is smoother. The WENO schemes which use the classical weights are discussed in Chapter 4.

In [6, 16, 17, 18] we helped develop the Zico weights formula,

$$\alpha_k \triangleq d_k \left[1 + \left(\frac{\tau}{\beta_k + \varepsilon} \right)^p \right], \quad \omega_k \triangleq \frac{\alpha_k}{\sum_{j=0}^{r-1} \alpha_j}, \quad k = 0, \dots, r - 1. \quad (3)$$

which is an improvement on the classical formula. The novelty in relation to (2) is the introduction of the global smoothness indicator τ , which measures the smoothness of the solution in the whole $2r - 1$ points stencil \mathcal{S} . This change in the formula made the WENO have better accuracy properties and sharper solutions. The WENO schemes based on the Zico weight formula are discussed in Chapter 5.

Yet another formula was introduced in [6]: the *min* weights. The formula is

$$\alpha_k \triangleq d_k \left[1 + \left(\frac{\max(\beta_k, \tau)}{\min(\beta_k, \tau) + \varepsilon} \right)^p \right], \quad \omega_k \triangleq \frac{\alpha_k}{\sum_{j=0}^{r-1} \alpha_j}, \quad k = 0, \dots, r - 1. \quad (4)$$

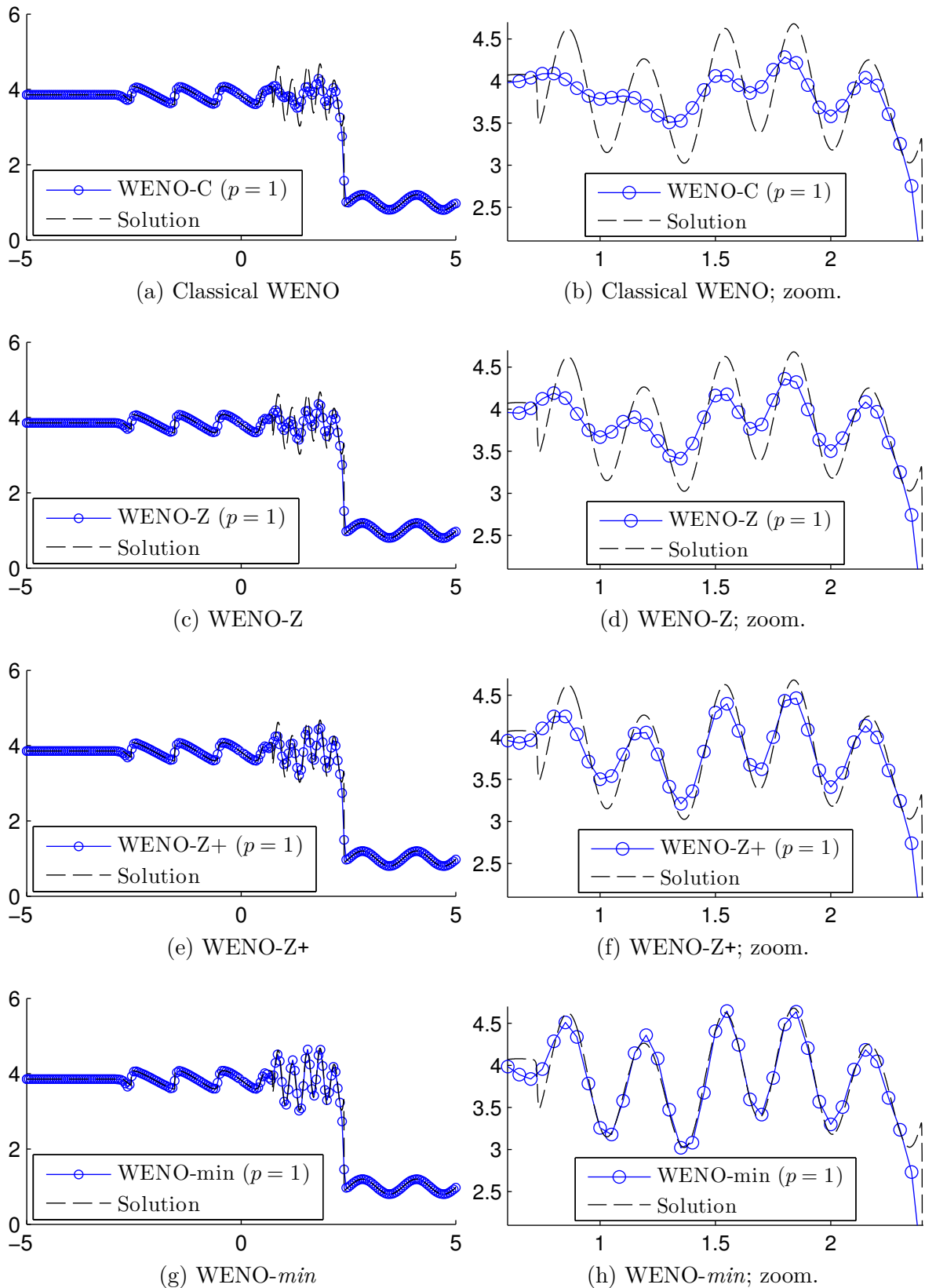
These weights make the solutions even sharper than (3) (as seen in Fig. 4). However, the resulting scheme is unstable (Fig. 5).

Part II deals with one of the motivations of this work, which was to find a WENO scheme which was nearly as sharp as WENO-*min* without its unstable nature. This was achieved through the new weights formula given by

$$\alpha_k \triangleq d_k \left[1 + \left(\frac{\tau + \varepsilon}{\beta_k + \varepsilon} \right)^p + \lambda \left(\frac{\beta_k + \varepsilon}{\tau + \varepsilon} \right) \right], \quad \omega_k \triangleq \frac{\alpha_k}{\sum_{j=0}^{r-1} \alpha_j}, \quad k = 0, \dots, r - 1. \quad (5)$$

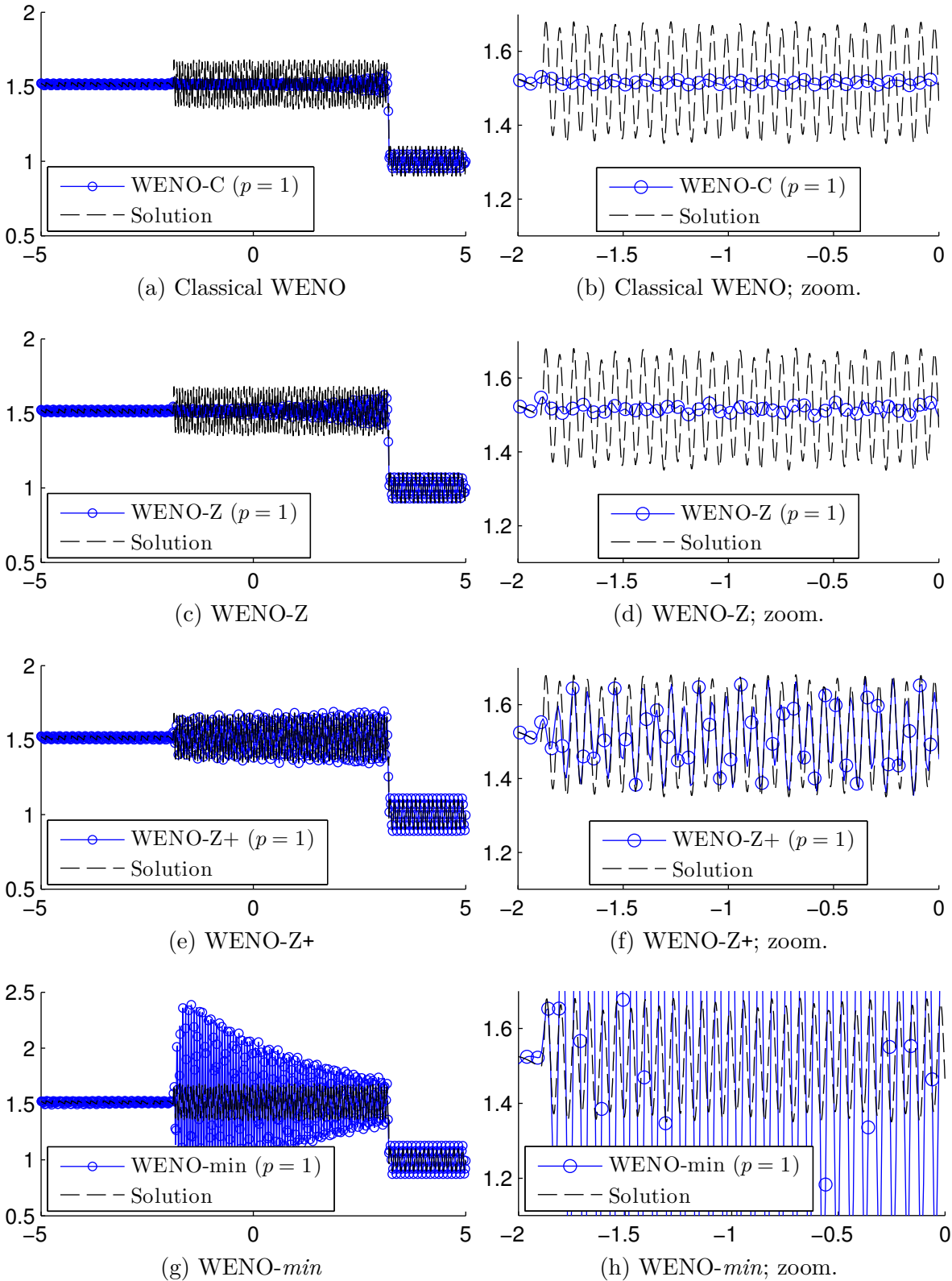
which is called the Zico+ weights, because it generalizes the weights (3) by introducing the sharpening term $\lambda \left(\frac{\beta_k + \varepsilon}{\tau + \varepsilon} \right)$. This term uses information which was already available

Figure 4 – Comparison between classical WENO, WENO-Z, WENO-Z+ and WENO-*min* in the Shu–Osher shock-entropy test



The figures show the density of the solution at $t = 1.8$. A coarse grid with $N = 200$ points was used. For all schemes, $\varepsilon = 10^{-40}$ and $p = 1$. CFL = 0.5.

Figure 5 – Comparison between classical WENO, WENO-Z, WENO-Z+ and WENO-*min* in the Titarev–Toro shock-entropy test



The figures show the density of the solution at $t = 5$. A coarse grid with $N = 1000$ points was used. For all schemes, $\varepsilon = 10^{-40}$ and $p = 1$. CFL = 0.5.

in (3) for increasing the contribution of the less smooth substencils. This may appear undesirable at first, but in fact the less smooth stencils carry useful information which should not be completely disregarded. By using them in a controlled way, the solution gets sharper without affecting the stability and its essentially non-oscillatory character (Figs. 4 and 5). The new parameter λ has the task of controlling the size of the sharpening term. Numerical results show that the new scheme is stable and sharper than the current WENO schemes (Section 8.2.2), sometimes being even sharper than higher-order WENO-Z schemes (Section 8.2.3).

The accuracy of the new WENO-Z+ scheme is analyzed in Chapter 9. It is a known fact that WENO schemes may lose accuracy near critical points [19, 16]. But, by imposing conditions on the parameters of the weights, it is possible to guarantee the optimal order of accuracy $2r - 1$ [20, 21, 22]. Here, we obtain sufficient asymptotic conditions on the parameters ε , p and λ for optimal accuracy of WENO-Z+, similar to the ones deduced in [22]. The issue of the relevance (or lack thereof) of the accuracy of WENO schemes at critical points is briefly discussed in Section 9.5.

Finally, the Appendix A lists the values of all constants and terms which appear in WENO schemes of orders 3 to 9, and the Appendix B contains the supporting theorems used in Chapter 9, along with their proofs.

The first-time reader of this thesis should take a look at the definitions of the classical and of the WENO-Z schemes at chapters 4 and 5 before going to chapters 6, 7 and 8, to get in touch with a more detailed account of the facts related in this introduction. In order to better appreciate the numerical results, a look at the problems descriptions at Section 2.5 is advised. For those interested in the accuracy analysis of the WENO schemes, Chapter 3 describes some properties of the smoothness indicators β_k and τ , which are common to all the schemes under study. The analysis is all based on asymptotic properties of the smoothness indicators, therefore, a prior look at the several asymptotic symbols Θ , Ω and O , described in the Definitions section (p. 21), is necessary for a clear understanding of the analytical results. The smoothness indicators, along with their ratios, determine the order of convergence of the WENO weights to the ideal weights, which in its turn determine the accuracy order of the WENO scheme. In Section 2.2, a set of sufficient conditions on the WENO weights for achieving optimal accuracy is developed; these must be understood before going to Chapter 9, where the main theorem relating the accuracy of the new scheme and the asymptotic properties of its parameters is stated and proved.

Part I

WENO schemes

1 Finite difference schemes for hyperbolic conservation laws

Here we describe how a generic conservative finite difference scheme for hyperbolic conservation laws works. More detailed accounts can be found in the references [5, 19, 6, 16, 22].

A hyperbolic conservation law is a system of first-order partial differential equations in the form

$$\begin{cases} \frac{\partial \mathbf{u}(\mathbf{x}, t)}{\partial t} + \nabla \cdot \mathbf{f}(\mathbf{u}(\mathbf{x}, t)) \equiv \frac{\partial \mathbf{u}(\mathbf{x}, t)}{\partial t} + \sum_{j=1}^d \frac{\partial \mathbf{f}^j(\mathbf{u}(\mathbf{x}, t))}{\partial x_j} = 0, \\ \mathbf{u}(\mathbf{x}, 0) = \mathbf{u}_0(\mathbf{x}), \end{cases} \quad (1.1)$$

where $\mathbf{u} : \mathbb{R}^d \times \mathbb{R} \rightarrow \mathbb{R}^m$, $\mathbf{u}_0 : \mathbb{R}^d \rightarrow \mathbb{R}^m$ and $\mathbf{f}^j \in C^1(\mathbb{R}^m, \mathbb{R}^m)$. Moreover, Eq. (1.1) must satisfy the following condition: define, for each \mathbf{f}^j , the $m \times m$ matrix

$$A^j \triangleq \begin{pmatrix} \frac{\partial f_1^j}{\partial u_1} & \cdots & \frac{\partial f_1^j}{\partial u_m} \\ \vdots & \ddots & \vdots \\ \frac{\partial f_m^j}{\partial u_1} & \cdots & \frac{\partial f_m^j}{\partial u_m} \end{pmatrix}.$$

We require that the matrix $A \triangleq \alpha_1 A^1 + \cdots + \alpha_d A^d$ has only real eigenvalues and is diagonalizable, for all $\alpha_1, \dots, \alpha_d \in \mathbb{R}$. Here, \mathbf{f} is called the *flux*.

In the finite difference approach we will be taking for solving Eq. (1.1), the spatial partial derivatives $\frac{\partial \mathbf{f}^j}{\partial x_j}$ are discretized in a dimension-by-dimension basis. In addition, the system

$$\frac{\partial \mathbf{u}(\mathbf{x}, t)}{\partial t} + \frac{\partial \mathbf{f}^j(\mathbf{u}(\mathbf{x}, t))}{\partial x_j} \equiv \frac{\partial \mathbf{u}(\mathbf{x}, t)}{\partial t} + A^j(\mathbf{u}(\mathbf{x}, t)) \frac{\partial \mathbf{u}(\mathbf{x}, t)}{\partial x_j} = 0$$

can be fully decoupled since A^j is diagonalizable. For these reasons, in our discussion it will be sufficient to consider the scalar case in one space dimension,

$$u_t + f(u)_x \equiv u_t + f'(u)u_x = 0. \quad (1.2)$$

Furthermore, for simplicity, only the case where $f'(u) \geq 0$ will be considered. In the general case, the flux must first be split in its increasing and decreasing parts, e.g. using the Lax–Friedrichs flux splitting:

$$f^\pm(u) \triangleq \frac{f(u) \pm Mu}{2}, \quad M \triangleq \max_u |f'(u)|. \quad (1.3)$$

Notice that

$$\frac{d}{dx} f^+(u) \geq 0, \quad \frac{d}{dx} f^-(u) \leq 0, \quad \text{and} \quad f^+(u) + f^-(u) = f(u),$$

so that $f^+(u)_x$ and $f^-(u)_x$ have positive and negative velocities, respectively. Thereafter, the discretization of both parts of the flux are done separately. It is sufficient to describe how the approximation of a flux with positive velocity is constructed, since $f^+(u)_x$ and $f^-(-u)_x$ are both fluxes with positive velocities (the approximation of $f^-(u)_x$ is done by approximating $f^-(-u)_x$ and flipping the result). In the end, the results of both discretizations are added to obtain a stable approximation to $f(u)_x$.

The details about the steps of characteristics decomposition (used for decoupling the system), multidimensional discretization, and flux splitting, used by all numerical schemes in the present work, can be found in [5] (here, we use Procedures 2.5 and 2.10 found there, with Lax–Friedrichs flux splitting, simple mean, full decoupling, and dimension-by-dimension discretization).

1.1 Fixed stencil schemes

Consider an uniform grid defined by the points $x_i = i \Delta x$, $i = 0, \dots, N$, with intermediate grid points $x_{i-\frac{1}{2}} = (i - \frac{1}{2})\Delta x$, $i = 0, \dots, N + 1$. For now, let us not worry with the time discretization of Eq. (1.2). Instead, for a fixed time t , consider the semi-discretized form of Eq. (1.2) by the method of lines, which yields a system of ordinary differential equations

$$\frac{du_i(t)}{dt} = - \left. \frac{\partial f}{\partial x} \right|_{x=x_i}, \quad i = 0, \dots, N - 1, \quad (1.4)$$

where $u_i(t)$ is a numerical approximation to the point value $u(x_i, t)$. Our goal is to find an R th-order discrete approximation $D_x f$ to $\partial_x f$ at x_i , using a fixed stencil \mathcal{S}_i of $R + 1$ points around x_i ,

$$\mathcal{S}_i = \{x_{i-k-1}, \dots, x_{i+l}\}, \quad k + l = R - 1.$$

Since we assumed $f'(x) > 0$, for satisfying the CFL stability condition it is necessary that \mathcal{S}_i should be an upwinding stencil. Therefore, we must have $x_{i-1} \in \mathcal{S}_i$ (which is equivalent to require that $k \geq 0$).

In order to be conservative — a necessary condition for the Lax–Wendroff theorem [2], which assures that a converging sequence of refined numerical solutions always converge to a weak solution of (1.2) — $D_x f$ must have the form

$$D_x f(x_i) = \frac{\hat{f}_{i+\frac{1}{2}} - \hat{f}_{i-\frac{1}{2}}}{\Delta x}, \quad i = 0, \dots, N - 1, \quad (1.5)$$

where

$$\hat{f}_{i+j} \equiv \hat{f}(u(x_{i-k-\frac{1}{2}+j}, t), \dots, u(x_{i+l-\frac{1}{2}+j}, t)) \equiv \hat{f}(x_{i-k-\frac{1}{2}+j}, \dots, x_{i+l-\frac{1}{2}+j})$$

satisfies the consistency condition $\hat{f}(x, \dots, x) = f(x)$ and \hat{f} is Lipschitz continuous on each argument [2, 13] (for simplicity of notation, from now on we will drop u and t and consider both f and \hat{f} as a function of x only, since t is fixed).

One way of achieving such approximation \hat{f} is through the numerical flux function $h(x)$ [13, 5], which is defined by the implicit relation

$$f(x) = \frac{1}{\Delta x} \int_{x-\frac{\Delta x}{2}}^{x+\frac{\Delta x}{2}} h(\xi) d\xi. \quad (1.6)$$

This special function satisfies $h(x) = f(x) + O(\Delta x^2)$ [13] and also the exact equality

$$f'(x) = \frac{h\left(x + \frac{\Delta x}{2}\right) - h\left(x - \frac{\Delta x}{2}\right)}{\Delta x},$$

whose proof is a simple Calculus exercise. Now, for $i = 0, \dots, N - 1$, we define $\hat{f}_{i+\frac{1}{2}}$ and $\hat{f}_{i-\frac{1}{2}}$ as $(R - 1)$ th degree polynomial interpolations of $h(x)$ respectively at the stencils $\mathcal{S}_{i+\frac{1}{2}} = \{x_{i-k}, \dots, x_{i+l}\}$ and $\mathcal{S}_{i-\frac{1}{2}} = \{x_{i-k-1}, \dots, x_{i+l-1}\}$, that is,

$$\hat{f}_{i\pm\frac{1}{2}} = h_{i\pm\frac{1}{2}} + a^R f_i^{(R)} \Delta x^R + O(\Delta x^{R+1}), \quad (1.7)$$

where the first asymptotic terms $(a^R f_i^{(R)} \Delta x^R)$ are identical for $\hat{f}_{i\pm\frac{1}{2}}$ because the grid is uniform and $\mathcal{S}_{i-\frac{1}{2}}$ is just $\mathcal{S}_{i+\frac{1}{2}}$ shifted one point to the left [22] (notice that, for upwinding, we must have $x_{i-1} \in \mathcal{S}_{i-\frac{1}{2}}$ and $x_i \in \mathcal{S}_{i+\frac{1}{2}}$). Immediately, we have

$$\hat{f}_{i+\frac{1}{2}} - \hat{f}_{i-\frac{1}{2}} = h_{i+\frac{1}{2}} - h_{i-\frac{1}{2}} + O(\Delta x^{R+1}).$$

It follows that

$$D_x f(x_i) \equiv \frac{\hat{f}_{i+\frac{1}{2}} - \hat{f}_{i-\frac{1}{2}}}{\Delta x} = \frac{h_{i+\frac{1}{2}} - h_{i-\frac{1}{2}} + O(\Delta x^{R+1})}{\Delta x} = f'(x_i) + O(\Delta x^R)$$

for $i = 0, \dots, N - 1$, and, as a result, we have an R th-order approximation $D_x f$ as desired.

For each $i = 0, \dots, N - 1$, the polynomial approximation $\hat{f}_{i+\frac{1}{2}}$ can be written as

$$\hat{f}_{i+\frac{1}{2}} = \sum_{j=0}^{R-1} c_{kj}^R f(x_{i-k+j}) = \hat{f}(x_{i-k}, \dots, x_{i+l}), \quad (1.8)$$

where the coefficients c_{kj}^R , which are given by the closed-form formula [5]

$$c_{kj}^R = \sum_{m=j+1}^R \frac{\sum_{\substack{l=0 \\ l \neq m}}^R \prod_{\substack{q=0 \\ q \neq m, l}}^R (R - k - q)}{\prod_{\substack{l=0 \\ l \neq m}}^R (m - l)},$$

depend on the order R , the left shift parameter k , and j , as the indexes imply, but not on i , Δx , or the original flux f . A table with values of c_{kj}^R up to order $R = 6$, and a more detailed discussion about the formula of c_{kj}^R , can be found in [6].

Since it is true that $\sum_{j=0}^{R-1} c_{kj}^R = 1$ for all R and k , it follows that $\hat{f}(x_{i-k}, \dots, x_{i+l})$ is both consistent to the flux f and Lipschitz continuous on each argument. Therefore, $D_x f$ is conservative, as required by the Lax–Wendroff theorem.

1.1.1 Time discretization

The approach following Eqs. (1.4) and (1.5) frees us to choose any desired time discretization scheme. For instance, one could use the Forward Euler scheme

$$\frac{U_i^{n+1} - U_i^n}{\Delta t} = \frac{\hat{f}_{i+\frac{1}{2}}(U^n) - \hat{f}_{i-\frac{1}{2}}(U^n)}{\Delta x},$$

the third-order strong stability-preserving explicit Runge–Kutta method (SSP-RK(3,3)) [5, 23]

$$\begin{aligned} U^{(1)} &= U^n + \frac{\Delta t}{\Delta x} [\hat{f}_{i+\frac{1}{2}}(U^n) - \hat{f}_{i-\frac{1}{2}}(U^n)] \\ U^{(2)} &= \frac{3}{4}U^n + \frac{1}{4}U^{(1)} + \frac{\Delta t}{4\Delta x} [\hat{f}_{i+\frac{1}{2}}(U^{(1)}) - \hat{f}_{i-\frac{1}{2}}(U^{(1)})] \\ U^{n+1} &= \frac{1}{3}U^n + \frac{2}{3}U^{(2)} + \frac{2\Delta t}{3\Delta x} [\hat{f}_{i+\frac{1}{2}}(U^{(2)}) - \hat{f}_{i-\frac{1}{2}}(U^{(2)})], \end{aligned} \quad (1.9)$$

the Adams–Bashforth methods, the ADER methods [24], etc. In this work, we use the SSP-RK(3,3) (1.9) as a time integrator in all numerical simulations.

1.1.2 The fifth-order upstream central scheme

For the purpose of illustration, consider the following fifth-order approximation to $h_{i+\frac{1}{2}}$:

$$\hat{f}_{i+\frac{1}{2}}^{\text{UC5}+} \triangleq \frac{2f_{i-2} - 13f_{i-1} + 47f_i + 27f_{i+1} - 3f_{i+2}}{60} = h_{i+\frac{1}{2}} + \mathcal{O}(\Delta x^5). \quad (1.10)$$

This approximation uses the 5 points stencil centered around x_i , and therefore has some level of upwinding for fluxes with positive velocity (that is, when $f'(x) \geq 0$). It follows that

$$\frac{\hat{f}_{i+\frac{1}{2}}^{\text{UC5}+} - \hat{f}_{i-\frac{1}{2}}^{\text{UC5}+}}{\Delta x} = \frac{-2f_{i-3} + 15f_{i-2} - 60f_{i-1} + 20f_i + 30f_{i+1} - 3f_{i+2}}{60\Delta x} = f'(x_i) + \mathcal{O}(\Delta x^5). \quad (1.11)$$

It is easy to construct a version of (1.11) for fluxes with negative velocity ($f'(x) \leq 0$); we just need to use a mirrored stencil, centered around x_{i+1} , for approximating $h_{i+\frac{1}{2}}$:

$$\hat{f}_{i+\frac{1}{2}}^{\text{UC5}-} \triangleq \frac{-3f_{i-1} + 27f_i + 47f_{i+1} - 13f_{i+2} + 2f_{i+3}}{60} = h_{i+\frac{1}{2}} + \mathcal{O}(\Delta x^5).$$

The resulting difference is also a fifth-order approximation to $f'(x_i)$:

$$\frac{\hat{f}_{i+\frac{1}{2}}^{\text{UC5}-} - \hat{f}_{i-\frac{1}{2}}^{\text{UC5}-}}{\Delta x} = \frac{-3f_{i-2} + 30f_{i-1} + 20f_i - 60f_{i+1} + 15f_{i+2} - 2f_{i+3}}{60\Delta x} = f'(x_i) + \mathcal{O}(\Delta x^5). \quad (1.12)$$

When a method for selecting between (1.11) and (1.12) (e.g., a flux partition like Eq. (1.3)) is used together with a time discretization method (e.g., Eq. (1.9)), the resulting scheme is called the *fifth-order upstream central scheme*. This scheme is relevant as a basis of comparison with fifth-order WENO schemes, as we shall see in the next sections.

2 WENO schemes

In what follows, we will consider only fluxes with positive velocity ($f'(x) \geq 0$). For fluxes with negative velocity, a simple mirroring and shifting of the stencils is sufficient [5].

The R th-order WENO polynomial approximation $\hat{f}_{i+\frac{1}{2}}^W$ to the numerical flux $h(x_{i+\frac{1}{2}})$ (1.6) is built through a convex combination of r polynomial approximations of order r , $\hat{f}_{i+\frac{1}{2}}^0, \hat{f}_{i+\frac{1}{2}}^1, \dots, \hat{f}_{i+\frac{1}{2}}^{r-1}$, where

$$\boxed{R = 2r - 1} \quad (2.1)$$

(R is the *scheme order* and r is the *substencil order*, or simply, *suborder*). Each approximation \hat{f}^k , $k = 0, \dots, r-1$, uses a corresponding r points fixed substencil $\mathcal{S}_{i+\frac{1}{2}}^k = \{x_{i-r+1+k}, x_{i-r+2+k}, \dots, x_{i+k}\}$ out of a global stencil of R points, $\mathcal{S}_{i+\frac{1}{2}} = \{x_{i-r+1}, x_{i-r+2}, \dots, x_{i+r-1}\}$. By Eq. (1.8), these polynomial approximations can be written as

$$\hat{f}_{i+\frac{1}{2}}^k = \sum_{j=0}^{r-1} c_{r-1-k,j}^r f(x_{i-r+1+k+j}) = \hat{f}(x_{i-r+1+k}, x_{i-r+2+k}, \dots, x_{i+k}), \quad k = 0, \dots, r-1.$$

The formulas of $\hat{f}_{i+\frac{1}{2}}^k$ for orders up to $R = 9$ can be found in Appendix A; for higher orders, these formulas can be found in [25, 26].

The WENO discretization $D_x^W f$ is defined as

$$D_x^W f(x_i) \triangleq \frac{\hat{f}_{i+\frac{1}{2}}^W - \hat{f}_{i-\frac{1}{2}}^W}{\Delta x}, \quad \hat{f}_{i\pm\frac{1}{2}}^W \triangleq \sum_{k=0}^{r-1} \omega_{i\pm\frac{1}{2}}^k \hat{f}_{i\pm\frac{1}{2}}^k, \quad i = 0, \dots, N-1, \quad (2.2)$$

where the *nonlinear weights* $\omega_{i\pm\frac{1}{2}}^k$ (often denoted ω_k for simplicity) must satisfy the following conditions:

Condition 1 (Convexity).

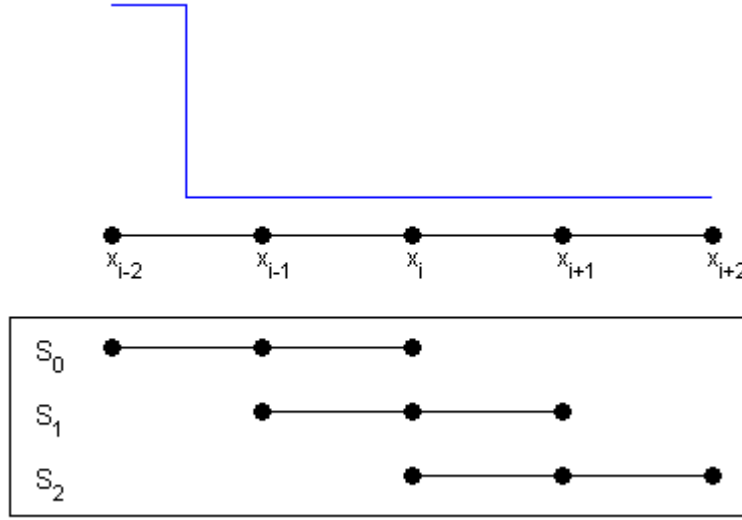
$$\sum_{k=0}^{r-1} \omega_k = 1, \quad \omega_k \geq 0, \quad k = 0, \dots, r-1.$$

Condition 2 (ENO property). If \mathcal{S}_D contains a discontinuity of f , but exists a substencil \mathcal{S}_C where the function is smooth, then $\omega_D = O(\Delta x^q)$ for some $q > 0$, and $\omega_C = \Theta(1)$.

Condition 3 (Optimality). If f is smooth, then

$$D_x^W f(x_i) = f'(x_i) + O(\Delta x^R), \quad i = 0, \dots, N-1.$$

Condition 1 is necessary for consistency and stability. Condition 2 implies that contribution of discontinuous stencils to $D_x^W f$ is small. Since the ultimate cause of oscillations in discontinuous numerical solutions is the interpolation across discontinuities of

Figure 6 – Stencil $\mathcal{S}_{i+\frac{1}{2}}$ and substencils $\mathcal{S}_{i+\frac{1}{2}}^0$, $\mathcal{S}_{i+\frac{1}{2}}^1$ and $\mathcal{S}_{i+\frac{1}{2}}^2$ of a fifth-order WENO scheme

the solution, condition 2 is the reason why WENO is essentially non-oscillatory. Condition 3 is for guaranteeing that, when the solution is smooth, the order of accuracy of $D_x^W f$ is the maximum allowed one by the $R + 1$ points stencil it uses (which is a union of $\mathcal{S}_{i+\frac{1}{2}}$ and $\mathcal{S}_{i-\frac{1}{2}} \equiv \{x_{i-r}, x_{i-r+1}, \dots, x_{i+r-2}\}$). This includes the case where f contains smooth extrema, which, as we shall see, is sometimes troublesome for WENO schemes.

2.1 The fifth-order WENO scheme

For the purpose of illustration, consider the WENO scheme of order $R = 5$. In this case, by Eq. (2.1), the substencil order is $r = 3$. Therefore, we have 3 polynomial approximations to $h_{i+\frac{1}{2}}$ of 2nd degree (see Appendix A),

$$\hat{f}_{i+\frac{1}{2}}^0 = \frac{2f_{i-2} - 7f_{i-1} + 11f_i}{6}, \quad \hat{f}_{i+\frac{1}{2}}^1 = \frac{-f_{i-1} + 5f_i + 2f_{i+1}}{6}, \quad \hat{f}_{i+\frac{1}{2}}^2 = \frac{2f_i + 5f_{i+1} - f_{i+2}}{6}, \quad (2.3)$$

each using their correspondent substencil $\mathcal{S}_{i+\frac{1}{2}}^k = \{x_{i-2+k}, x_{i-1+k}, x_{i+k}\}$, $k = 0, \dots, r - 1$. By Eq. (2.2), the WENO discretization is given by

$$D_x^W f(x_i) = \frac{\hat{f}_{i+\frac{1}{2}}^W - \hat{f}_{i-\frac{1}{2}}^W}{\Delta x}, \quad \hat{f}_{i\pm\frac{1}{2}}^W = \omega_{i\pm\frac{1}{2}}^0 \hat{f}_{i\pm\frac{1}{2}}^0 + \omega_{i\pm\frac{1}{2}}^1 \hat{f}_{i\pm\frac{1}{2}}^1 + \omega_{i\pm\frac{1}{2}}^2 \hat{f}_{i\pm\frac{1}{2}}^2, \quad i = 0, \dots, N - 1.$$

Figure 6 shows the global stencil $\mathcal{S}_{i+\frac{1}{2}}$ around x_i and the substencils $\mathcal{S}_{i+\frac{1}{2}}^0$, $\mathcal{S}_{i+\frac{1}{2}}^1$ and $\mathcal{S}_{i+\frac{1}{2}}^2$. Notice that f has a discontinuity on $\mathcal{S}_{i+\frac{1}{2}}^0$, but is smooth on $\mathcal{S}_{i+\frac{1}{2}}^1$ and $\mathcal{S}_{i+\frac{1}{2}}^2$. In this case, Condition 2 imposes that $\omega_0 = O(\Delta x^q)$ (that is, ω_0 is “small”) and, therefore,

the contribution of the oscillatory approximation $\hat{f}_{i+\frac{1}{2}}^0$ to $\hat{f}^W i + \frac{1}{2}$ is small, making the solution essentially non-oscillatory.

2.2 Ideal weights and accuracy of WENO schemes

When the solution is smooth, the R points stencil WENO approximation $\hat{f}_{i+\frac{1}{2}}^W$ must be of order R by Condition 3. However, it is not immediate how $\hat{f}_{i+\frac{1}{2}}^W$ could achieve this, since, by Eq. (2.2), it is a convex combination of $\hat{f}_{i+\frac{1}{2}}^k$, $k = 0, \dots, r-1$, which are all r th-order approximations to $h(x)$. Fortunately, there exist some constants d_k , which are called the *ideal weights*, which satisfy

$$\sum_{k=0}^{r-1} d_k \hat{f}_{i\pm\frac{1}{2}}^k = h_{i\pm\frac{1}{2}} + A^R f_i^{(R)} \Delta x^R + O(\Delta x^{R+1}), \quad (2.4)$$

where, similarly to Eq. (1.7), the coefficient A^R is the same for $x_{i-\frac{1}{2}}$ and $x_{i+\frac{1}{2}}$ and does not depend on k , and

$$\sum_{k=0}^{r-1} d_k = 1, \quad d_k \geq 0, \quad k = 0, \dots, r-1. \quad (2.5)$$

Therefore, the ideal weights satisfy the Conditions 1 and 3. In [21], the existence of ideal weights for any given order R is demonstrated, and a closed-form formula is provided,

$$d_k = \frac{\binom{r-1}{k} \binom{r}{k}}{\binom{R}{r}}, \quad k = 0, \dots, r-1.$$

The values of d_k for orders up to 9 are given in Appendix A; for higher orders, these formulas can be found in [25, 26].

2.2.1 The fifth-order case

For fifth-order WENO,

$$d_0 = \frac{1}{10}, \quad d_1 = \frac{3}{5}, \quad d_2 = \frac{3}{10}.$$

Therefore, by (2.3), we have

$$\begin{aligned} d_0 \hat{f}_{i+\frac{1}{2}}^0 + d_1 \hat{f}_{i+\frac{1}{2}}^1 + d_2 \hat{f}_{i+\frac{1}{2}}^2 &= \\ &= \frac{1}{10} \cdot \frac{2f_{i-2} - 7f_{i-1} + 11f_i}{6} + \frac{3}{5} \cdot \frac{-f_{i-1} + 5f_i + 2f_{i+1}}{6} + \frac{3}{10} \cdot \frac{2f_i + 5f_{i+1} - f_{i+2}}{6} \\ &= \frac{2f_{i-2} - 13f_{i-1} + 47f_i + 27f_{i+1} - 3f_{i+2}}{60}, \end{aligned}$$

which is exactly the term $\hat{f}_{i+\frac{1}{2}}^{\text{UC5+}}$ of the fifth-order upstream central scheme (1.10). Similar relations hold for higher orders.

2.2.2 Achieving the optimality condition

Virtually all existing WENO schemes adopt the same strategy (devised in [15]) for satisfying the optimality condition, which consists on defining the nonlinear weights ω_k in such a way that it approximates the ideal weights up to a convenient order. This is done by first noticing that

$$\begin{aligned}
\hat{f}_{i\pm\frac{1}{2}}^W &= \sum_{k=0}^{r-1} d_k \hat{f}_{i\pm\frac{1}{2}}^k + \sum_{k=0}^{r-1} (\omega_{i\pm\frac{1}{2}}^k - d_k) \hat{f}_{i\pm\frac{1}{2}}^k \\
&= h_{i\pm\frac{1}{2}} + A^R f_i^R \Delta x^R + O(\Delta x^{R+1}) + \sum_{k=0}^{r-1} (\omega_{i\pm\frac{1}{2}}^k - d_k) \left(h_{i\pm\frac{1}{2}} + a_k^r f_i^{(r)} \Delta x^r + O(\Delta x^{r+1}) \right) \\
&= h_{i\pm\frac{1}{2}} + A^R f_i^R \Delta x^R + O(\Delta x^{R+1}) \\
&\quad + \sum_{k=0}^{r-1} (\omega_{i\pm\frac{1}{2}}^k - d_k) a_k^r f_i^{(r)} \Delta x^r + \sum_{k=0}^{r-1} [(\omega_{i\pm\frac{1}{2}}^k - d_k) O(\Delta x^{r+1})], \tag{2.6}
\end{aligned}$$

which follows by Condition 1 and Eqs. (1.7), (2.4) and (2.5). From Eq. (2.6), it is immediate that if $\omega_{i\pm\frac{1}{2}}^k - d_k$ is small, then $\hat{f}_{i\pm\frac{1}{2}}^W = h_{i\pm\frac{1}{2}} + A^R f_i^R \Delta x^R + O(\Delta x^{R+1})$, and this implies the Condition 3.

Remark 2. It should be stressed that the $O(\Delta x^{r+1})$ term in Eq. (2.6) depends on k and is different for $x_{i-\frac{1}{2}}$ and $x_{i+\frac{1}{2}}$; this is why it must appear inside the summation.

Now, we will formalize the aforementioned strategy in two propositions. They impose sufficient conditions on the size of $\omega_{i\pm\frac{1}{2}}^k - d_k$ so that WENO achieves the optimal order R for smooth solutions.

Proposition 1. *If the nonlinear weights satisfy the condition*

$$\omega_{i\pm\frac{1}{2}}^k - d_k = O(\Delta x^r), \quad k = 0, \dots, r-1, \quad i = 0, \dots, N-1, \tag{2.7}$$

then the corresponding WENO scheme satisfies the optimality condition (Condition 3).

Proof. By Eq. (2.5),

$$\begin{aligned}
\hat{f}_{i\pm\frac{1}{2}}^W &= h_{i\pm\frac{1}{2}} + A^R f_i^R \Delta x^R + O(\Delta x^{R+1}) + \sum_{k=0}^{r-1} O(\Delta x^r) a_k^r f_i^{(r)} \Delta x^r + \sum_{k=0}^{r-1} [O(\Delta x^r) O(\Delta x^{r+1})] \\
&= h_{i\pm\frac{1}{2}} + A^R f_i^R \Delta x^R + O(\Delta x^{R+1}).
\end{aligned}$$

Therefore, by Eq. (2.2),

$$D_x^W f = \frac{h_{i+\frac{1}{2}} - h_{i-\frac{1}{2}}}{\Delta x} + \frac{A^R f_i^R \Delta x^R - A^R f_i^R \Delta x^R}{\Delta x} + \frac{O(\Delta x^{R+1})}{\Delta x} = f'(x_i) + O(\Delta x^R),$$

and the scheme satisfies Condition 3. \square

Proposition 2. *If the nonlinear weights satisfy the conditions*

$$\begin{cases} \omega_{i\pm\frac{1}{2}}^k - d_k = O(\Delta x^{r-1}), \\ \omega_{i+\frac{1}{2}}^k - \omega_{i-\frac{1}{2}}^k = O(\Delta x^r), \end{cases} \quad k = 0, \dots, r-1, \quad i = 0, \dots, N-1, \quad (2.8)$$

then the corresponding WENO scheme satisfies the optimality condition (Condition 3).

Proof. By Eq. (2.5),

$$\hat{f}_{i\pm\frac{1}{2}}^W = h_{i\pm\frac{1}{2}} + A^R f_i^R \Delta x^R + \sum_{k=0}^{r-1} (\omega_{i\pm\frac{1}{2}}^k - d_k) a_k^r f_i^{(r)} \Delta x^r + O(\Delta x^{R+1}).$$

By Eq. (2.2), it follows that

$$\begin{aligned} D_x^W f &= \frac{h_{i+\frac{1}{2}} - h_{i-\frac{1}{2}}}{\Delta x} + \frac{\sum_{k=0}^{r-1} (\omega_{i+\frac{1}{2}}^k - \omega_{i-\frac{1}{2}}^k) a_k^r f_i^{(r)} \Delta x^r}{\Delta x} + O(\Delta x^R) \\ &= f'(x_i) + \frac{\sum_{k=0}^{r-1} O(\Delta x^r) a_k^r f_i^{(r)} \Delta x^r}{\Delta x} + O(\Delta x^R) = f'(x_i) + O(\Delta x^R). \quad \square \end{aligned}$$

2.3 Time integration and linear stability

Fifth-order WENO schemes are linearly unstable when coupled with forward Euler time integration or second-order explicit Runge–Kutta methods, but are linearly stable when used together with any third-order Runge–Kutta method [27] — in particular, the third-order SSP-RK(3,3) method (1.9), which, for many years, has been the time integrator of choice for combining with WENO schemes (see e.g. [15, 5, 19, 16], and many others). For this reason, in this work we use the SSP-RK(3,3) method as a time integrator in all numerical simulations.

Notice that, in order to achieve the formal order R in smooth solutions, one needs to use $\Delta t = C\Delta x^{R/3}$ when coupling SSP-RK(3,3) with an R th-order WENO scheme. However, in all of the numerical tests which involve discontinuities, the effective accuracy order is close to 1, no matter the power of Δx in the expression of Δt [5]. Thus, we use $\Delta t = C\Delta x^{R/3}$ in accuracy tests (whose solutions do not contain discontinuities) and $\Delta t = C\Delta x$ in all other tests.

2.4 Analysis of WENO schemes

When analyzing WENO schemes, in most cases the work can be done in the $x_{i+\frac{1}{2}}$ -centered stencil $\mathcal{S}_{i+\frac{1}{2}} = \{x_{i-r+1}, x_{i-r+2}, \dots, x_{i+r-1}\}$ only. Since the grid index i is arbitrary, the results are carried over to $\mathcal{S}_{i-\frac{1}{2}} = \{x_{i-r}, x_{i-r+1}, \dots, x_{i+r-2}\}$, because $\mathcal{S}_{i-\frac{1}{2}}$ is just $\mathcal{S}_{i+\frac{1}{2}}$

shifted one point to the left. For instance, in Proposition 1, it is sufficient to show that $\omega_{i+\frac{1}{2}}^k - d_k = O(\Delta x^r)$, $k = 0, \dots, r-1$ and arbitrary i ; if this is true, it is evident that $\omega_{i-\frac{1}{2}}^k - d_k = O(\Delta x^r)$, $k = 0, \dots, r-1$ also holds.

There are exceptions where the analysis on $\mathcal{S}_{i+\frac{1}{2}}$ and $\mathcal{S}_{i-\frac{1}{2}}$ must be done separately. An example is Proposition 2, which has a condition on $\delta_i \omega^k$. In such cases, the subscripts $i \pm \frac{1}{2}$ will be used for avoiding confusion. In all other cases, whenever the i subscript is dropped, consider that we are doing the analysis in $\mathcal{S}_{i+\frac{1}{2}}$.

2.4.1 The discontinuous/continuous ratio: a relative measure of dissipativity

Let \mathcal{S} be an R points stencil, and two r points substencils \mathcal{S}_C and \mathcal{S}_D . Suppose \mathcal{S}_C is smooth (that is, f is smooth in \mathcal{S}_C), while \mathcal{S}_D is not. Let's call the ratio ω_D/ω_C , between the weights of a discontinuous substencil and a continuous one, the *discontinuous/continuous ratio*. It is a measure of the dissipativity of a WENO scheme which we would like to formally introduce in this work.

Consider ω^I and ω^{II} two different weight definitions, corresponding to two different schemes, WENO I and WENO II, respectively. If it can be shown that

$$\frac{\omega_D^I}{\omega_C^I} > \frac{\omega_D^{II}}{\omega_C^{II}} \quad (2.9)$$

whenever \mathcal{S}_D is discontinuous and \mathcal{S}_C is continuous, this means that WENO I assigns relatively more weight to discontinuous substencils than WENO II does. This may seem undesirable at first, since the WENO schemes were designed for avoiding discontinuous substencils via ENO property (Condition 2). However, the discontinuous stencils carry useful information about the solution which should not be completely disregarded. Moreover, the relative upwinding, which occurs when the weights of discontinuous substencils are small, increases the dissipativity of the scheme. By increasing the weights of discontinuous substencils, the upwinding process is softened and as a result WENO I is less dissipative than WENO II. A less dissipative scheme gives sharper discontinuities. Likewise, in coarse grids it resolves smooth, large gradient structures better, because at these numerical scales the large gradients are detected as relative discontinuities. Of course, there's a balance here: the weights of discontinuous substencils cannot be *too* large, otherwise the resulting scheme will be oscillatory and/or unstable.

So far, the numerical results corroborate that if two schemes I and II satisfy (2.9), then WENO I has sharper results than WENO II, in general.

2.4.2 Operation count

Throughout this work, we will count the operations done when computing a weight ω_k as a labeled triple $\{\cdot\pm, \cdot\times, \cdot\div\}$, where $\text{flops}(\omega_k) = \{a\pm, b\times, c\div\}$ denotes that it is necessary

to do a sums (or subtractions), b products and c divisions in order to compute ω_k . We opted for doing so because, in some computer architectures, a division costs more than a product, which in turn costs more than sums and subtractions.

Most weight formulas also involve powers. We prefer to not calculate the costs of a power operation directly, since the cost vary with the power in question and the specific implementation of the power operation (for instance, a power of two can be implemented as a single product, or as a more generic (and costly) function which deals with any power). Instead, whenever a power of p needs to be computed, we will denote its cost as $\text{flops}(\text{pow}(p))$.

Some formulas also involve conditional expressions. These have a cost which is architecture-dependent, and will be denoted as $\text{conditional}()$.

2.4.3 Unnormalized weights

Virtually all WENO schemes in existence can be written in the form

$$\omega_k = \frac{\alpha_k}{\sum_{j=0}^{r-1} \alpha_j}, \quad \alpha_k \geq 0, \quad k = 0, \dots, r-1, \quad (2.10)$$

where α_k are the *unnormalized weights*. In this way, ω_k immediately satisfies the convexity condition (Condition 1).

It also follows that the discontinuous/continuous ratio can be expressed in terms of unnormalized weights: suppose \mathcal{S}_D is discontinuous and \mathcal{S}_C is continuous, both substencils of \mathcal{S} . Then,

$$\frac{\omega_D}{\omega_C} = \frac{\alpha_D}{\sum_{j=0}^{r-1} \alpha_j} \bigg/ \frac{\alpha_C}{\sum_{j=0}^{r-1} \alpha_j} = \frac{\alpha_D}{\alpha_C}.$$

Moreover, the ENO property (Condition 2) can be verified in terms of the discontinuous/continuous ratio α_D/α_C : suppose we have $\alpha_D/\alpha_C = O(\Delta x^q)$ for some $q > 0$. Then, as $\Delta x \rightarrow 0$,

$$\omega_D \leq \frac{\alpha_D}{\alpha_C + \alpha_D} = \frac{\alpha_D}{\alpha_C} \frac{1}{1 + \frac{\alpha_D}{\alpha_C}} = \Theta\left(\frac{\alpha_D}{\alpha_C}\right).$$

It follows that $\omega_D = O(\Delta x^q)$. As a result, $\omega_C = \Theta(1)$ because of Condition 1 (which ω satisfies by (2.10)), and the ENO property is achieved. This can be summarized in the following proposition:

Proposition 3. *Suppose the weights of a WENO scheme are defined in terms of unnormalized weights, as in Eq. (2.10). If, for every \mathcal{S} which has a continuous substencil \mathcal{S}_C and a discontinuous one \mathcal{S}_D the relation $\alpha_D/\alpha_C = O(\Delta x^q)$ holds, for some $q > 0$, then, as $\Delta x \rightarrow 0$, the WENO scheme satisfies the ENO property.*

Since all WENO schemes studied here are defined in terms of unnormalized weights, in most of times when comparing the operation count of two different schemes it will be

sufficient to compare the costs of computing the unnormalized weights, since the cost of the normalization (2.10) is the same for two WENO schemes of same order.

2.5 Testing WENO schemes

For numerically validating the schemes presented here, some standard tests found in the literature are used. These tests are setups of two hyperbolic conservation laws: the linear advection equation

$$u_t + u_x = 0, \quad u(x, 0) = u_0(x), \quad (2.11)$$

and the Euler equations of compressible flow for an ideal gas, in 1D

$$\begin{bmatrix} \rho \\ \rho u \\ E \end{bmatrix}_t + \begin{bmatrix} \rho u \\ \rho u^2 + p \\ u(E + p) \end{bmatrix}_x = 0, \quad E = \frac{p}{\gamma - 1} + \frac{1}{2}\rho u^2, \quad \begin{bmatrix} \rho(x, 0) \\ u(x, 0) \\ p(x, 0) \end{bmatrix} = \begin{bmatrix} \rho_0(x) \\ u_0(x) \\ p_0(x) \end{bmatrix}.$$

Here, ρ is the mass density of the fluid; u is the velocity; E is the total energy per unit length; p is the pressure; and γ is the adiabatic index. For monoatomic gases, $\gamma = 5/3$; for diatomic, $\gamma = 7/5$.

The tests can be grouped into three categories:

2.5.1 Stability tests

2.5.1.1 Interacting blast waves

This Euler 1D test was developed in [28] and consists in two interacting blast waves. The strong shocks in the solution are computationally hard to solve; schemes with unstable tendencies often fail to converge in this test. The domain is $x \in [0, 1]$ with reflexive boundary conditions. The initial setup is

$$(\rho_0, u_0, p_0) = \begin{cases} (1, 0, 1000), & x < 0.1, \\ (1, 0, 100), & x > 0.9, \\ (1, 0, 0.01), & \text{otherwise.} \end{cases}$$

For this test, $\gamma = 7/5$. The test is run up to the final time $T = 0.038$. Since there is no known expression for the exact solution of this problem, the numerical solution by the WENO-Z scheme with $N = 8000$ points (shown in Fig. 7) is used as a reference solution.

2.5.1.2 ADR analysis

We will follow the approach of [8] for applying a nonlinear version of the Approximate Dispersion Relation analysis to the WENO schemes. The analysis is done this way: consider a grid with N points, set

$$\phi_n = \frac{2\pi n}{N}.$$

We then solve the advection problem (2.11) with the initial condition given by the discrete wave $e^{im\phi_n}$, $m = 0, \dots, N-1$, using the WENO scheme being analyzed, up to a very small final time $T = 10^{-10}$ (in order to make the error from the time integration negligible) and periodic boundary conditions. The complex exponent of the amplification factor of the numerical solution at ϕ_n is defined as $i\Phi(\phi_n)$. By making $n = 0, \dots, N/2$, we cover all wavenumbers in the grid ($0 \leq \phi_n \leq \pi$). In this way, we get the amplification Φ for all wavenumbers. See [8, 29] for details.

Here, we will be using a grid with $N = 2000$ points for the ADR analysis, and only the imaginary part of Φ , which is related with the dissipation of the scheme, will be considered. Ideally, $\text{Im}(\Phi)$ should be 0, but in practice $\text{Im}(\Phi) \sim 0$ in a range of low wavenumbers and decreases with ϕ for higher wavenumbers. The larger the range of wavenumbers for which $\text{Im}(\Phi) \sim 0$, and the larger the value $\text{Im}(\Phi)$ for higher wavenumbers, the less dissipative is the scheme. Positive values of $\text{Im}(\Phi)$ means that the scheme is actually amplifying the waves, which may be an evidence of instability. However, since the WENO schemes are nonlinear, in practice some nonlinear mechanism may compensate for this increase, though, and the scheme might as well remain stable.

2.5.2 Oscillation tests

These tests contain jump discontinuities in their solutions. Therefore, they are suited for testing if a given WENO scheme is indeed essentially non-oscillatory in practice.

2.5.2.1 GSTE test

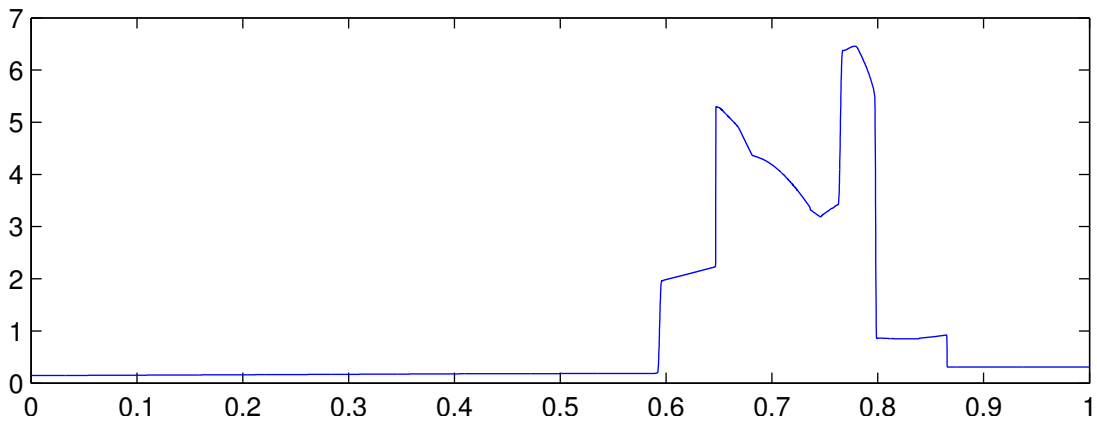
The acronym stands for Gaussian-square-triangle-ellipse, which is the shape of the function which is advected to the right [15]. The domain is $x \in [-1, 1]$ with periodic boundary, and the initial condition of this linear advection test is

$$u_0(x) = \begin{cases} \frac{1}{6} [G(x, \beta, z - \delta) + 4G(x, \beta, z) + G(x, \beta, z + \delta)], & x \in [-0.8, -0.6] \\ 1, & x \in [-0.4, -0.2] \\ 1 - |10(x - 0.1)|, & x \in [0, 0.2] \\ \frac{1}{6} [F(x, \alpha, a - \delta) + 4F(x, \alpha, a) + F(x, \alpha, a + \delta)], & x \in [0.4, 0.6] \\ 0, & \text{otherwise} \end{cases}$$

$$G(x, \beta, z) = e^{-\beta(x-z)^2}, \quad F(x, \alpha, a) = \sqrt{\max(1 - \alpha^2(x-a)^2, 0)},$$

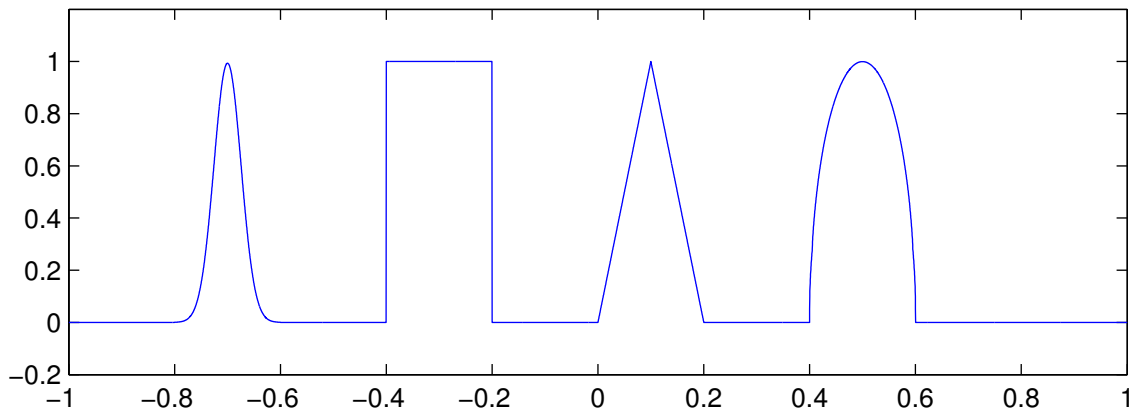
with $z = -0.7$, $\delta = 0.005$, $\beta = (\log 2)/36\delta^2$, $a = 0.5$ and $\alpha = 10$. The exact solution at final time $T = 2$ (which is exactly the initial condition) is shown in Fig. 8.

Figure 7 – Reference solution of the interacting blast waves problem



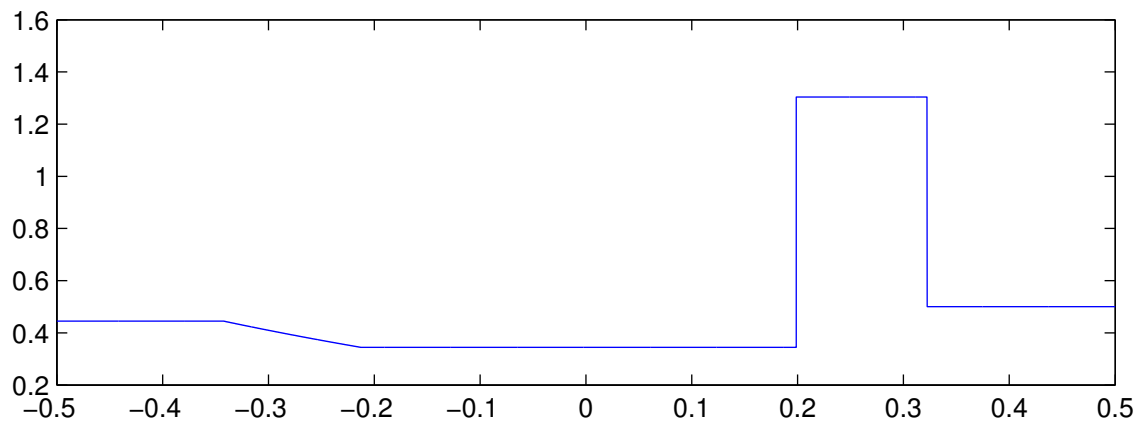
The figure shows the density of the solution at $T = 0.038$.

Figure 8 – Initial condition (and solution) of the GSTE problem



The figure shows the solution at $T = 2k$, $k \in \mathbb{N}$.

Figure 9 – Solution of Lax's Riemann problem



The figure shows the density of the solution at $T = 0.13$.

2.5.2.2 Riemann problem of Lax

This Riemann problem was introduced in [30]. The domain is $x \in [-0.5, 0.5]$ with free boundary, the initial condition is

$$(\rho_0, u_0, p_0) = \begin{cases} (0.445, 0.698, 3.528), & x \leq 0, \\ (0.5, 0, 0.571), & x > 0, \end{cases}$$

the final time is $T = 0.13$, and $\gamma = 7/5$. The reference solution at the final time is computed using an exact Riemann solver [3], and it is shown in Fig. 9. It consists in a left rarefaction wave, a central contact discontinuity and a right shock.

2.5.2.3 Riemann problem of Sod¹

This other Riemann problem was introduced in [31]. The domain is $x \in [-5, 5]$ with free boundary, the initial condition is

$$(\rho_0, u_0, p_0) = \begin{cases} (1, 0, 1), & x \leq 0, \\ (1/8, 0, 1/10), & x > 0, \end{cases}$$

final time is $T = 2$, and $\gamma = 7/5$. Again, the reference solution (Fig. 10) is computed by an exact Riemann solver, and it also consists in a left rarefaction wave, a central contact discontinuity and a right shock, albeit with a different shape.

2.5.3 Features tests

These tests involve both shocks and fine structures, and are used for testing the resolution power of WENO schemes.

2.5.3.1 Shock-entropy wave² test of Shu–Osher

This test was introduced in [13]. The domain of this Euler 1D test is $x \in [-5, 5]$ with free boundary, the initial condition is

$$(\rho_0, u_0, p_0) = \begin{cases} (27/7, 4\sqrt{35}/9, 31/3), & x < -4, \\ (1 + \sin(5x)/5, 0, 1), & x \geq -4, \end{cases}$$

final time is $T = 1.8$ and $\gamma = 7/5$. Since there is no known expression for the exact solution of this problem, the numerical solution by the WENO-Z scheme with $N = 8000$ (Fig. 11) is used as a reference solution.

¹ Also known in the literature as “shock tube problem of Sod”.

² Also known in the literature as “shock-density” or “shock-turbulence”.

Figure 10 – Solution of Sod’s Riemann problem

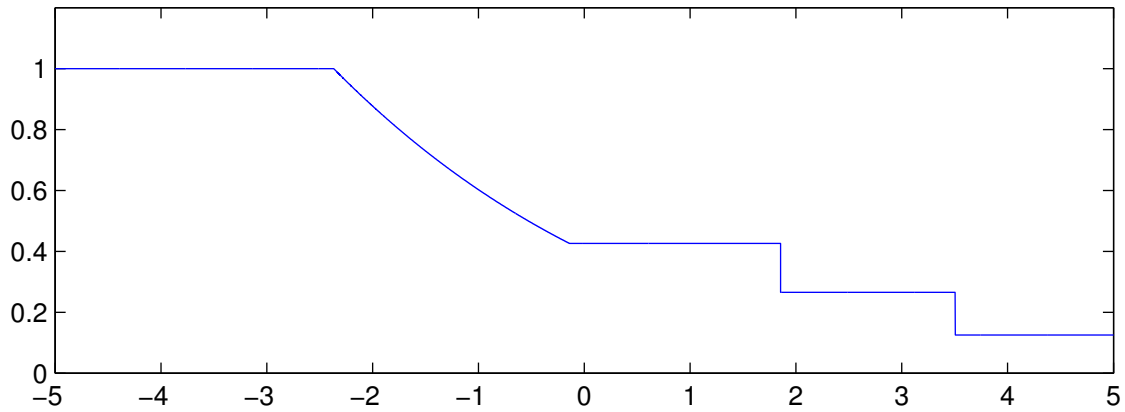


Figure 11 – Reference solution of shock-entropy wave problem of Shu–Osher

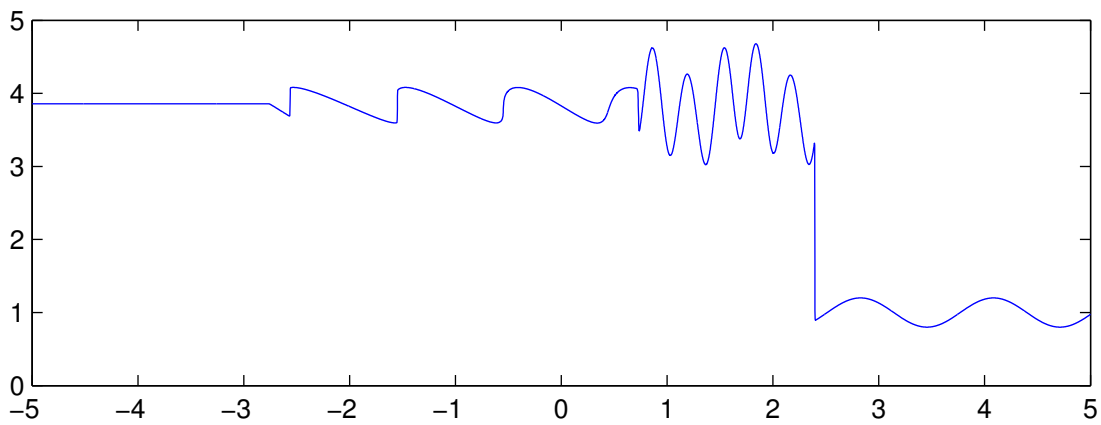
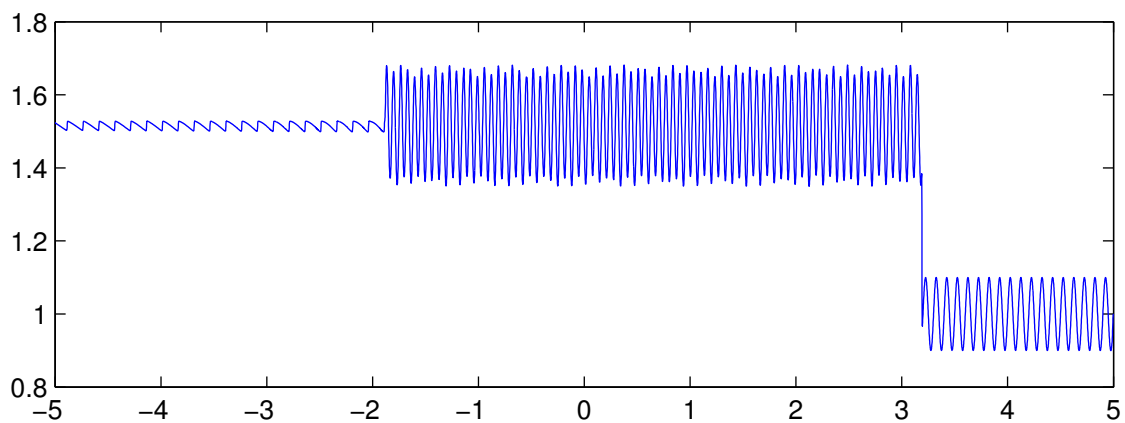


Figure 12 – Reference solution of shock-entropy wave problem of Titarev–Toro



2.5.3.2 Shock-entropy wave test of Titarev–Toro

This test, introduced in [32], is a variation of the Shu–Osher test, with a different initial condition

$$(\rho_0, u_0, p_0) = \begin{cases} (1.515695, 0.523346, 1.805000), & x < -4.5, \\ (1 + \sin(20\pi x)/10, 0, 1), & x \geq -4.5, \end{cases}$$

and final time, $T = 5$. Again, the numerical solution by the WENO-Z scheme with $N = 8000$ (Fig. 12) is used as a reference solution.

2.5.4 Accuracy test

WENO schemes may lose accuracy near critical points [19, 21, 22]. The goal of this test is to evaluate the order of accuracy of the WENO scheme at critical points of different orders (Definition 1), and see if the design order R is achieved or if the scheme loses accuracy.

The accuracy test consists on comparing the WENO discrete derivative $D_x^W f$ (cf. Eq. (2.2)) with the actual derivative f' of a given function $f(x)$ at the grid points x_i , $i = 0, \dots, N - 1$, with increasing grid sizes N . The L^1 error of $D_x^W f$, $e_1(N)$, is defined as

$$e_1(N) = \sum_{i=0}^{N-1} \left| D_x^W f(x_i) - f'(x_i) \right| \Delta x.$$

Given $M < N$, the L^1 numerical order of accuracy (shortly, L^1 order) from M to N , $o_1(M, N)$, is given by

$$o_1(M, N) = \log \left(\frac{e_1(M)}{e_1(N)} \right) / \log \left(\frac{N}{M} \right).$$

For this test, we use the family of functions

$$g_n(x) = e^{\frac{3}{4}(x-1)} x^{n+1}, \quad x \in [-1, 1].$$

The functions $g_n(x)$ are normalized, so that $\|g_n\|_{L^\infty[-1,1]} = 1$. Moreover, $g_n(x)$ has a single critical point of order n at $x = 0$ (except $g_0(x)$, which has no critical points) [22].

3 Smoothness indicators

So far, we have dealt with generic properties of WENO schemes, without going into details about the actual weights formulation. Before we move on, we need to introduce the smoothness indicators — mathematical objects which detect discontinuities in the solution, and are used in the formulation of WENO weights for achieving the ENO property (Condition 2).

Definition 5. Let f be a smooth by parts function defined in a collection of stencils $\mathcal{S} \equiv \mathcal{S}[x_i, \Delta x]$ fixed around a given point x_i ,

$$\mathcal{S}[x_i, \Delta x] = \{x_i + k_1\Delta x, x_i + k_2\Delta x, \dots, x_i + k_m\Delta x\}, \quad k_j \in \mathbb{R}, \quad k_1 < k_2 < \dots < k_m.$$

A *smoothness indicator*¹ $\mu(f, \mathcal{S})$ of order q , where $q > 0$, is a real positive function which satisfies

$$\mu(f, \mathcal{S}) = \begin{cases} O(\Delta x^q), & \text{if } f \text{ is continuous at } x_i, \\ \Theta(1), & \text{otherwise,} \end{cases}$$

as $\Delta x \rightarrow 0$.

This means that $\mu(f, \mathcal{S})$ gets smaller as $\Delta x \rightarrow 0$ if f is continuous at x_i , but it remains close to a fixed value (which depends on f) otherwise.

The smoothness indicators are defined in asymptotic terms, but in practice they are used differently. Since, in numerical applications, we usually desire to run a problem only once, we don't get a sequence of grid spaces Δx going to zero. Instead, the value of $\mu(f, \mathcal{S})$ is inspected for a fixed Δx , and if it is “small”, then we may assume f is continuous in the whole stencil $\mathcal{S}[x_i, \Delta x]$; otherwise, if it is “large”, then it is probably has a discontinuity somewhere inside said stencil (not necessarily at x_i !). Here, “small” and “large” are to be taken in relative terms — there is no threshold value under which the function is definitely continuous.²

In this work we follow the convention of leaving the function being availed by μ implicit, since it will always clear by the context, and making μ inherit any super/subscripts of \mathcal{S} as needed. For instance, $\mu(f, \mathcal{S}_k)$ will often be denoted μ_k .

¹ Also commonly called “smoothness measurement” or “smoothness estimator”.

² In fact, for each smoothness indicator μ , it is usually not hard to construct a function f and a stencil \mathcal{S} such that f is discontinuous in \mathcal{S} but $\mu(f, \mathcal{S}) = 0$.

3.1 A simple smoothness indicator

To elucidate how a typical smoothness indicator work, consider a smooth by parts function f and the stencil $\mathcal{S} = \{x_{i-1}, x_i, x_{i+1}\}$ around x_i , where $x_{i\pm 1} = x_i \pm \Delta x$. Let us define (recall Definition 4)

$$\mu \triangleq \left(\delta_i^{(2\Delta x)}[f] \right)^2 \Delta x^2 = \left(\frac{f(x_{i+1}) - f(x_{i-1})}{2} \right)^2,$$

which is the square of the centered second-order finite difference approximation to $f'(x_i)\Delta x$. We shall see that μ is a smoothness indicator of order 2.

First, suppose f is C^1 on \mathcal{S} . Taylor series around x_i gives

$$\mu = \left(f'(x_i)\Delta x + O(\Delta x^2) \right)^2 = (f'(x_i))^2 \Delta x^2 + O(\Delta x^3) = O(\Delta x^2).$$

In this case, it's clear that $\mu = O(\Delta x^2)$. But even when f is only continuous the same result holds. Suppose, without loss of generality, that f has a discontinuity in the first derivative at x_i but is smooth elsewhere (since f is smooth by parts, this is always the case as $\Delta x \rightarrow 0$). Then

$$f(x_i) = f(x_{i\pm 1}) \mp f'(x_{i\pm 1})\Delta x + O(\Delta x^2),$$

and

$$\begin{aligned} \mu &= \left(\frac{f(x_i) + f'(x_{i+1})\Delta x + O(\Delta x^2) - f(x_i) + f'(x_{i-1})\Delta x + O(\Delta x^2)}{2} \right)^2 \\ &= \left(\frac{f'(x_{i+1}) + f'(x_{i-1})}{2} \Delta x + O(\Delta x^2) \right)^2 \\ &= \left(\frac{f'(x_{i+1}) + f'(x_{i-1})}{2} \right)^2 \Delta x^2 + O(\Delta x^3) = O(\Delta x^2). \end{aligned}$$

Now, on the other hand, suppose f is discontinuous at x_i . Then,

$$\lim_{\Delta x \rightarrow 0} \mu = \left(\frac{\lim_{x \rightarrow x_i^+} f(x) - \lim_{x \rightarrow x_i^-} f(x)}{2} \right)^2 = \left(\frac{[f]_{x_i}}{2} \right)^2 = \Theta(1),$$

as claimed.

Typically, smoothness indicators are powers of finite difference approximations to derivatives (like this example), or more generally, combinations of such powers of approximations. In the next sections we shall see some of the smoothness indicators used in the literature.

3.2 Forward differences

Let $\Delta^{(n)} [f_i]$ be the n th-order undivided forward difference defined by (cf. Definition 4)

$$\begin{aligned}\Delta^{(0)} [f_i] &\triangleq f_i, \\ \Delta^{(n)} [f_i] &\triangleq \Delta^{(n-1)} f_{i+1} - \Delta^{(n-1)} f_i.\end{aligned}$$

Notice that $\Delta^{(n)} [f_i] = O(\Delta x^n)$ if f is smooth (the order decreases to $\Delta^{(n)} [f_i] = O(\Delta x^m)$ if f is continuous but has only $m - 1 < n$ derivatives), and $\Delta^{(n)} [f_i] = \Theta(1)$ if f is discontinuous in the domain (a complete proof of this can be found in [6]).

Let

$$\mathcal{S}^r(x_i) = \{x_{i-r+1}, x_{i-r+2}, \dots, x_i\};$$

here, r is the substencil order as in Eq. (2.1). We define the Forward Differences smoothness indicator as

$$FD(f, \mathcal{S}^r(x_i)) \triangleq \sum_{j=1}^{r-1} \left(\sum_{l=1}^j \frac{(\Delta^{(r-j)} [f_{i-r+l}])^2}{j} \right). \quad (3.1)$$

For simplicity, we will denote $FD(f, \mathcal{S}^r(x_i))$ as FD .

For suborder $r = 2$, the formula for FD is

$$FD = (\Delta^{(1)} [f_{i-1}])^2 = (f_i - f_{i-1})^2 = (f'_i)^2 \Delta x^2 + O(\Delta x^3),$$

and, for $r = 3$,

$$\begin{aligned}FD &= \frac{(\Delta^{(1)} [f_{i-2}])^2 + (\Delta^{(1)} [f_{i-1}])^2}{2} + (\Delta^{(2)} [f_{i-2}])^2 \\ &= \frac{(f_{i-1} - f_{i-2})^2 + (f_i - f_{i-1})^2}{2} + (f_i - 2f_{i-1} + f_{i-2})^2 \\ &= (f'_i)^2 \Delta x^2 + (f''_i)^2 \Delta x^4 + O(\Delta x^3).\end{aligned}$$

It is clear that FD is a smoothness measurement of order 2.

The forward differences are used by ENO schemes [11, 13], and was the first smoothness measurement proposed for WENO [14]. But, as we shall see in the next section, the smoothness indicator β of Jiang–Shu, which succeeded it, is more suitable for WENO schemes in general.

3.3 The smoothness indicator β of Jiang–Shu

By far, the smoothness indicator most currently used by WENO schemes is the Jiang–Shu β , which was developed in [15]. Its use is so widespread that it can be considered the *de facto* standard smoothness indicator for WENO schemes.

Convention 1. Thorough this work, the symbol β we will be used for denoting the Jiang–Shu smoothness indicator specifically; when speaking of a generic smoothness indicator, the symbol μ will be used instead.

Definition 6. The Jiang–Shu smoothness indicators of suborder r are given by

$$\beta_k \triangleq \sum_{l=1}^{r-1} \Delta x^{2l-1} \int_{x_{i-\frac{1}{2}}}^{x_{i+\frac{1}{2}}} \left(\frac{d^l}{dx^l} \hat{f}^k(x) \right)^2 dx, \quad k = 0, \dots, r-1. \quad (3.2)$$

Observe that β_k is a normalized sum of the L^2 version of the total variation of all derivatives of the $(r-1)$ th degree approximation polynomial $\hat{f}^k(x)$ to the numerical flux $h(x)$ (see Section 1.1 for the definition of $h(x)$). As such, the less smooth $h(x)$ is on \mathcal{S}_k (the stencil where $\hat{f}^k(x)$ interpolates $h(x)$), the higher the total variation of $\hat{f}^k(x)$ in $[x_{i-\frac{1}{2}}, x_{i+\frac{1}{2}}]$ and, therefore, the higher the value of β_k .

For the purpose of illustration, consider the case $R = 5$ ($r = 3$), which uses the global stencil $\mathcal{S} = \{x_{i-2}, x_{i-1}, x_i, x_{i+1}, x_{i+2}\}$ and substencils $\mathcal{S}_0 = \{x_{i-2}, x_{i-1}, x_i\}$, $\mathcal{S}_1 = \{x_{i-1}, x_i, x_{i+1}\}$ and $\mathcal{S}_2 = \{x_i, x_{i+1}, x_{i+2}\}$. These are the same stencils used by fifth-order WENO schemes for the polynomial approximations \hat{f} and \hat{f}^k , $k = 0, \dots, r-1$ (cf. Section 2.1). Direct evaluation of Eq. (3.2) gives

$$\begin{aligned} \beta_0 &= \frac{1}{4} (f_{i-2} - 4f_{i-1} + 3f_i)^2 + \frac{13}{12} (f_{i-2} - 2f_{i-1} + f_i)^2, \\ \beta_1 &= \frac{1}{4} (-f_{i-1} + f_{i+1})^2 + \frac{13}{12} (f_{i-1} - 2f_i + f_{i+1})^2, \\ \beta_2 &= \frac{1}{4} (-3f_i + 4f_{i+1} - f_{i+2})^2 + \frac{13}{12} (f_i - 2f_{i+1} + f_{i+2})^2. \end{aligned}$$

When $h(x)$ is smooth, Taylor series expansion shows that all of the above β_k satisfy

$$\beta_k = (f'_i \Delta x + O(\Delta x^3))^2 + \frac{13}{12} (f''_i \Delta x^2 + O(\Delta x^3))^2, \quad k = 0, 1, 2,$$

and therefore $\beta_k = O(\Delta x^2)$. On the other hand, suppose \mathcal{S}_D (fixed at x_i) contains a discontinuity of $h(x)$ at x_i . Then, the total variation of $\hat{f}^D(x)$ does not go to zero as $\Delta x \rightarrow 0$, which implies $\beta_D = \Theta(1)$. In sum, β is a smoothness indicator of order 2.

Part of the success of β_k is due to the fact that it uses distinct formulas for measuring the smoothness of each substencil, which makes it less sensitive to critical points than the forward divided differences used in the original WENO [15].

Formulas of β_k for orders up to $R = 9$ can be found in Appendix A; for higher orders, these formulas can be found in [25, 26]. In Appendix B, some general and fundamental properties of β that makes them so useful for WENO schemes are described.

3.4 The global smoothness indicator τ

The global smoothness indicator τ is used by the WENO-Z scheme for measuring the smoothness in the whole R points stencil \mathcal{S} [6, 16, 17, 18]. It consists in a combination of

R	r	τ	$\theta(\tau)_{opt}$
3	2	$ \beta_0 - \beta_1 $	3
5	3	$ \beta_0 - \beta_2 $	5
7	4	$ \beta_0 + 3\beta_1 - 3\beta_2 - \beta_3 $	7
9	5	$ \beta_0 + 2\beta_1 - 6\beta_2 + 2\beta_3 + \beta_4 $	8
11	6	$ \beta_0 + \beta_1 - 8\beta_2 + 8\beta_3 - \beta_4 - \beta_5 $	9
13	7	$ \beta_0 + 36\beta_1 + 135\beta_2 - 135\beta_4 - 36\beta_5 - \beta_6 $	11

Table 1 – The global optimal order smoothness indicator τ and its leading truncation order $\theta(\tau)_{opt}$ of the $(2r - 1)$ order WENO-Z scheme.

the local smoothness indicators β_k , $k = 0, \dots, r - 1$, in such a way that it maximizes the order of τ .

Table 1 shows the expressions of τ for orders up to $R = 13$. $\theta(\tau)_{opt}$ denotes the optimal order of τ for a given r , for smooth regions and in the absence of critical points. We can see that the optimal order of τ increases with r . In fact, for $r \geq 3$, it can be shown that $\theta(\tau)_{opt}$ satisfies

$$\theta(\tau)_{opt} = r + 1 + \left\lfloor \frac{\sqrt{8r - 7} - 1}{2} \right\rfloor.$$

This will be done in a future work.

Remark 3. In previous works [16, 18, 22], we chose to include a subscript τ_{2r-1} for letting the dependency of τ on the design order $2r - 1$ of the scheme explicit. But now we have opted to drop the subscript for clarity and consistency, mainly because d_k and μ_k have formulas which also depend on $2r - 1$ but most authors do not feel the need of adding a subscript on them for making it explicit.

4 Classical weight schemes

4.1 Classical weight formula

The classical weight formula was developed in the original WENO paper [14], and it was later revised and improved to the present form in [15]. The unnormalized weights α^C are defined as

$$\alpha_k^C \triangleq \frac{d_k}{(\mu_k + \varepsilon)^p}, \quad k = 0, \dots, r-1. \quad (4.1)$$

Here, d_k are the ideal weights (Section 2.2); μ_k is a smoothness measurement (Chapter 3); ε is the *sensitivity parameter*, originally a small positive constant introduced in the formula to avoid a division by zero (since we could have $\mu_k = 0$); and p is the *power parameter*. The classical weights ω^C are simply a normalization of α^C ,

$$\omega_k^C \triangleq \frac{\alpha_k^C}{\sum_{j=0}^{r-1} \alpha_j^C}, \quad k = 0, \dots, r-1, \quad (4.2)$$

so that $\sum_{j=0}^{r-1} \omega_j^C = 1$. The superscript “C” stand for “classical”¹, and for simplicity it will be dropped when there is not a risk of ambiguity.

4.1.1 ENO property

Let us see how the weights (4.2) satisfy the ENO property (Condition 2). Suppose that \mathcal{S}_C is continuous and \mathcal{S}_D is not. Hence, by Definition 5, $\mu_C = O(\Delta x^q)$ for some positive q and $\mu_D = \Theta(1)$. So, we have

$$\frac{\alpha_D^C}{\alpha_C^C} = \frac{d_D (\mu_C + \varepsilon)^p}{d_C (\mu_D + \varepsilon)^p} = \Theta(1) \frac{(O(\Delta x^q) + \varepsilon)^p}{(\Theta(1))^p} = O(\Delta x^{pq}) + \Theta(\varepsilon^p), \quad (4.3)$$

and the ENO property follows from Proposition 3. Moreover,

$$\omega_D^C = O(\Delta x^{pq}) + \Theta(\varepsilon^p). \quad (4.4)$$

Remark 4. The role of parameters ε and p are evident from Eq. 4.4: if, and only if, ε is small enough, we have $\omega_D^C \sim O(\Delta x^{pq})$ and the ENO property holds. Likewise, a big ε dominates the denominator of 4.1, interfering with μ ’s sensitivity to discontinuities — hence the name “sensitivity parameter”. Also, from 4.4 is clear that the power parameter p has the effect of amplifying the ENO property; that is, the bigger the p , the smaller the weight of a discontinuous substencil.

¹ The superscript “JS” (for “Jiang–Shu”) is more common in the literature [19, 16]. Although the contributions of Guang-Shan Jiang and Chi-Wang Shu [15] to the development of the classical WENO scheme were crucial to its success, the pioneering work of Xu-Dong Liu, Stanley Osher and Tony Chan [14] is equally important. The superscript “C” will be used to honor all 5 authors.

4.1.2 Operation count

The cost of the unnormalized weights per substencil is

$$\text{flops}(\alpha_k^c) = \{1\pm, 0\times, 1\div\} + \text{flops}(\mu_k) + \text{flops}(\text{pow}(p)),$$

and the total cost per stencil is

$$\text{flops}(\alpha^c) = \{r\pm, 0\times, r\div\} + r \text{flops}(\mu_k) + r \text{flops}(\text{pow}(p)).$$

Therefore, the total cost of the normalized weights is

$$\text{flops}(\omega^c) = \text{flops}(\alpha^c) + \{(r-1)\pm, 0\times, r\div\}.$$

4.2 The original WENO scheme

The original WENO scheme was developed by Liu, Osher and Chan in [14]. It uses the classical weights (4.1) coupled with the divided differences smoothness indicators (3.1), and a different $\Theta(1)$ term, C_k , instead of the ideal weights d_k . The use of C_k doesn't change the result of Eq. (4.3) about the ENO property. But it does change the formal order of accuracy: the original weights were designed for improving the ENO accuracy order from r to $r+1$ only. For this reason, the original WENO is deprecated in favor of the classical WENO scheme of Jiang and Shu, but it was nevertheless an important work for its brilliant and pioneering ideas.

4.3 The classical WENO scheme (WENO-C)

The improved WENO scheme proposed by Jiang and Shu [15] was so successful that, for years, it has become a synonymous with WENO. It is by far the most popular WENO scheme, in terms of citations². For this reason, in this work it shall be called the *classical WENO scheme*, or WENO-C.

The scheme uses the classical formula (4.1) coupled with the smoothness indicator β (Section 3.3), which was another innovation proposed by the authors. The final formula reads

$$\alpha_k^c \triangleq \frac{d_k}{(\beta_k + \varepsilon)^p}, \quad \omega_k^c \triangleq \frac{\alpha_k^c}{\sum_{j=0}^{r-1} \alpha_j^c}, \quad k = 0, \dots, r-1. \quad (4.5)$$

The classical WENO was later extended to orders higher than 5 in [25] and to even higher orders in [26].

WENO-C is a milestone in the history of the WENO schemes, but, as we shall see in the next sections, it is too dissipative when compared with the newer, more improved WENO schemes.

² 2533 as of April 2014, according to Google Scholar.

4.4 The mapped WENO scheme (WENO-M)

The smoothness measurement β improved the accuracy of the WENO scheme near critical points when compared to the original forward differences, but the classical WENO scheme still lost accuracy near critical points. Andrew Henrick, Tariq Aslam and Joseph Powers studied this issue in [19] and, as a solution, they proposed a mapping function g_k ,

$$g_k(\omega) \triangleq \frac{(d_k + d_k^2 - 3d_k\omega + \omega^2)\omega}{d_k^2 - 2d_k\omega + \omega}, \quad \omega \in [0, 1], \quad (4.6)$$

which has the following properties:

$$\begin{cases} g_k(\omega_k) = d_k + O(\Delta x^3) & \text{if } \omega_k = d_k + O(\Delta x), \\ g_k(0) = 0, \quad g_k(1) = 1, \\ g_k \text{ is monotonically increasing in } [0, 1]. \end{cases}$$

Applying it to the classical weights (4.5), a new set of weights ω^M is obtained,

$$\alpha_k^M \triangleq g_k(\omega_k^C), \quad \omega_k^M \triangleq \frac{\alpha_k^M}{\sum_{j=0}^{r-1} \alpha_j^M}, \quad k = 0, \dots, r-1. \quad (4.7)$$

The mapping (4.6) does not improve the accuracy of the classical WENO scheme in the rare case where several derivatives of f vanish at the same point, meaning f is very flat near the critical point. However, the mapped WENO is less dissipative than the classical WENO (see Section 5.3). We wished to give an analytical prove of this fact via discontinuous/continuous ratio, but due to time constraints we will have to leave this to a future work. Nevertheless, numerical results show the discontinuous/continuous ratio of the mapped weights (4.7) is larger than the classical weights' (this was studied in detail in [18, Section 5]).

4.4.1 Operation count

The operation count for the unnormalized mapped weights for the whole stencil can be optimized to

$$\text{flops}(\alpha^M) = \text{flops}(\omega^C) + \{7r\pm, 4r\times, r\div\}$$

which gives

$$\begin{aligned} \text{flops}(\omega^M) &= \text{flops}(\alpha^M) + \{(r-1)\pm, 0\times, r\div\} \\ &= \text{flops}(\omega^C) + \{(8r-1)\pm, 4r\times, 2r\div\}, \end{aligned}$$

a substantial cost increase.

5 Zico weight schemes

5.1 Zico weight formula

In [6, 16], we helped develop a new weight formula. Its name, “Zico”¹, is a homage to Bruno’s then newborn son, which has the same name of the great Brazilian footballer.

The Zico unnormalized weights α^z are given by

$$\alpha_k^z \triangleq d_k \left[1 + \left(\frac{\nu}{\mu_k + \varepsilon} \right)^p \right], \quad k = 0, \dots, r-1, \quad (5.1)$$

and the Zico weights ω^z , like the classical ones (Eq. (4.2)), are just a normalization of α^z ,

$$\omega_k^z \triangleq \frac{\alpha_k^z}{\sum_{j=0}^{r-1} \alpha_j^z}, \quad k = 0, \dots, r-1.$$

The superscripts “Z” stand for “Zico” and they will also be dropped when they can be inferred from the context. The parameters ε and p , the ideal weights d_k (Section 2.2) and the smoothness indicator μ_k , are completely analogous to the ones from the classical weight formula (4.1). The novelty in formula (5.1) is the inclusion of the *global smoothness indicator* ν , a smoothness indicator (Definition 5) which measures the smoothness of the whole stencil \mathcal{S} . It has the same value on all substencils $k = 0, \dots, r-1$.

Initially [16, Eq. 27], we have seen formula (5.1) as a simple modification to the classical formula (4.1) through the artifact of a new “smoothness indicator” M , given by

$$M_k = \frac{(\mu_k + \varepsilon)^p}{(\mu_k + \varepsilon)^p + \nu^p}, \quad (5.2)$$

so that

$$\alpha_k^z = \frac{d_k}{M_k} = d_k \left[\frac{(\mu_k + \varepsilon)^p + \nu^p}{(\mu_k + \varepsilon)^p} \right] = d_k \left[1 + \left(\frac{\nu}{\mu_k + \varepsilon} \right)^p \right]. \quad (5.3)$$

The formula $\alpha_k = d_k/M_k$ seem analogous to Eq. (4.1), at least for the $p = 1$ case. This view has influenced some recent works on new WENO schemes [33, 34]. Nevertheless, now we would like to argue against the practice of classifying Eqs. (4.1) and (5.1) as a single formula based on relations (5.2) and (5.3) above, for two reasons:

- M_k is not a smoothness indicator in the sense of Definition 5, so the analogy between Eqs. (4.1) and (5.3) is false. In fact, $M_k = \Theta(1)$ regardless of the smoothness of the measured function, so one cannot say anything about the smoothness of a function f by the value of M_k . As a matter of fact, calling M_k a smoothness indicator is a misnomer.

¹ IPA: [ˈziku]

- The WENO schemes which use the Zico weights have distinct accuracy and dissipative properties than the ones which use the classical weights. They are so distinct that it is more useful and precise to treat Eqs. (4.1) and (5.1) as different weight formulas.

5.1.1 ENO property

To verify that the Zico weights satisfy the ENO property, suppose that \mathcal{S}_C is continuous and \mathcal{S}_D is not. Again, by Definition 5, $\mu_C = O(\Delta x^q)$ for some positive q , $\mu_D = \Theta(1)$ and also $\nu = \Theta(1)$ (since \mathcal{S} contains the discontinuity in \mathcal{S}_D). Therefore,

$$\begin{aligned} \frac{\alpha_D^Z}{\alpha_C^Z} &= \frac{d_D}{d_C} \frac{\left(\frac{\mu_C + \varepsilon}{\nu}\right)^p + \left(\frac{\mu_C + \varepsilon}{\mu_D + \varepsilon}\right)^p}{1 + \left(\frac{\mu_C + \varepsilon}{\nu}\right)^p} = \Theta(1) \frac{\left(\frac{O(\Delta x^q) + \varepsilon}{\Theta(1)}\right)^p + \left(\frac{O(\Delta x^q) + \varepsilon}{\Theta(1)}\right)^p}{1 + \left(\frac{O(\Delta x^q) + \varepsilon}{\Theta(1)}\right)^p} \\ &= O(\Delta x^{pq}) + \Theta(\varepsilon^p), \end{aligned} \quad (5.4)$$

and we have the same asymptotic result as the classical formula (Eq. (4.4)). Remark 4 about ε and p also holds here.

5.1.2 Discontinuous/continuous ratio

We have seen from Eqs. (4.3) and (5.4) that the discontinuous/continuous ratio of both the classical and Zico formulas have exactly the same asymptotic behavior. But this does not mean the ratios are equal: recalling that $\mu_C = O(\Delta x^q) < \mu_D = \Theta(1)$ as $\Delta x \rightarrow 0$, we have

$$\frac{\alpha_D^Z}{\alpha_C^Z} = \frac{d_D}{d_C} \frac{(\mu_C + \varepsilon)^p (\mu_D + \varepsilon)^p + \nu^p}{(\mu_D + \varepsilon)^p (\mu_C + \varepsilon)^p + \nu^p} > \frac{d_D}{d_C} \frac{(\mu_C + \varepsilon)^p}{(\mu_D + \varepsilon)^p} = \frac{\alpha_D^C}{\alpha_C^C}.$$

Therefore, the discontinuous/continuous ratio is larger for the Zico formula than for the classical one when the same parameters ε , p and smoothness indicator μ_C are used. This means the Zico formula assigns larger weights to discontinuous substencils than the classical formula does. But the fact is the classical formula is too much dissipative to begin with, and it leaves a lot of room for increasing the weights of discontinuous substencils while remaining essentially non-oscillatory. Numerical results has shown that schemes based on Zico weights are as robust and non-oscillatory as ones based on classical weights, but remarkably less dissipative [18, 22].

5.1.3 Operation count

The cost of the unnormalized weights per substencil is

$$\text{flops } \alpha_k^Z = \{2\pm, 1\times, 1\div\} + \text{flops}(\mu_k) + \text{flops}(\nu) + \text{flops}(\text{pow}(p)),$$

and the total cost per stencil is

$$\begin{aligned} \text{flops}(\alpha^Z) &= \{2r\pm, r\times, r\div\} + r \text{ flops}(\mu_k) + \text{flops}(\nu) + r \text{ flops}(\text{pow}(p)) \\ &= \text{flops}(\alpha^C) + \{r\pm, r\times, 0\div\} + \text{flops}(\nu). \end{aligned}$$

This gives

$$\begin{aligned} \text{flops}(\omega^Z) &= \text{flops}(\alpha^Z) + \{(r-1)\pm, 0\times, r\div\} \\ &= \text{flops}(\alpha^C) + \{(2r-1)\pm, r\times, r\div\} + \text{flops}(\nu) \\ &= \text{flops}(\omega^C) + \{r\pm, r\times, 0\div\} + \text{flops}(\nu), \end{aligned}$$

which is just a slight increase to the total cost of the normalized classical weights.

5.2 The Zico WENO scheme (WENO-Z)

The Zico WENO scheme was first described in [6, 16] and later expanded in [17, 18]. It uses the Zico weights (5.1) coupled with the smoothness indicators β_k of Jiang–Shu (Section 3.3) and a combination of β as the global smoothness indicator τ (Section 3.4). The WENO-Z weights read

$$\alpha_k^Z \triangleq d_k \left[1 + \left(\frac{\tau}{\beta_k + \varepsilon} \right)^p \right], \quad \omega_k^Z \triangleq \frac{\alpha_k^Z}{\sum_{j=0}^{r-1} \alpha_j^Z}, \quad k = 0, \dots, r-1. \quad (5.5)$$

The WENO-Z scheme has better accuracy and dissipative properties than WENO-C, thanks to the Zico formula (5.1). It is able to recover the optimal order of accuracy at the same critical points that WENO-M does, but at a much smaller computational cost (see [16, 18], and Sections 4.4.1 and 5.1.3). The numerical results show that WENO-Z and WENO-M have comparable resolution power, while both are clearly less dissipative than WENO-C, when the same parameters are employed (see the next section).

5.3 A comparison between classical and Zico weight schemes

In this section, we give a brief comparison between the aforementioned WENO-C, WENO-M, and WENO-Z schemes.

Computational cost. WENO-C is the cheapest scheme (Section 4.1.2). The normalized WENO-Z weights needs r sums and r multiplications more (Section 5.1.3), plus the cost of the computation of the global smoothness indicator τ , which is not more than $(r-1)$ sums and an absolute value operation (Section 3.4). The more computationally expensive scheme is WENO-M, which has $8r-1$ sums, $4r$ products, and $2r$ divisions more than WENO-C (Section 4.4.1). Recently, an independent study concluded, for fifth order, that WENO-Z and WENO-M spend $\sim 8\%$ and $\sim 20\%$ more wall time than WENO-C, respectively [29].

Accuracy. For fifth order, when $\varepsilon = 10^{-40}$ and $p = 2$ are used, WENO-C loses accuracy at simple critical points (i.e., of order 1), while WENO-C and WENO-Z do not. Still, at critical points of order 2, all three schemes lose accuracy [19, 16].

However, choosing a suitable ε corrects the accuracy of WENO-C and WENO-Z, making the mapping procedure redundant. For WENO-C of any order and p , it is necessary that $\varepsilon = \Omega(\Delta x^2)$ (i.e., $\varepsilon = \Delta x^q$, with $q \leq 2$) [21]. The downside is that $\varepsilon = \Omega(\Delta x^2)$ is too large, which makes WENO-C prone to oscillations [22]. For WENO-Z, a similar condition, $\varepsilon = \Omega(\Delta x^{q(R,p)})$, is required; the difference is that the maximum allowed power $q(R,p)$ grows with both the order R and power parameter p [22]. As an illustration, for fifth order, with $p = 2$, the condition is $\varepsilon = \Omega(\Delta x^4)$. This allows for much smaller ε than WENO-C does, therefore avoiding oscillations.

Discontinuous/continuous ratio. The discontinuous/continuous ratio of WENO-Z is strictly greater than that of WENO-C (Section 5.1.2). Numerically, it was indicated in [18] that WENO-M has a greater discontinuous/continuous ratio than WENO-Z, which indeed has a greater ratio than WENO-C. We don't have an analytical proof of this yet.

Sharpness. For fifth-order, near shocks and general features of the solution, WENO-M is the sharper scheme, followed by WENO-Z, with WENO-C being more dissipative than the other two. However, for shock-entropy tests, WENO-Z gives sharper results in the high-frequency waves region, followed by WENO-M and WENO-C. Figures 13 and 14 exemplify this general trend. More numerical results can be found in [18, 29].

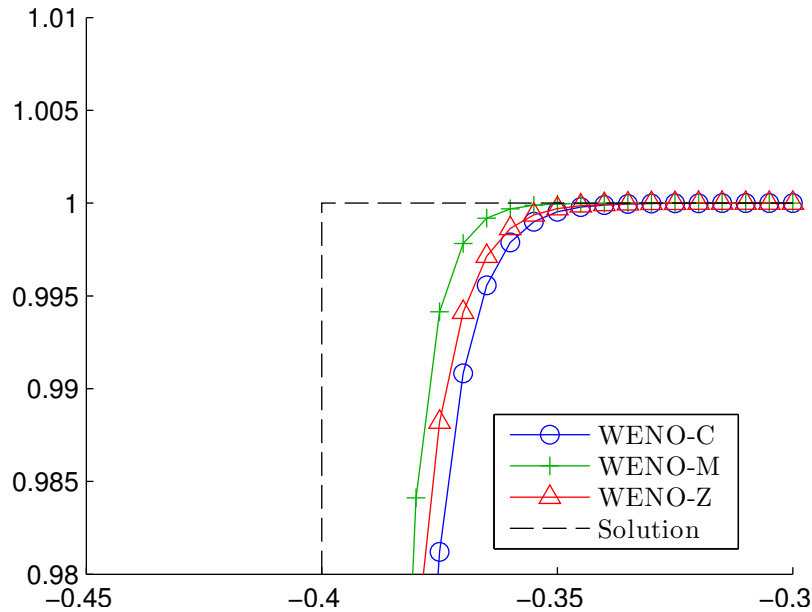
Stability. For fifth-order, with $p = 2$, all three schemes are fairly stable in practice. With $p = 1$, WENO-M is sometimes unstable (e.g., in the interacting blast waves test).

In sum, WENO-Z is the most cost-effective scheme among the three in terms of sharpness [29], and it also has better accuracy properties than WENO-C. The high cost of WENO-M, and the high dissipativity of WENO-C, makes them less attractive option nowadays.

5.4 Other schemes

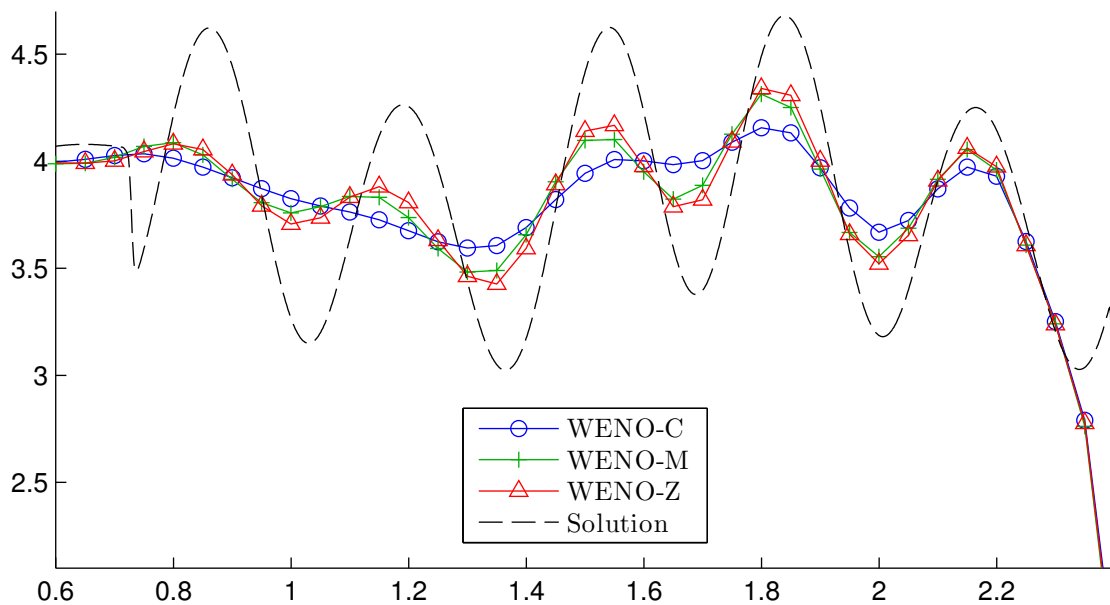
Other WENO schemes which are based in the Zico formula (5.1), albeit with different global smoothness indicators than WENO-Z's τ (Eq. (5.5)), can be found in the literature, such as: the ESWENO (energy stable WENO) [20, 35], the WENO-NS [34], the mapped WENO-Z [29], and many others. They generally achieve sharper results — and are costlier — than WENO-Z. Our wish was to study them and compare their results with WENO-Z and the new scheme we implemented, but, unfortunately, this was not possible due to time constraints.

Figure 13 – Numerical solution of the Gaussian-square-triangle-ellipse linear test by the WENO-C, WENO-M, and WENO-Z schemes



The figure shows a zoom in the square wave of the solution at $t = 2$. $N = 200$ points were used. CFL = 0.5.

Figure 14 – Numerical solution of the shock-entropy problem of Shu–Osher by the WENO-C, WENO-M, and WENO-Z schemes



The figure show a zoom in the region of high-frequency waves of the density of the solutions at $t = 1.8$. A grid with $N = 200$ points was used. CFL = 0.5.

Part II

A new WENO scheme

6 Towards a new WENO scheme

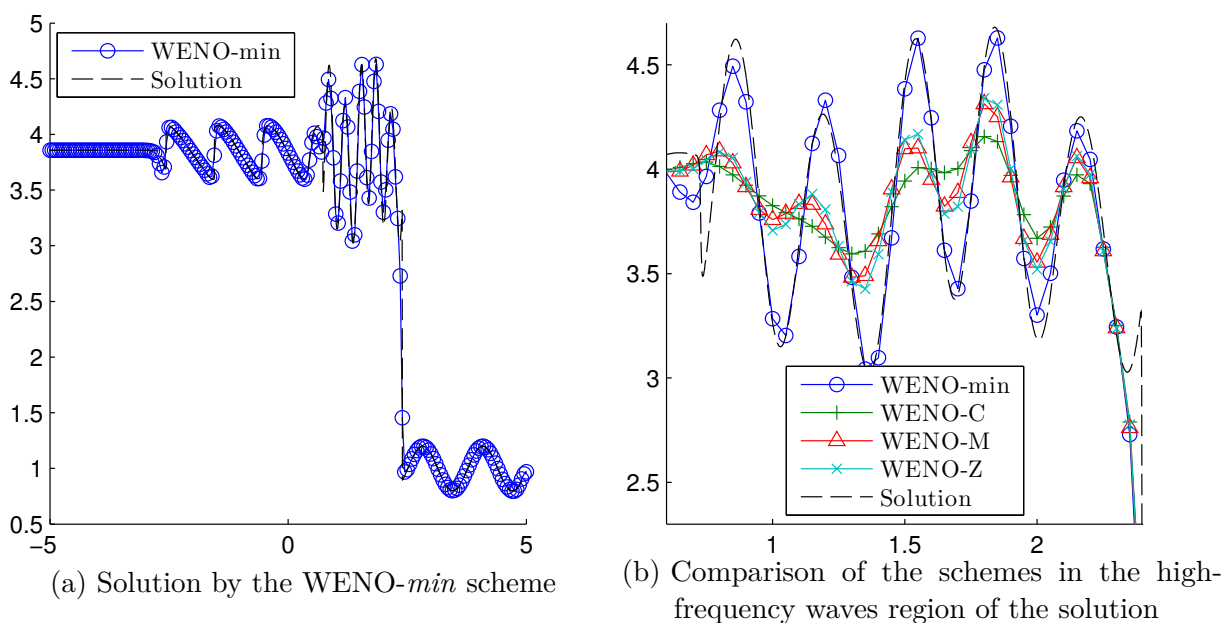
Besides the Zico weights, an experimental weight formula was also introduced in [6]: the *min* weights. They were defined as

$$\alpha_k^{min} \triangleq d_k \left[1 + \left(\frac{\max(\mu_k, \nu)}{\min(\mu_k, \nu) + \varepsilon} \right)^p \right], \quad \omega_k^{min} \triangleq \frac{\alpha_k^{min}}{\sum_{j=0}^{r-1} \alpha_j^{min}}, \quad k = 0, \dots, r-1.$$

This is similar to the Zico formula (5.1), but instead of having ν in the numerator and μ_k in the denominator, it has $\max(\mu_k, \nu)$ and $\min(\mu_k, \nu)$, respectively (hence the name “*min*”). This change made WENO-*min* scheme much less dissipative than the then-current WENO schemes (WENO-C, WENO-M and WENO-Z). The results of the shock-entropy test were particularly encouraging, as shown in Fig. 15. The grid with 200 points is not enough for the other schemes to resolve the high-frequency waves of the solution, but WENO-*min* already resolves them.

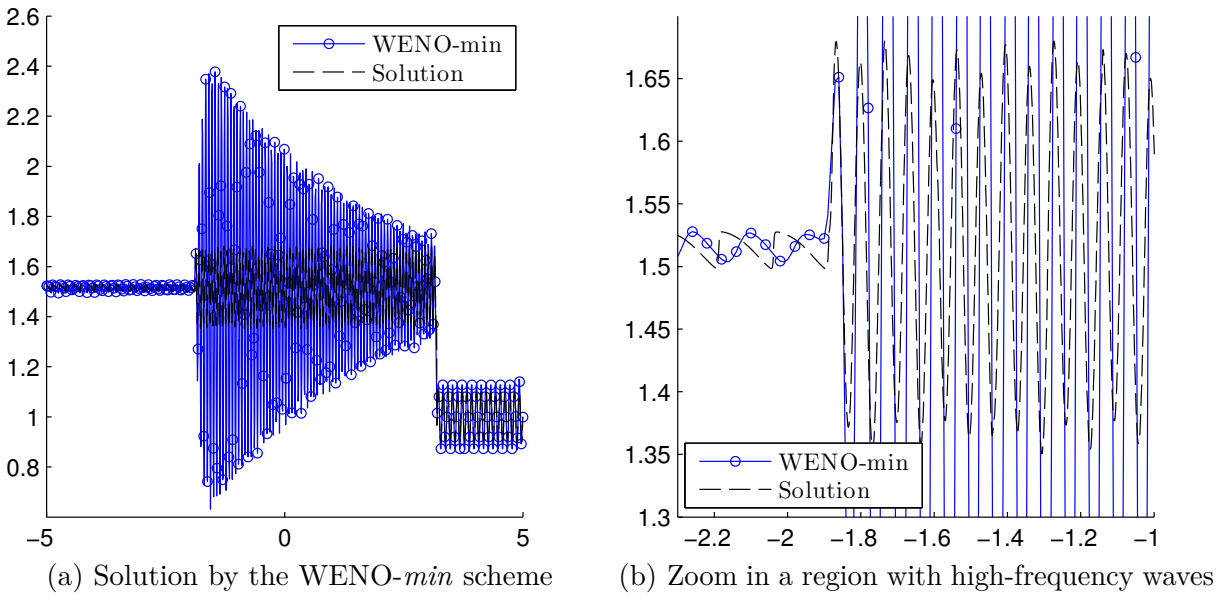
However, while the WENO-Z scheme was eventually published later [16], two issues prevented WENO-*min* to enjoy the same fate. First, at the time we already knew it was unstable and had an oscillatory tendency. The impressive results for the Shu–Osher shock-entropy problem seemed too good to be true, and in fact they were: the Titarev–Toro shock-entropy test, which has higher frequency waves in the solution and a longer final

Figure 15 – Numerical solution of the shock-entropy problem of Shu–Osher by the WENO-*min*, WENO-C, WENO-M and WENO-Z schemes



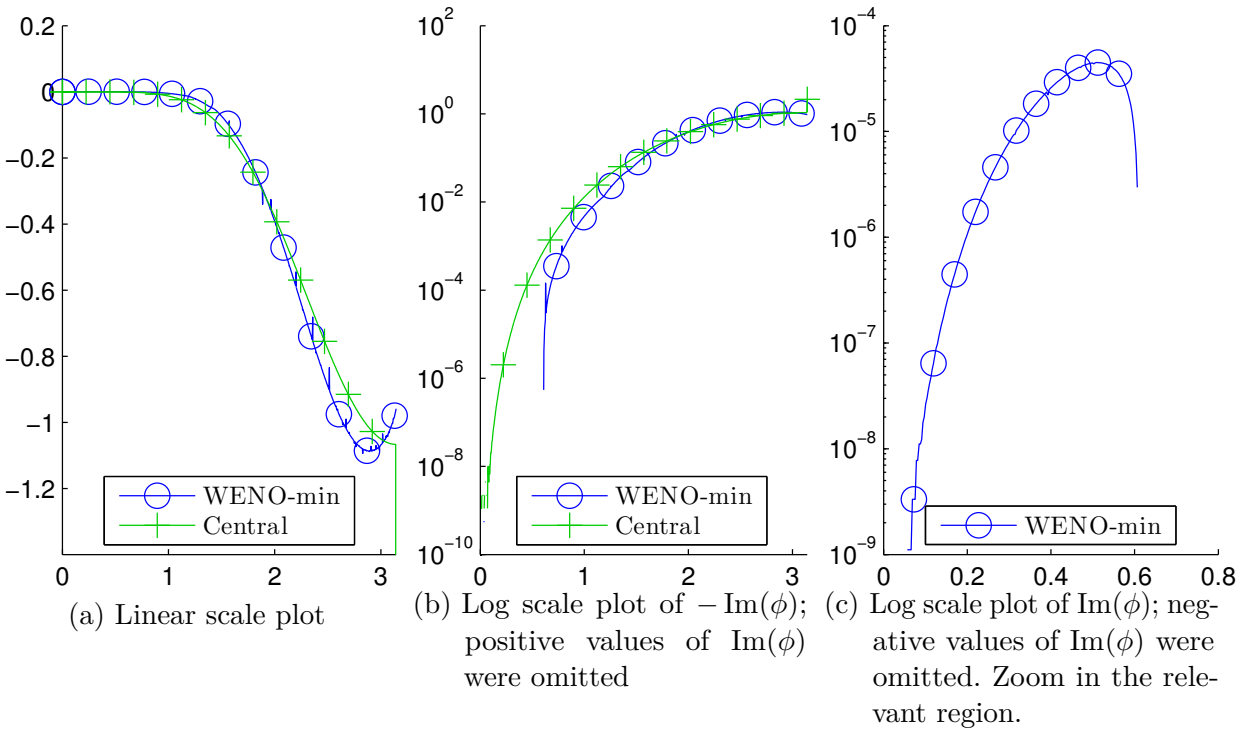
The figures show the density of the solution at $t = 1.8$. A grid with $N = 200$ points was used. $CFL = 0.5$.

Figure 16 – Numerical solution of the shock-entropy problem of Titarev–Toro by the WENO-*min* scheme with a small grid



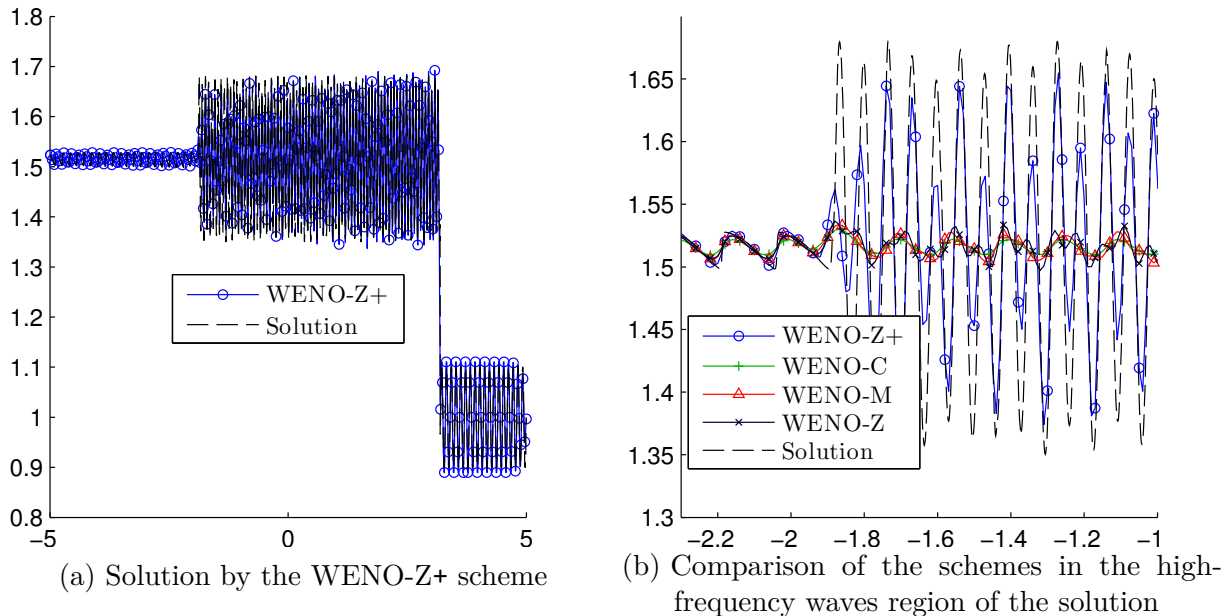
The figures show the density of the solution at $t = 5$. A grid with $N = 1000$ points was used. $CFL = 0.5$.

Figure 17 – ADR analysis of WENO-*min* scheme: imaginary part of ϕ



The higher the value of $\text{Im}(\phi)$, the less dissipative is the scheme. Positive values of $\text{Im}(\phi)$ indicates instability. Here, 2000 wavenumbers were used.

Figure 18 – Numerical solution of the shock-entropy problem of Titarev–Toro by the WENO-Z+, WENO-C, WENO-M and WENO-Z schemes with a small grid



The figures show the density of the solution at $t = 5$. A grid with $N = 1000$ points was used. CFL = 0.5.

time, showed that the WENO-*min* solution greatly overshooted the expected solution (Fig. 16). Similarly, the ADR analysis evidenced that WENO-*min* was unstable. Notice, in Fig. 17c, that WENO-*min* has a large range of wavenumbers for which $\text{Im}(\phi)$ is positive, that extends from 0 to approximately $\pi/5$. This means that WENO-*min* makes these waves actually grow, which could lead to instability. The solution of WENO-*min* for the Titarev–Toro problem grows very slowly with time, but only because it is a relatively mild test. For the interacting blast waves problem, which involves strong shocks and is computationally harder to solve, the numerical solution by the WENO-*min* scheme actually blows up with $N = 800$.

The second issue is that, at the time WENO-*min* was developed, we wasn't able to explain why did it have such impressive results for the Shu–Osher test. We already knew that replacing ν and μ_k by $\max(\mu_k, \nu)$ and $\min(\mu_k, \nu)$ made the discontinuous/continuous rate increase, and therefore the WENO-*min* was less dissipative than WENO-Z — but this alone wasn't enough to explain the shock-entropy results.

The motivation behind this part of the thesis was to find a way of achieving the impressive results of WENO-*min* in a stable and essentially non-oscillatory manner. At first, two existing techniques were employed in the attempt to stabilize WENO-*min*: the monotonicity-preserving limiters of Suresh and Huynh [36, 25], and the energy stable artificial dissipation operator of Yamaleev and Carpenter [20, 35], but the results were not satisfactory. Then, after these attempts, a deeper understanding of the *min* formula led to

the development of a new weight formula

$$\alpha_k^{Z+} \triangleq d_k \left[1 + \left(\frac{\nu + \varepsilon}{\mu_k + \varepsilon} \right)^p + \lambda \left(\frac{\mu_k + \varepsilon}{\nu + \varepsilon} \right)^p \right], \quad \omega_k^{Z+} \triangleq \frac{\alpha_k^{Z+}}{\sum_{j=0}^{r-1} \alpha_j^{Z+}}, \quad k = 0, \dots, r-1,$$

which we call the Zico+ weights, because it is a generalization of the Zico weights (5.1) by the means of an addition of the sharpening term $\lambda \left(\frac{\mu_k + \varepsilon}{\nu + \varepsilon} \right)^p$ to the Zico weight formula. The new scheme WENO-Z+ has remarkably better results on the shock-entropy problems than WENO-C, WENO-M and WENO-Z (Fig. 18), and it passes the ADR analysis and interacting blast waves tests for stability.

This Part is structured as follows: in Chapter 7, the WENO-*min* scheme is described. In particular, in Section 7.2.1 it is explained why it is unstable. Finally, in Chapter 8, we describe and study the WENO-Z+ scheme. Detailed numerical experiments with the new scheme are shown in Section 8.2.

7 The experimental WENO-min scheme

7.1 The *min* weight formula

The *min* weights [6] are defined as

$$\alpha_k^{min} \triangleq d_k \left[1 + \left(\frac{\max(\mu_k, \nu)}{\min(\mu_k, \nu) + \varepsilon} \right)^p \right] = d_k \left[\frac{(\min(\mu_k, \nu) + \varepsilon)^p + \max(\mu_k, \nu)^p}{(\min(\mu_k, \nu) + \varepsilon)^p} \right], \quad (7.1)$$

$$\omega_k^{min} \triangleq \frac{\alpha_k^{min}}{\sum_{j=0}^{r-1} \alpha_j^{min}}, \quad k = 0, \dots, r-1.$$

For $p = 1$ (which is typically the case), Eq. (7.1) simplifies to

$$\alpha_k^{min} = d_k \left[\frac{\mu_k + \nu + \varepsilon}{\min(\mu_k, \nu) + \varepsilon} \right], \quad (7.2)$$

and the name of the scheme comes from the min operator in the denominator of Eq. (7.2).

Eq. (7.1) can also be written in a conditional form

$$\alpha_k^{min} = \begin{cases} d_k \left[1 + \left(\frac{\nu}{\mu_k + \varepsilon} \right)^p \right] \equiv \alpha_k^Z, & \text{if } \mu_k \leq \nu, \\ d_k \left[1 + \left(\frac{\mu_k}{\nu + \varepsilon} \right)^p \right], & \text{if } \mu_k > \nu. \end{cases} \quad (7.3)$$

This form is more convenient for operation counting, and also for understanding how the WENO-*min* scheme works. This is discussed in Section 7.2. First, let us show some basic properties of the *min* formula.

7.1.1 ENO property

To show that the *min* weights satisfy the ENO property (Condition 2), assume S_C is a continuous substencil and S_D is a discontinuous one. Therefore, as $\Delta x \rightarrow 0$, $\min(\mu_C, \nu) = \mu_C = O(\Delta x^q)$ for some $q > 0$, and $\max(\mu_C, \nu) = \nu = \Theta(1)$. Also, because both $\mu_D = \Theta(1)$ and $\nu = \Theta(1)$, we have $\min(\mu_D, \nu) = \Theta(1)$ and $\max(\mu_D, \nu) = \Theta(1)$. So,

$$\begin{aligned} \frac{\alpha_D}{\alpha_C} &= \frac{d_D}{d_C} \frac{\left(\frac{\min(\mu_C, \nu) + \varepsilon}{\max(\mu_C, \nu)} \right)^p + \left(\frac{\min(\mu_C, \nu) + \varepsilon}{\min(\mu_D, \nu) + \varepsilon} \right)^p \left(\frac{\max(\mu_D, \nu)}{\max(\mu_C, \nu)} \right)^p}{1 + \left(\frac{\min(\mu_C, \nu) + \varepsilon}{\max(\mu_C, \nu)} \right)^p} \\ &= \Theta(1) \frac{\left(\frac{O(\Delta x^q) + \varepsilon}{\Theta(1)} \right)^p + \left(\frac{O(\Delta x^q) + \varepsilon}{\Theta(1)} \right)^p \left(\frac{\Theta(1)}{\Theta(1)} \right)^p}{1 + \left(\frac{O(\Delta x^q) + \varepsilon}{\Theta(1)} \right)^p} \\ &= O(\Delta x^{pq}) + \Theta(\varepsilon^p), \end{aligned}$$

Again, the *min* formula has the same asymptotic behavior as the classical (4.3) and Zico (5.4) formulas and Remark 4 applies.

7.1.2 Discontinuous/continuous ratio

The weight ω_D^{min} of the discontinuous substencil \mathcal{S}_D is greater or equal to the Zico weight ω_D^Z with same parameters ε , p and smoothness indicators μ , ν :

$$\begin{aligned} \frac{\alpha_D^{min}}{\alpha_C^{min}} &= \frac{d_D}{d_C} \frac{(\min(\mu_C, \nu) + \varepsilon)^p}{(\min(\mu_C, \nu) + \varepsilon)^p + \max(\mu_C, \nu)^p} \left[1 + \left(\frac{\max(\mu_D, \nu)}{\min(\mu_D, \nu) + \varepsilon} \right)^p \right] \\ &\geq \frac{d_D}{d_C} \frac{(\mu_C + \varepsilon)^p}{(\mu_C + \varepsilon)^p + \nu^p} \left[1 + \left(\frac{\nu}{\mu_D + \varepsilon} \right)^p \right] = \frac{\alpha_D^Z}{\alpha_C^Z}; \end{aligned}$$

the last inequality holds because $\mu_C < \nu$ as $\Delta x \rightarrow 0$, $\max(\mu_D, \nu) \geq \nu$ and $\min(\mu_D, \nu) \leq \mu_D$. This makes the *min* weights less dissipative than the Zico ones.

7.1.3 Operation count

Based on the conditional form (7.3), the operation count for each substencil is

$$\begin{aligned} \text{flops}(\alpha_k^{min}) &= \{2\pm, 1\times, 1\div\} + \text{flops}(\text{pow}(p)) + \text{flops}(\nu) + \text{flops}(\mu_k) + \text{conditional}() \\ &= \text{flops}(\alpha_k^Z) + \text{conditional}(), \end{aligned}$$

and for the whole stencil is

$$\begin{aligned} \text{flops}(\alpha^{min}) &= \{2r\pm, r\times, r\div\} + r \text{ flops}(\text{pow}(p)) + \text{flops}(\nu) + r \text{ flops}(\mu_k) + r \text{ conditional}() \\ &= \text{flops}(\alpha^Z) + r \text{ conditional}(). \end{aligned}$$

Here, `conditional()` stands for the cost of the conditional operation in Eq. (7.3). So, basically, the computational cost per stencil of the *min* weights is equal to the cost of Zico weights plus the cost of r conditional operations, which is architecture-dependent. Finally, the total cost of the normalized weights per stencil is

$$\begin{aligned} \text{flops}(\omega^{min}) &= \text{flops}(\alpha^{min}) + \{(r-1)\pm, 0\times, r\div\} \\ &= \text{flops}(\omega^Z) + r \text{ conditional}() \\ &= \text{flops}(\omega^C) + \{r\pm, r\times, 0\div\} + \text{flops}(\nu) + r \text{ conditional}(). \end{aligned}$$

7.2 The WENO-*min* scheme

The WENO-*min* scheme is the *min* formula (7.1) coupled with the smoothness indicators β_k of Jiang–Shu (Section 3.3) and the τ global smoothness indicators (Section 3.4), the

same smoothness indicators used by WENO-Z. Its formula is

$$\alpha_k^{min} = d_k \left[1 + \left(\frac{\max(\beta_k, \tau)}{\min(\beta_k, \tau) + \varepsilon} \right)^p \right], \quad \omega_k^{min} = \frac{\alpha_k^{min}}{\sum_{j=0}^{r-1} \alpha_j^{min}}, \quad k = 0, \dots, r-1. \quad (7.4)$$

The default values for the parameters are $\varepsilon = 10^{-40}$ and $p = 1$.

7.2.1 Stability analysis

We have seen in Chapter 6 that the WENO-*min* has impressive results on the Shu–Osher shock-entropy test when compared to WENO-C, WENO-M and WENO-Z (Fig. 15), but it is ultimately unstable. The analysis in this section aims for explaining why.

Consider

$$\eta_k^z \triangleq \frac{\tau}{\beta_k + \varepsilon}, \quad \eta_k^{-z} \triangleq \frac{\beta_k}{\tau + \varepsilon}. \quad (7.5)$$

η_k^z is the term which appears in the WENO-Z weight formula (cf. Eq. (5.5))

$$\alpha_k^z = d_k [1 + (\eta_k^z)^p], \quad (7.6)$$

and η_k^{-z} is its “inverse” (if we disregard ε , that is). Eq. (7.4) is more conveniently written in the conditional form

$$\alpha_k^{min} = \begin{cases} d_k [1 + (\eta_k^z)^p] \equiv \alpha_k^z, & \text{if } \beta_k \leq \tau, \\ d_k [1 + (\eta_k^{-z})^p], & \text{if } \beta_k > \tau. \end{cases} \quad (7.7)$$

If we had $\beta_k \leq \tau$ all the time, then $\alpha_k^{min} \equiv \alpha_k^z$ and the WENO-*min* would be identical to WENO-Z. Therefore, what distinguishes the *min* formula from Zico, the reason for the great shock-entropy results and also for the instability of WENO-*min*, is the term η_k^{-z} , which appears in the formula when $\beta_k > \tau$.

Let us see how the terms η_k^z and η_k^{-z} work. From Eq. (7.5), the value of η_k^z is larger in the substencils \mathcal{S}_k where the solution is smoother, while the value of η_k^{-z} is smaller in such substencils. Thus, η_k^{-z} works as the opposite of a smoothness indicator. This is the ultimate cause of instability in WENO-*min*. The following example will illustrate this.

Consider $f(x) = \sin(4\pi x)$, defined on the uniform, periodic grid

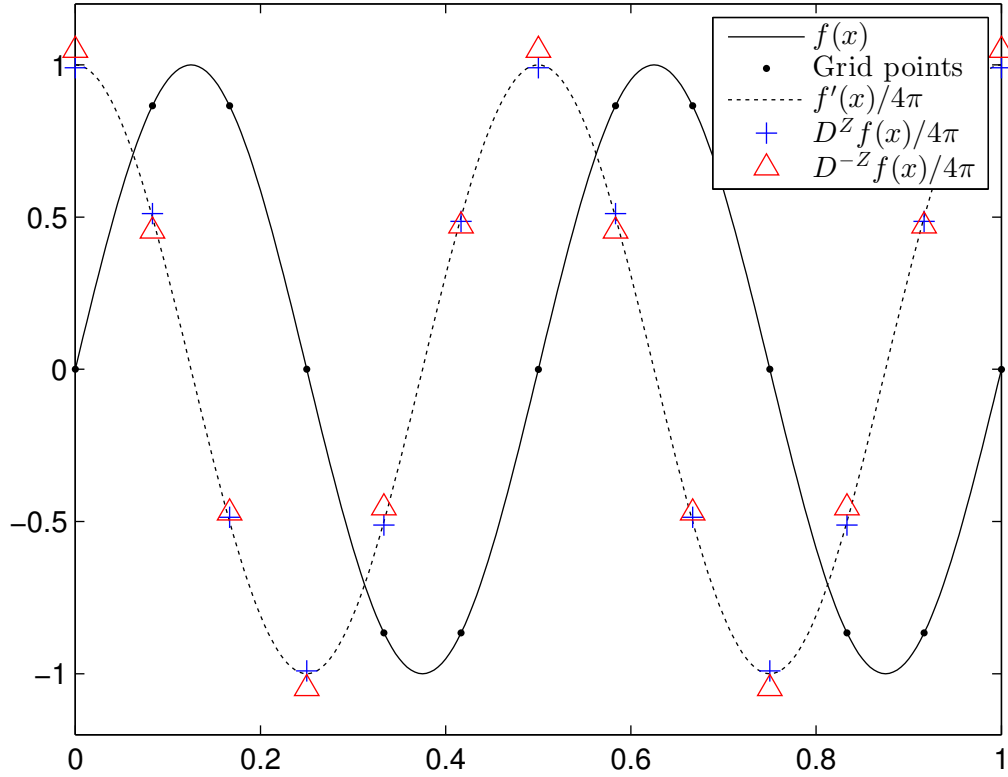
$$x_n = n\Delta x, \quad n = 0, \dots, 12, \quad (7.8)$$

and $\Delta x = 1/12$. Let us define the “anti-Zico” weights as

$$\alpha_k^{-z} = d_k [1 + (\eta_k^{-z})^p], \quad \omega_k^{-z} = \frac{\alpha_k^{-z}}{\sum_{j=0}^{r-1} \alpha_j^{-z}}, \quad k = 0, \dots, r-1. \quad (7.9)$$

These are not useful as WENO weights, since they don’t satisfy the ENO property (assume \mathcal{S}_C continuous and \mathcal{S}_D discontinuous):

$$\frac{\alpha_D^{-z}}{\alpha_C^{-z}} = \frac{d_D}{d_C} \frac{1 + \left(\frac{\beta_D}{\tau + \varepsilon} \right)^p}{1 + \left(\frac{\beta_C}{\tau + \varepsilon} \right)^p} = \Theta(1) \frac{1 + \left(\frac{\Theta(1)}{\Theta(1) + \varepsilon} \right)^p}{1 + \left(\frac{O(\Delta x^q)}{\Theta(1) + \varepsilon} \right)^p} = \Theta(1).$$

Figure 19 – Discrete approximations $D^z f$ and $D^{-z} f$ to the derivative of $f(x) = \sin(4\pi x)$ 

The exact derivative $f'(x)$ (dotted line) and the discrete approximations $D^z f(x_n)$ (blue plus symbols) and $D^{-z} f(x_n)$ (red triangles) are scaled by a factor of $1/4\pi$ for a better view. The grid points are $x_n = n\Delta x$, $n = 0, \dots, 12$, with $\Delta x = 1/12$.

They nevertheless work for continuous solutions, since they approximate the ideal weights when all substencils are continuous — a fact whose proof is given in Appendix C — and defining them will be useful for illustration purposes.

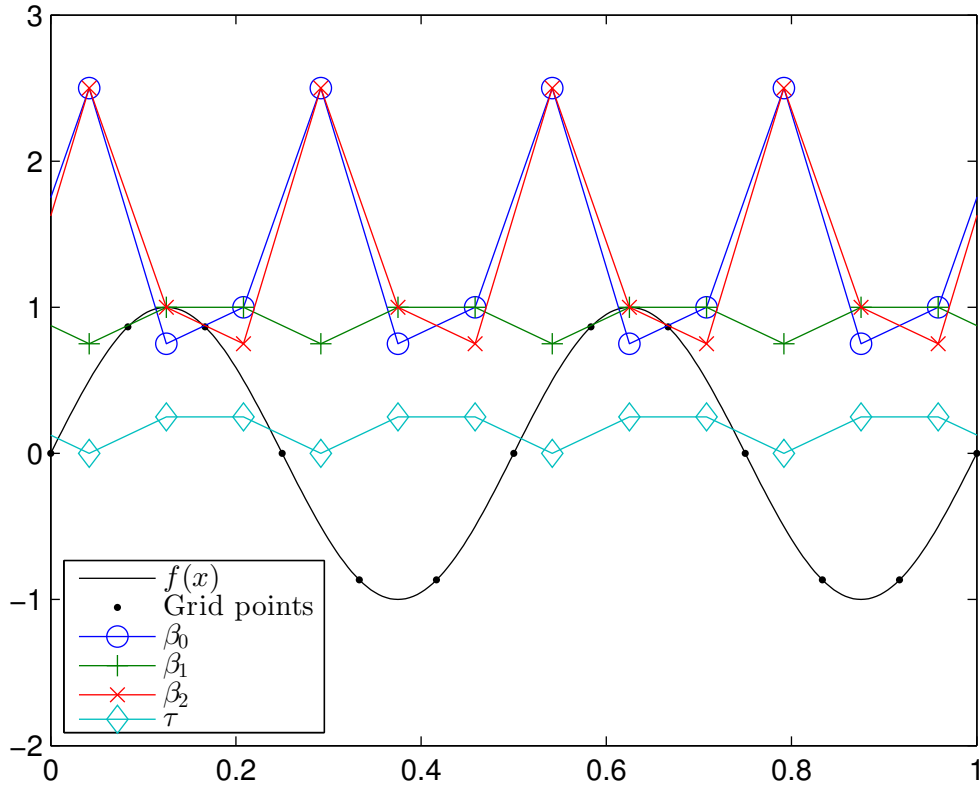
Here, we will be working with schemes of order $R = 5$, but the same conclusions are valid for any order. The fifth-order WENO-Z discrete derivative operator D_x^z is given by

$$D_x^z f(x_n) \triangleq \frac{\sum_{k=0}^2 \omega_{n+\frac{1}{2}}^{z,k} \hat{f}_{n+\frac{1}{2}}^k - \sum_{k=0}^2 \omega_{n-\frac{1}{2}}^{z,k} \hat{f}_{n-\frac{1}{2}}^k}{\Delta x} = f'(x_n) + O(\Delta x^5). \quad (7.10)$$

Similarly, the “anti-Zico” discrete derivative is defined as

$$D_x^{-z} f(x_n) \triangleq \frac{\sum_{k=0}^2 \omega_{n+\frac{1}{2}}^{-z,k} \hat{f}_{n+\frac{1}{2}}^k - \sum_{k=0}^2 \omega_{n-\frac{1}{2}}^{-z,k} \hat{f}_{n-\frac{1}{2}}^k}{\Delta x} \approx f'(x_n) \quad (7.11)$$

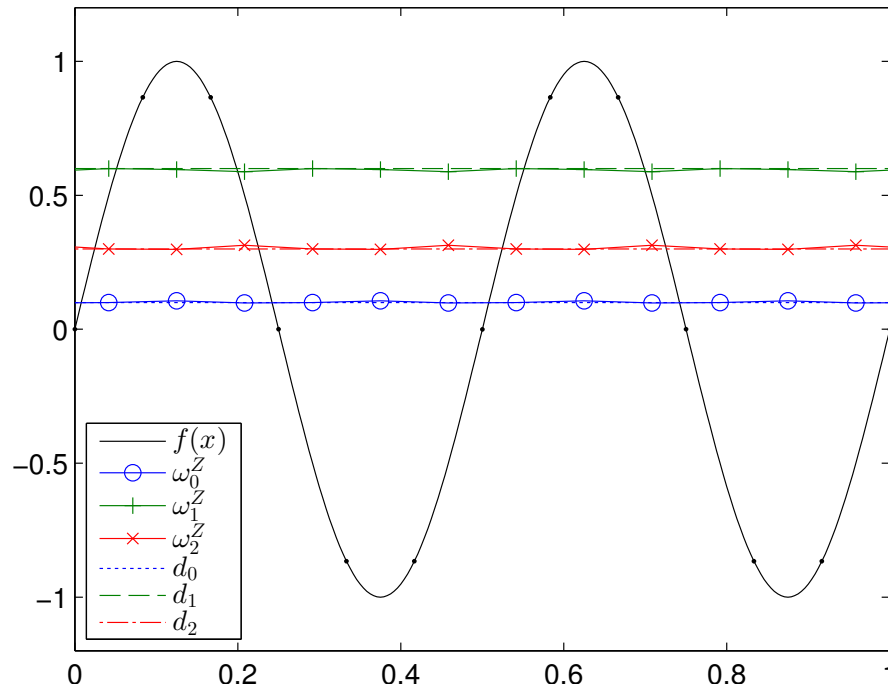
(here, we are not concerned with the order of this approximation). Figure 19 shows that $D_x^{-z} f(x_n)$ surpasses $f'(x_n) \equiv 4\pi \cos(4\pi x_n)$ at critical points of $f'(x)$ (that is, $x_n = 0, 0.25, 0.5$, etc.), while $D_x^z f(x_n)$ remains close, but under it. Since $D_x^{-z} f(x_n)$ has a greater

Figure 20 – Values of smoothness indicators β and τ for $f(x) = \sin(4\pi x)$ 

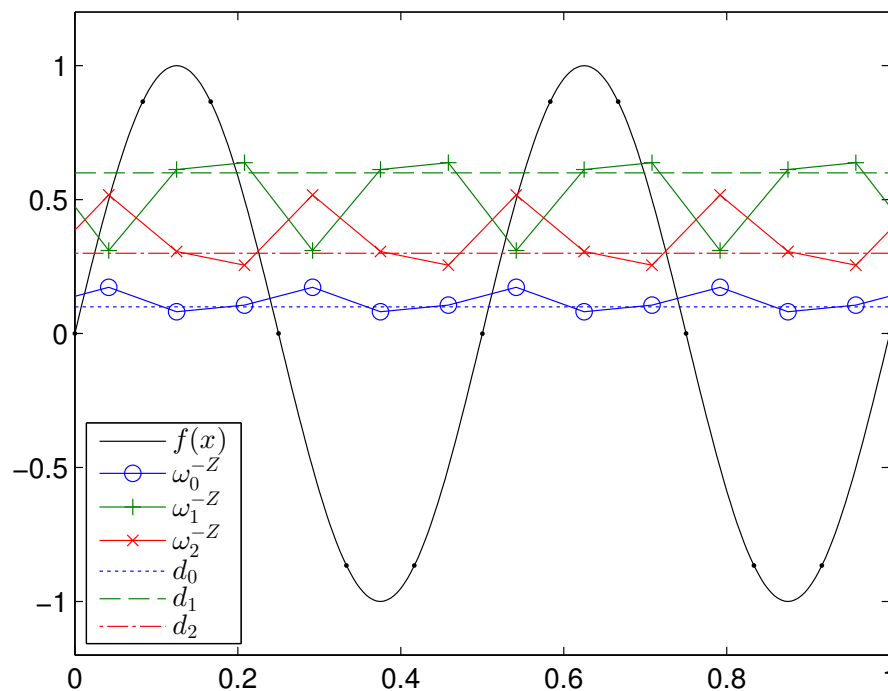
The solid black line is $f(x)$, with grid points $x_n = n\Delta x$ marked by dots, where $n = 0, \dots, 12$ and $\Delta x = 1/12$. The markers show the smoothness indicators computed at the interfaces $x_{n+\frac{1}{2}} = (n + 1/2)\Delta x$, $n = 0, \dots, 11$.

sup norm than $f'(x)$, this leads to instability when this process is iterated by a time integrator. On the other hand, $D_x^z f(x_n)$ has a slightly smaller sup norm than $f'(x)$, so this indicates that iterating $D_x^z f(x_n)$ is stable in this case (due to the nonlinear nature of D_x^z and D_x^{-z} , these are only indications, not established facts).

To understand why the approximation $D_x^{-z} f(x_i)$ overshoots $f'(x_i)$ at $x_i = 0.5$ and why $D_x^z f(x_i)$ does not, let us examine the weights ω^z and ω^{-z} . Figure 20 shows the smoothness indicators β and τ , and Figure 21 show the weights ω^z and ω^{-z} , all computed at the interfaces $x_{n+\frac{1}{2}} = (n + \frac{1}{2})\Delta x$, $n = 0, \dots, 11$. The first thing that stands out is how the WENO-Z weights remain fairly close to the ideal ones in the whole domain, while the “anti-Zico” weights oscillates away from them. In particular, at $x_{i+\frac{1}{2}}$ (≈ 0.54), the weights ω_0^{-z} and ω_2^{-z} are much greater, and ω_1^{-z} is much smaller, than their ideal counterparts. In other words, ω_1^{-z} , the central weight, transfers “mass” to the lateral weights ω_0^{-z} and ω_2^{-z} . $\hat{f}_{i+\frac{1}{2}}^0(x)$ and $\hat{f}_{i+\frac{1}{2}}^2(x)$ happen to be the two reconstruction polynomials with the highest

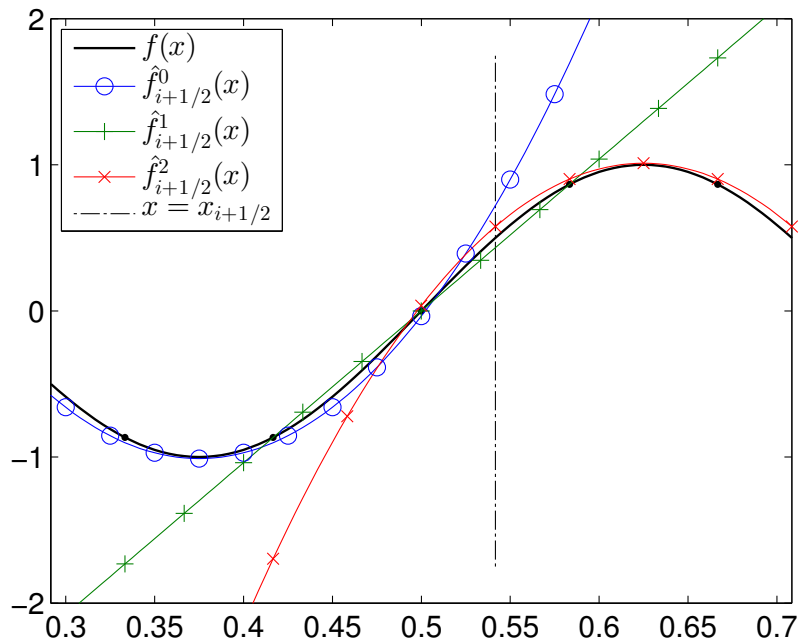
Figure 21 – WENO-Z weights ω^z and “anti-Zico” weights ω^{-z} for $f(x) = \sin(4\pi x)$ 

(a) WENO-Z weights

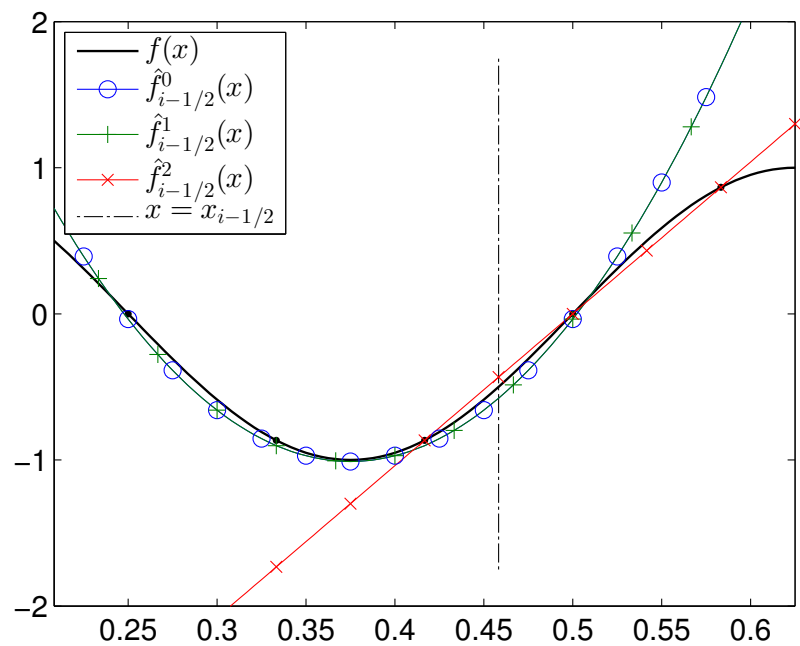


(b) “Anti-Zico” weights

The blue dotted lines, the green dashed lines, and the red dash-dotted lines correspond to the ideal weights $d_0 \equiv 0.1$, $d_1 \equiv 0.6$, and $d_2 \equiv 0.3$, resp. The blue lines with circles, the green lines with plus symbols, and the red lines with crosses correspond to the computed weights — respectively, above, they are the WENO-Z weights ω_0^z , ω_1^z , and ω_2^z , and, below, the “anti-Zico” weights ω_0^{-z} , ω_1^{-z} , and ω_2^{-z} . The markers show the weights computed at the interfaces $x_{n+\frac{1}{2}} = (n + 1/2)\Delta x$, $n = 0, \dots, 11$, with $\Delta x = 1/12$.

Figure 22 – Reconstruction polynomials $\hat{f}_{i+\frac{1}{2}}^0(x)$, $\hat{f}_{i+\frac{1}{2}}^1(x)$, and $\hat{f}_{i+\frac{1}{2}}^2(x)$ at the stencil $\mathcal{S}_{i+\frac{1}{2}}$ 

The solid black line is $f(x)$, with grid points marked by dots. The dash-dotted vertical line marks the location of $x_{i+\frac{1}{2}} \approx 0.54$.

Figure 23 – Reconstruction polynomials $\hat{f}_{i-\frac{1}{2}}^0(x)$, $\hat{f}_{i-\frac{1}{2}}^1(x)$, and $\hat{f}_{i-\frac{1}{2}}^2(x)$ at the stencil $\mathcal{S}_{i-\frac{1}{2}}$ 

The solid black line is $f(x)$, with grid points marked by dots. The dash-dotted vertical line marks the location of $x_{i-\frac{1}{2}} \approx 0.46$. Note that $\hat{f}_{i-\frac{1}{2}}^0(x)$ and $\hat{f}_{i-\frac{1}{2}}^1(x)$ coincide.

values at $x_{i+\frac{1}{2}}$, as Figure 22 shows, so

$$\sum_{k=0}^2 \omega_{i+\frac{1}{2}}^{-z,k} \hat{f}_{i+\frac{1}{2}}^k > \sum_{k=0}^2 d_k \hat{f}_{i+\frac{1}{2}}^k.$$

This is so because $\hat{f}_{i+\frac{1}{2}}^0(x)$ and $\hat{f}_{i+\frac{1}{2}}^2(x)$ are the polynomials with higher total variations around $x_i = 0.5$. Similarly, at $x_{i-\frac{1}{2}} (\approx 0.46)$, ω_0^{-z} and ω_1^{-z} are greater than d_0 and d_1 , resp., and they correspond to the polynomials with the lowest values at $x_{i-\frac{1}{2}}$, $\hat{f}_{i-\frac{1}{2}}^0(x)$ and $\hat{f}_{i-\frac{1}{2}}^1(x)$ (shown in Figure 23). Therefore,

$$\sum_{k=0}^2 \omega_{i-\frac{1}{2}}^{-z,k} \hat{f}_{i-\frac{1}{2}}^k < \sum_{k=0}^2 d_k \hat{f}_{i-\frac{1}{2}}^k.$$

Using Eq. (7.11), this gives

$$D_x^{-z} f(x_i) > f'(x_i) + O(\Delta x^5) \sim f'(x_i),$$

and this is why $D_x^{-z} f$ overshoots f' at $x_i = 0.5$. The same analysis applied to the WENO-Z weights gives

$$D_x^z f(x_i) < f'(x_i) + O(\Delta x^5) \sim f'(x_i).$$

In this example, the phenomenon is exacerbated because the grid (7.8) is coarse. In particular, every 5 points stencil in this grid contains a critical point, which increases the disparities of total variation between substencils. Nevertheless, this situation is typical, although it happens at a smaller scale at finer grids.

Now, to understand why WENO-min is unstable, suppose f is smooth on a given stencil \mathcal{S} . Then, generally, β_k is larger than τ on each substencil of \mathcal{S} , because the order of τ is higher than the order of β . An exception is when f has a very flat critical point in \mathcal{S} — in this case, we may have $\beta_k \leq \tau$. But if f has only simple critical points like in the example $f(x) = \sin(4\pi x)$ above, then $\beta_k > \tau$ in the whole domain (as Fig. 20 shows). In such cases, by Eq. (7.7) $\alpha^{min} \equiv \alpha^{-z}$ in the whole domain; but, as we have seen, the “anti-Zico” discrete derivative operator is unstable.

In conclusion, the term η_k^{-z} (Eq. (7.5)) is the ultimate responsible for the instability of WENO-min. But there is a bright side to it: when the size of η_k^{-z} is controlled, it acts as a *sharpening term* (or *steepening term*) near critical points, smooth structures and discontinuities, while keeping the scheme stable. It seems the right dose differentiates a poison and a remedy. In the next chapter, we present a new scheme which uses the sharpening properties of η_k^{-z} to its advantage.

8 A new improved WENO scheme

8.1 Designing a new weight formula

In the previous chapter we have seen that the *min* weight formula conditionally chooses between two terms (cf. Eq. (7.5))

$$\eta_k^z \triangleq \frac{\nu}{\mu_k + \varepsilon}, \quad \eta_k^{-z} \triangleq \frac{\mu_k}{\nu + \varepsilon},$$

depending on the size of μ_k and ν (cf. Eq. (7.7)),

$$\alpha_k^{\min} = d_k [1 + (\eta_k)^p], \quad \eta_k = \begin{cases} \eta_k^z, & \text{if } \mu_k \leq \nu, \\ \eta_k^{-z}, & \text{if } \mu_k > \nu. \end{cases} \quad (8.1)$$

Also, we have noted that while η_k^{-z} is the ultimate responsible for the instability of the WENO-*min* scheme, it has potential as a sharpening term.

What if, instead of merely choosing between η_k^z and η_k^{-z} , we combined both terms in the weight formula, but controlling the size of η_k^{-z} so as to make the scheme stable? This idea led to a new weight formula, which generalizes and improves upon the Zico weights. First, we will modify the terms η_k^z and η_k^{-z} a bit, by defining the new terms

$$\eta_k \triangleq \frac{\nu + \varepsilon}{\mu_k + \varepsilon}, \quad \eta_k^{-1} \triangleq \frac{\mu_k + \varepsilon}{\nu + \varepsilon} = (\eta_k)^{-1}. \quad (8.2)$$

In comparison to η_k^z , η_k^{-z} , the terms η_k , η_k^{-1} have additional epsilons in their numerators. This change is introduced for computational reasons: since η_k is the reciprocal of η_k^{-1} , some computations are simplified and the operation count decreases as a result (this is detailed in Section 8.1.3). Also, we will see in Chapter 9 that this makes the weights have better and more easily proven accuracy properties.

Now, we define the new weights as

$$\alpha_k^{z+} \triangleq d_k \left[1 + (\eta_k)^p + \lambda \eta_k^{-1} \right] = d_k \left[1 + \left(\frac{\nu + \varepsilon}{\mu_k + \varepsilon} \right)^p + \lambda \left(\frac{\mu_k + \varepsilon}{\nu + \varepsilon} \right) \right], \quad (8.3)$$

$$\omega_k^{z+} \triangleq \frac{\alpha_k^{z+}}{\sum_{j=0}^{r-1} \alpha_j^{z+}}, \quad k = 0, \dots, r-1.$$

This is essentially the Zico unnormalized weight (5.1) with the addition of the sharpening term $\lambda \eta_k^{-1}$ inside the parentheses and epsilons in the numerators. For this reason, we call this new formula the Zico+ weights. The new parameter λ is used for controlling the size of η_k^{-1} . It must be small enough so the scheme is stable and essentially non-oscillatory, but large enough for effectively improving the sharpness of the solutions.

Remark 5. Eq. (8.3) could be more generally written as

$$\alpha_k^{z^+} = d_k \left[1 + (\eta_k)^p + \lambda(\eta_k^{-1})^{p_2} \right].$$

However, preliminary numerical results displayed instability when $p_2 = 2$. This happens because the sharpening term η_k^{-1} is too amplified in this case. For this reason, we are fixing $p_2 = 1$ in Eq. (8.3).

Now, let us show the properties of the new weights.

8.1.1 ENO property

As usual, consider \mathcal{S}_C continuous and \mathcal{S}_D discontinuous. Assuming $\lambda = O(1)$ (that is, λ does not asymptotically grow with Δx), we have

$$\begin{aligned} \frac{\alpha_D}{\alpha_C} &= \frac{d_D}{d_C} \frac{\left(\frac{\mu_C + \varepsilon}{\nu + \varepsilon}\right)^p + \left(\frac{\mu_C + \varepsilon}{\mu_D + \varepsilon}\right)^p + \lambda \frac{(\mu_C + \varepsilon)^p (\mu_D + \varepsilon)}{(\nu + \varepsilon)^{p+1}}}{1 + \left(\frac{\mu_C + \varepsilon}{\nu + \varepsilon}\right)^p + \lambda \left(\frac{\mu_C + \varepsilon}{\nu + \varepsilon}\right)^{p+1}} \\ &= \Theta(1) \frac{\left(\frac{O(\Delta x^q) + \varepsilon}{\Theta(1)}\right)^p + \left(\frac{O(\Delta x^q) + \varepsilon}{\Theta(1)}\right)^p + O(1) \frac{(O(\Delta x^q) + \varepsilon)^p \Theta(1)}{\Theta(1)}}{1 + \left(\frac{O(\Delta x^q) + \varepsilon}{\Theta(1)}\right)^p + O(1) \left(\frac{O(\Delta x^q) + \varepsilon}{\Theta(1)}\right)^{p+1}} \\ &= O(\Delta x^{pq}) + \Theta(\varepsilon^p), \end{aligned}$$

which is the same asymptotic expression as the other weight formulas studied so far. Note that the asymptotic behavior does not depend on the new parameter λ , given that $\lambda = O(1)$.

8.1.2 Discontinuous/continuous ratio

Their discontinuous/continuous ratio is

$$\frac{\alpha_D^{z^+}}{\alpha_C^{z^+}} = \frac{d_D}{d_C} \frac{(\mu_C + \varepsilon)^p (\mu_D + \varepsilon)^p + (\nu + \varepsilon)^p + \lambda(\mu_D + \varepsilon)^{p+1}/(\nu + \varepsilon)}{(\mu_D + \varepsilon)^p (\mu_C + \varepsilon)^p + (\nu + \varepsilon)^p + \lambda(\mu_C + \varepsilon)^{p+1}/(\nu + \varepsilon)}.$$

This is greater than the discontinuous/continuous ratio of the Zico weights, if ε is small:

$$\begin{aligned} \frac{\alpha_D^{z^+}}{\alpha_C^{z^+}} &> \frac{d_D}{d_C} \frac{(\mu_C + \varepsilon)^p (\mu_D + \varepsilon)^p + (\nu + \varepsilon)^p}{(\mu_D + \varepsilon)^p (\mu_C + \varepsilon)^p + (\nu + \varepsilon)^p} \\ &\sim \frac{d_D}{d_C} \frac{(\mu_C + \varepsilon)^p (\mu_D + \varepsilon)^p + \nu^p}{(\mu_D + \varepsilon)^p (\mu_C + \varepsilon)^p + \nu^p} = \frac{\alpha_D^Z}{\alpha_C^Z}. \end{aligned} \quad (8.4)$$

The inequality in (8.4) holds due to the following: for simplifying the notation, let $a_j = (\mu_j + \varepsilon)^p + (\nu + \varepsilon)^p$ and $b_j = \lambda(\mu_j + \varepsilon)^{p+1}/(\nu + \varepsilon)$. Since $a_D, a_C > 0$,

$$\frac{a_D + b_D}{a_C + b_C} > \frac{a_D}{a_C} \quad \Leftrightarrow \quad \frac{1 + b_D/a_D}{1 + b_C/a_C} > 1 \quad \Leftrightarrow \quad \frac{b_D}{a_D} > \frac{b_C}{a_C} \quad \Leftrightarrow \quad b_D a_C - b_C a_D > 0.$$

Hence, if $b_D a_C - b_C a_D > 0$, Eq. 8.4 holds. Finally, since $\mu_D > \mu_C$ as $\Delta x \rightarrow 0$,

$$\begin{aligned} \frac{\nu + \varepsilon}{\lambda} (b_D a_C - b_C a_D) &= \\ &= (\mu_D + \varepsilon)^{p+1} [(\mu_C + \varepsilon)^p + (\nu + \varepsilon)^p] - (\mu_C + \varepsilon)^{p+1} [(\mu_D + \varepsilon)^p + (\nu + \varepsilon)^p] \\ &= (\mu_D - \mu_C) (\mu_D + \varepsilon)^p (\mu_C + \varepsilon)^p + [(\mu_D + \varepsilon)^{p+1} - (\mu_C + \varepsilon)^{p+1}] (\nu + \varepsilon)^p \\ &> 0. \end{aligned}$$

Remark 6. The relation (8.4) is not a proof that $\alpha_D^{Z+}/\alpha_C^{Z+} > \alpha_D^Z/\alpha_C^Z$, it is merely an indication. However, since ε is usually very small, this is very often the case.

8.1.3 Operation count

From Eqs. (8.2), (8.3),

$$\eta_k = \frac{\nu + \varepsilon}{\mu_k + \varepsilon}, \quad \alpha_k^{Z+} = d_k \left[1 + (\eta_k)^p + \frac{\lambda}{\eta_k} \right].$$

Hence, the flop count per substencil is

$$\begin{aligned} \text{flops}(\alpha_k^{Z+}) &= \{4\pm, 1\times, 2\div\} + \text{flops}(\text{pow}(p)) + \text{flops}(\nu) + \text{flops}(\mu_k) \\ &= \text{flops}(\alpha_k^Z) + \{2\pm, 0\times, 1\div\}, \end{aligned}$$

and the total cost per stencil is

$$\begin{aligned} \text{flops}(\alpha^{Z+}) &= \{4r\pm, r\times, 2r\div\} + r \text{ flops}(\text{pow}(p)) + \text{flops}(\nu) + r \text{ flops}(\mu_k) \\ &= \text{flops}(\alpha^Z) + \{2r\pm, 0\times, r\div\}. \end{aligned}$$

Therefore, the Zico+ weights are a little costlier than the Zico weights. If, however, we had used η_k^Z and η_k^{-Z} instead of η_k and η_k^{-1} in the definition of Zico+ weights, we would have needed an extra product per substencil:

$$\begin{aligned} \text{flops} \left(d_k \left[1 + \eta_k^Z + \lambda \eta_k^{-Z} \right] \right) &= \text{flops} \left(d_k \left[1 + \left(\frac{\nu}{\mu_k + \varepsilon} \right)^p + \lambda \left(\frac{\mu_k}{\nu + \varepsilon} \right) \right] \right) \\ &= \{4\pm, 2\times, 2\div\} + 2 \text{ flops}(\text{pow}(p)) + \text{flops}(\nu) + \text{flops}(\mu_k) \\ &= \text{flops}(\alpha_k^{Z+}) + \{0\pm, 1\times, 0\div\} + \text{flops}(\text{exp}(p)). \end{aligned}$$

The total cost of the normalized weights per stencil is

$$\begin{aligned} \text{flops}(\omega^{Z+}) &= \text{flops}(\alpha^{Z+}) + \{(r-1)\pm, 0\times, r\div\} \\ &= \text{flops}(\omega^Z) + \{2r\pm, 0\times, r\div\} \\ &= \text{flops}(\omega^C) + \{3r\pm, r\times, r\div\} + \text{flops}(\nu). \end{aligned}$$

8.2 The new WENO-Z+ scheme

The WENO-Z+ scheme is composed by the Zico+ formula (8.3), using the local smoothness indicators β_k of Jiang–Shu (Section 3.3) and the τ global smoothness indicators (Section 3.4). The default values for the parameters are $\varepsilon = 10^{-40}$ and $p = 2$. The value of parameter λ was empirically determined — for order $R = 5$ and $p = 1$ or 2 , the choice $\lambda = \Delta x^{2/3}$ gives good results in terms of stability, mitigation of oscillations, steepness and resolution power, at least for the standard tests. Preliminary tests show that, for higher orders, λ may assume constant values with no harm to stability. However, the research on the new WENO with higher orders is still on its early steps, and it will be the subject of future works. In this section, we focus on the 5th order WENO-Z+ scheme.

8.2.1 The parameter λ

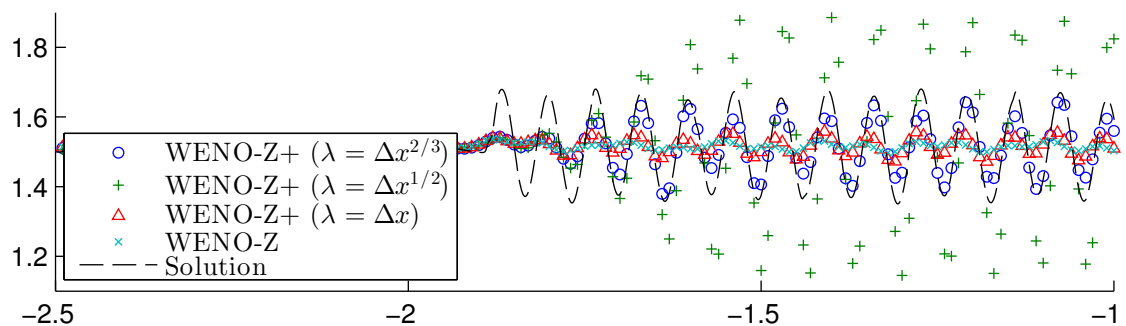
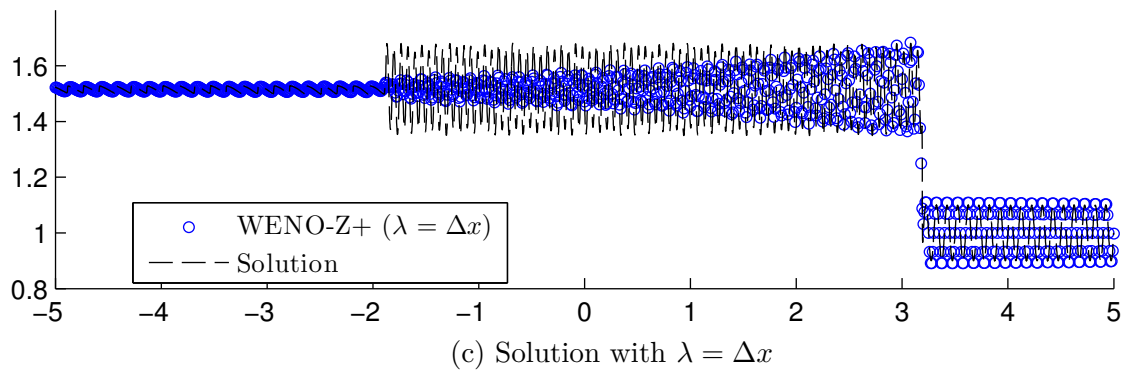
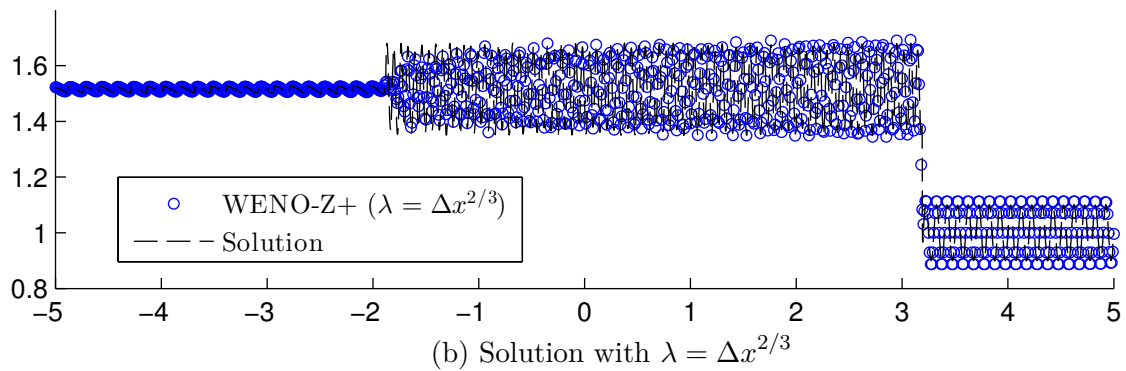
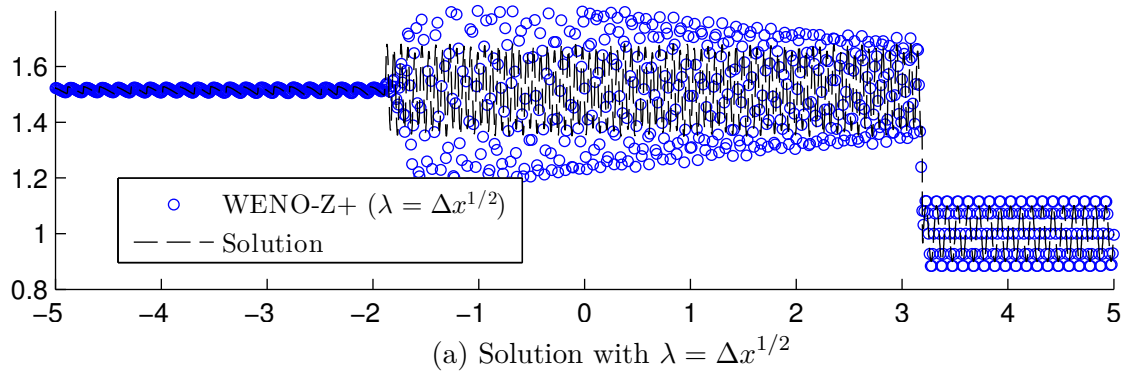
Here, we will show how the parameter λ can be used to fine-tune the steepness of the WENO-Z+ scheme. We have investigated the behavior of WENO-Z+ with three different choices for the parameter λ : $\Delta x^{1/2}$, $\Delta x^{2/3}$ and Δx . The higher the λ , the greater the contribution of the sharpening term η_k^{-1} ; therefore, WENO-Z+ is expected to be the less dissipative with $\lambda = \Delta x^{1/2}$ and more dissipative with $\lambda = \Delta x$, with $\lambda = \Delta x^{2/3}$ giving intermediate results. The results in this section empirically justify the choice $\lambda = \Delta x^{2/3}$ as a good compromise between stability and sharpness.

Remark 7. There is no guarantee, however, that $\lambda = \Delta x^{2/3}$ will work well in every situation. In some specific problems, the scheme may need more numerical dissipation in order to maintain stability. In these cases, one should use a smaller λ .

In all tests, $\varepsilon = 10^{-40}$ and $p = 2$ for all schemes.

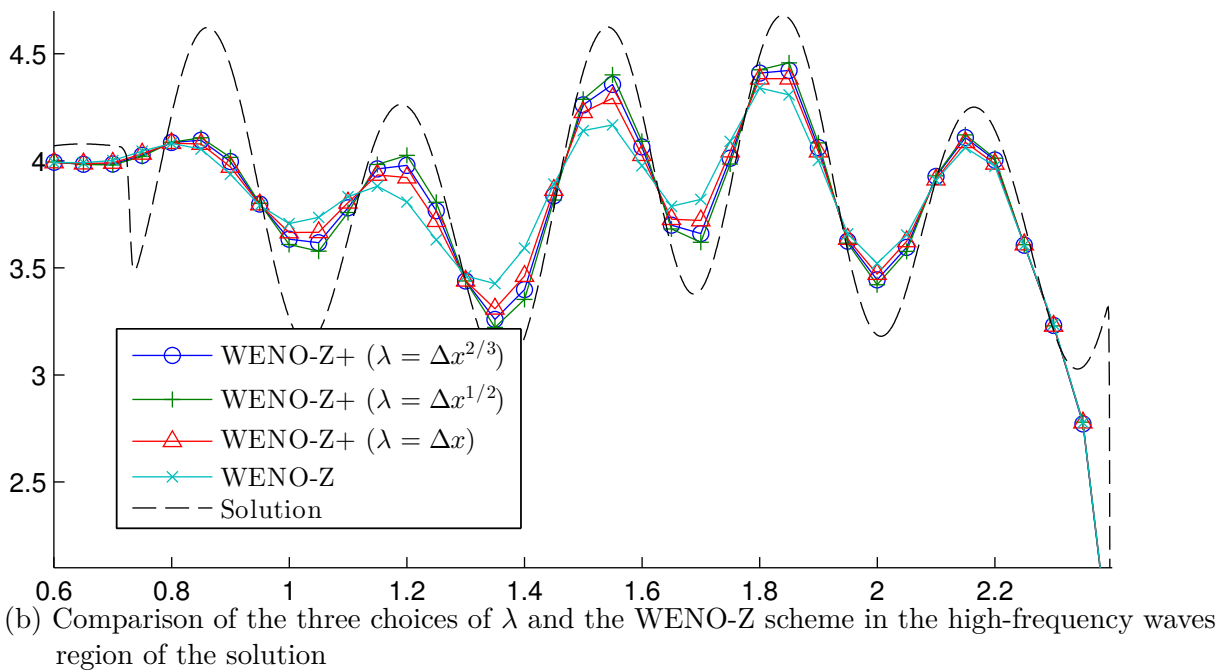
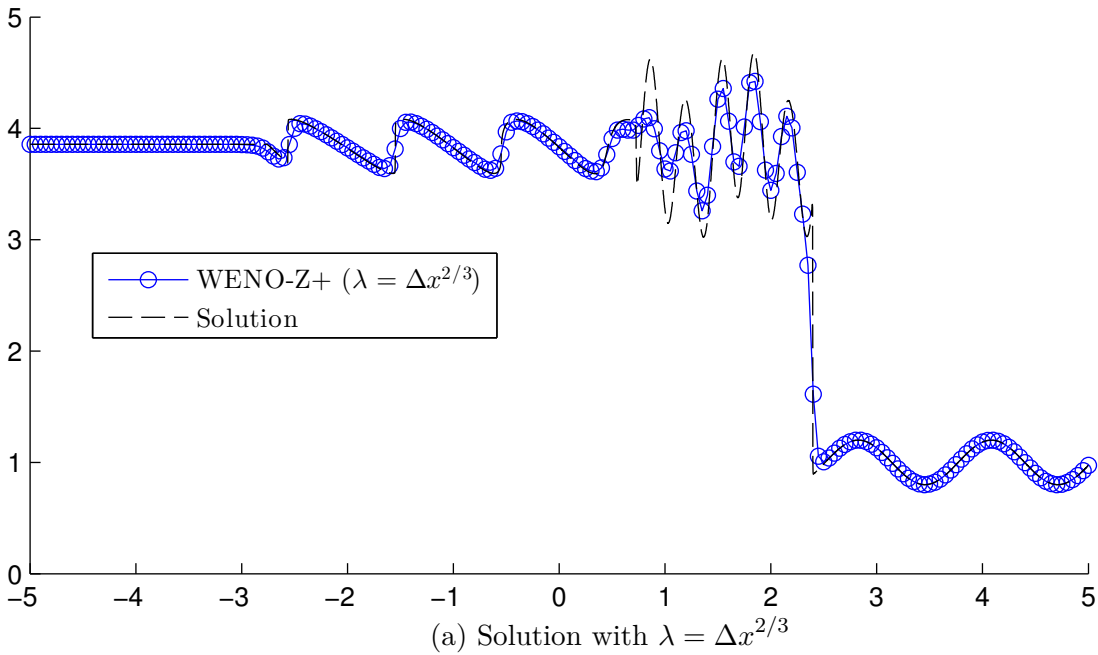
Shock-entropy test of Titarev–Toro. Figure 24 compares the results of the Titarev–Toro shock-entropy test with $N = 1000$ points for the 5th order WENO-Z+ scheme with the three different values for the parameter λ above, and the reference scheme WENO-Z. The figure shows that $\lambda = \Delta x^{1/2}$ makes the wave greatly overshoot the solution, which is an indication of instability. On the other hand, $\lambda = \Delta x$ makes the scheme too dissipative: the results are comparable to the simpler and less costly WENO-Z (Fig. 24d). The choice $\lambda = \Delta x^{2/3}$ gives the best results, resolving most of the waves with a good approximation to their amplitudes already with this relatively small number of points.

Shock-entropy test of Shu–Osher. Figure 25 shows the results of the Shu–Osher shock-entropy test with $N = 200$ points. Figure 25a displays WENO-Z+ with $\lambda = \Delta x^{2/3}$ alone, since, at this scale, the results with other choices for λ are too similar. Figure 25b shows that WENO-Z+ is sharper than WENO-Z. It shows how λ can be used as a fine-tuner, in which a smaller λ makes the WENO-Z+ sharper.

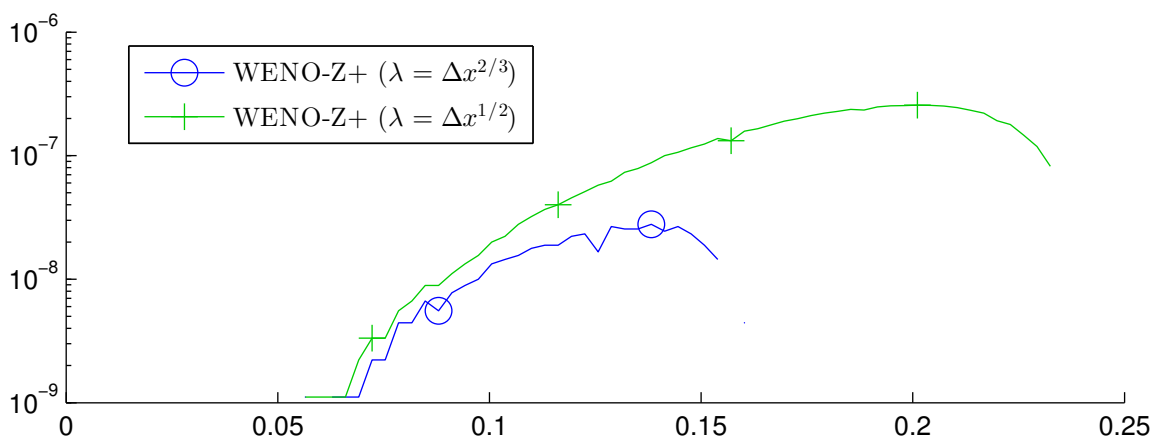
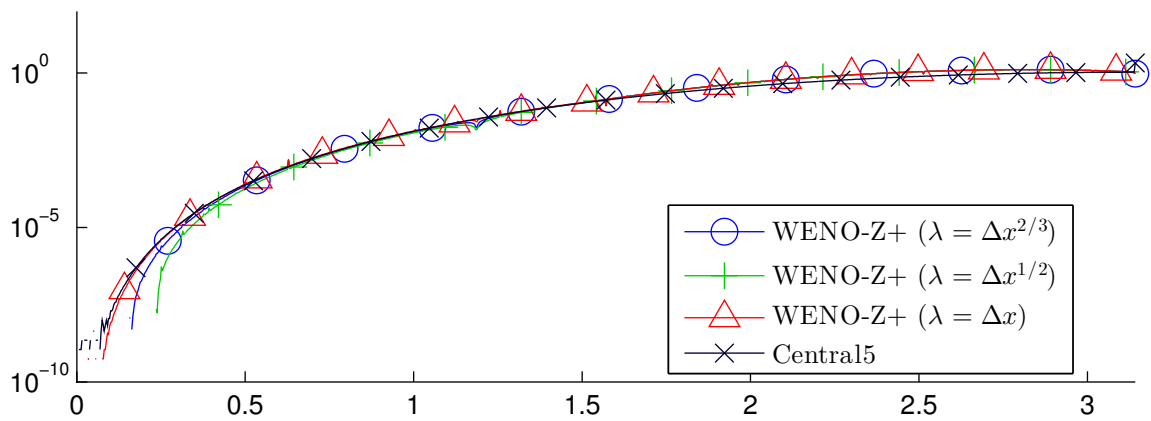
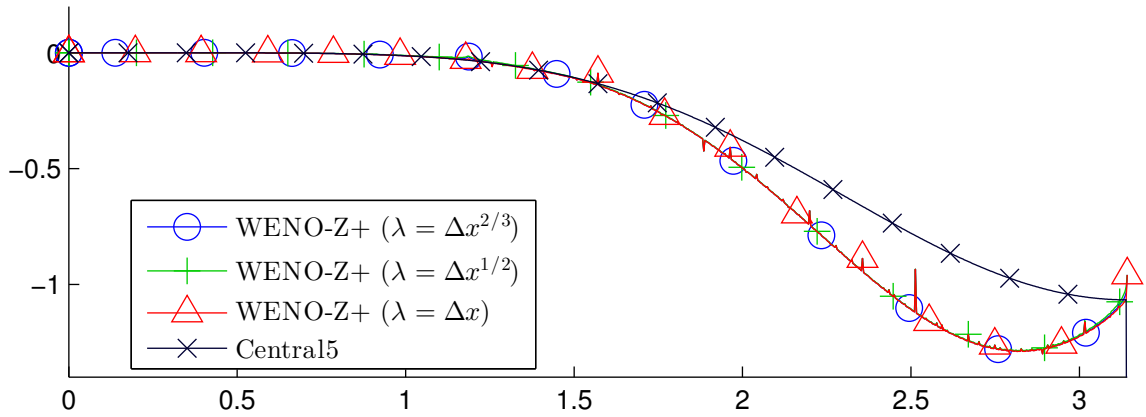
Figure 24 – Numerical solution of the shock-entropy problem of Titarev–Toro by the WENO-Z+ scheme with different λ 

The figures show the density of the solution at $t = 5$. A grid with $N = 1000$ points was used. For all schemes, $\varepsilon = 10^{-40}$ and $p = 2$. CFL = 0.5.

Figure 25 – Numerical solution of the shock-entropy problem of Shu–Osher by the WENO-Z+ scheme with different λ



The figures show the density of the solution at $t = 1.8$. A grid with $N = 200$ points was used. $\text{CFL} = 0.5$.

Figure 26 – ADR analysis of WENO-Z+ scheme with different λ : imaginary part of ϕ 

The higher the value of $\text{Im}(\phi)$, the less dissipative is the scheme. Positive values of $\text{Im}(\phi)$ indicates instability. Here, 2000 wavenumbers were used.

ADR analysis. Figure 26 shows the results of the imaginary part of ϕ , in linear (Fig. 26a) and log scale of negative (Fig. 26b) and positive values (Fig. 26c), for the three variations of WENO-Z+ and the reference scheme, the fifth-order upstream central scheme (see Section 1.1.2), labeled Central5. The results are very similar, except for the lower left corner in Fig. 26b, where $\text{Im}(\phi)$ assume positive values for $\lambda = \Delta x^{1/2}$ and $\lambda = \Delta x^{2/3}$. The value of ϕ being positive means that the schemes actually make the waves at these wavenumbers grow, instead of being dissipated, which indicates instability. We can see that the positive interval is larger for $\lambda = \Delta x^{1/2}$ and smaller for $\lambda = \Delta x^{2/3}$. However, the positive interval for $\lambda = \Delta x^{2/3}$ is small, as are the corresponding values of $\text{Im}(\phi)$. In practice, the nonlinear nature of the WENO-Z+ weights compensate for this small positive range, and WENO-Z+ with $\lambda = \Delta x^{2/3}$ was stable and essentially non-oscillatory in all standard tests.

Notice that both the range and amplitude of the positive part of $\text{Im}(\phi)$ are smaller than in the WENO-*min* case (Fig. 17).

Interacting blast waves. For the interacting blast waves test with $N = 800$ points and $\text{CFL} = 0.5$, WENO-Z+ is unstable with $\lambda = \Delta x^{1/2}$, but it is stable with $\lambda = \Delta x^{2/3}$ and $\lambda = \Delta x$. Since the results are too similar for these two choices of λ , the results are not shown here.

Other tests. We have also run the Riemann problems of Lax and Sod and the Gaussian-square-triangle-ellipse linear test. The results similarly show that $\lambda = \Delta x^{2/3}$ occupy an intermediate position between the less dissipative, $\lambda = \Delta x^{1/2}$, and the more dissipative, $\lambda = \Delta x$, although the scale of the differences is very small in these problems. For brevity, these results are not shown.

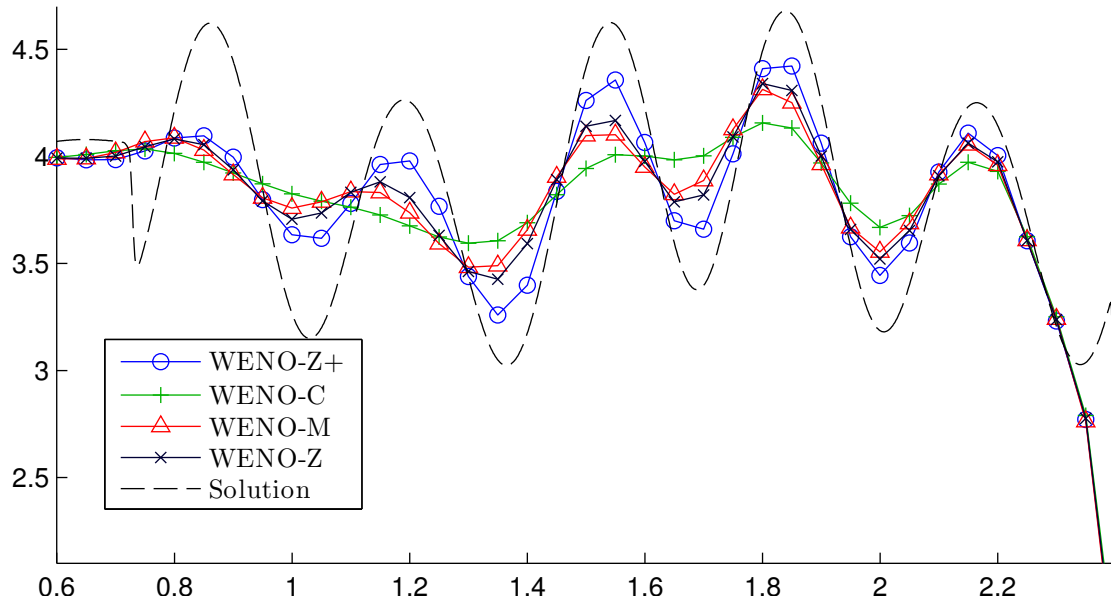
8.2.2 Comparison with other WENO schemes

Here, we compare the new WENO-Z+ scheme with the classical WENO, the WENO-M and WENO-Z schemes. From now on, we will assume that the value of parameter λ of WENO-Z+ is $\Delta x^{2/3}$ in all tests. All schemes use $p = 2$ and $\varepsilon = 10^{-40}$, for a fair comparison.

Shock-entropy tests. Figure 27 shows the results of the shock-entropy problem of Shu–Osher with $N = 200$ points, and Figure 28 shows the results of the shock-entropy problem of Titarev–Toro with $N = 1000$ points. The results of WENO-Z+ are much sharper than the others, especially in the Titarev–Toro test.

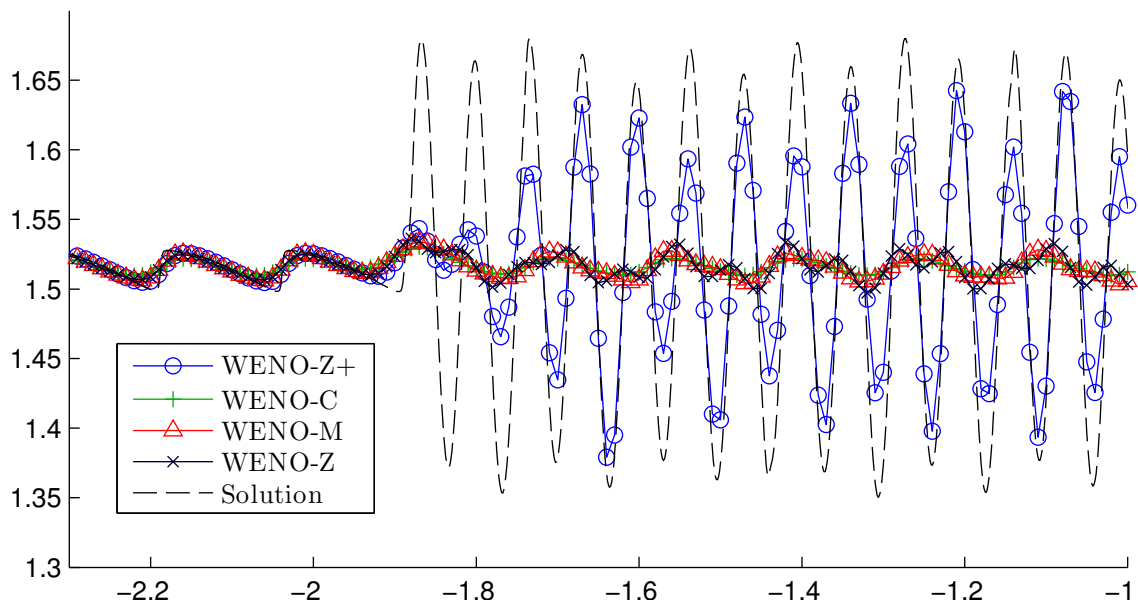
Interacting blast waves. Figure 29 shows a zoom in the results of the interacting blast waves problem, with $N = 200$ points. In this problem, WENO-Z+ is not significantly less dissipative than WENO-Z. In fact, WENO-M, WENO-Z, and WENO-Z+ give comparable results, with WENO-C being more dissipative than the other three. It should be noted that WENO-M with $p = 1$ is unstable for this test, while the other three schemes are not.

Figure 27 – Numerical solution of the shock-entropy problem of Shu–Osher by the WENO-Z+, WENO-C, WENO-M, and WENO-Z schemes



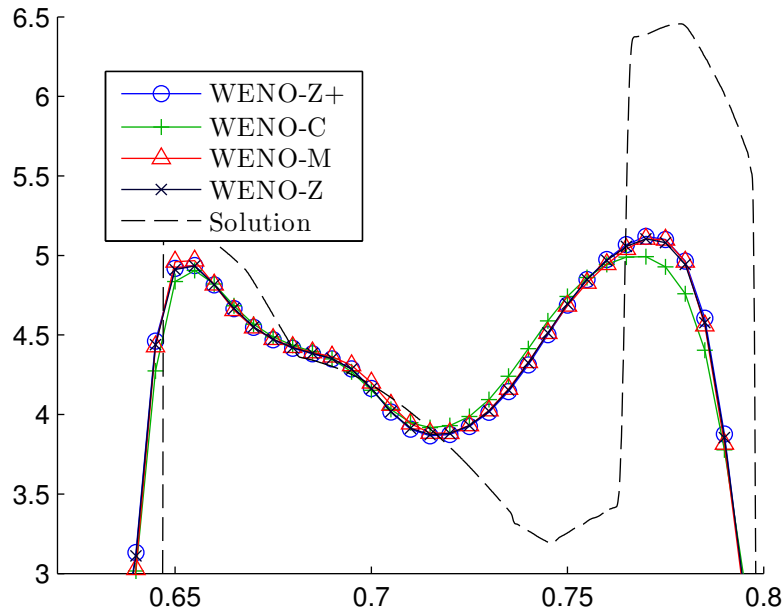
The figure show a zoom in the region of high-frequency waves of the density of the solutions at $t = 1.8$. A grid with $N = 200$ points was used. CFL = 0.5.

Figure 28 – Numerical solution of the shock-entropy problem of Titarev–Toro by the WENO-Z+, WENO-C, WENO-M, and WENO-Z schemes



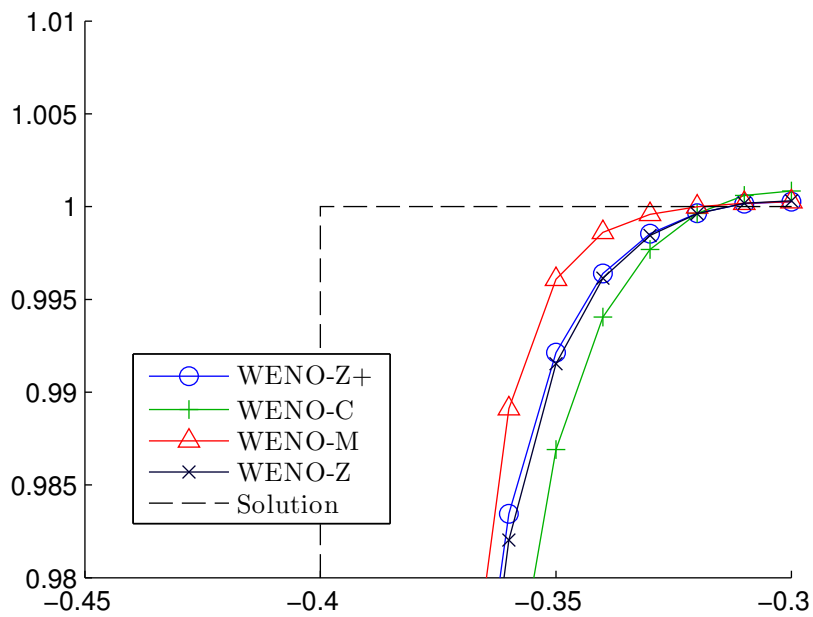
The figure show a zoom in the region of high-frequency waves of the density of the solutions at $t = 5$. A grid with $N = 1000$ points was used. CFL = 0.5.

Figure 29 – Numerical solution of the blast waves problem by the WENO-Z+, WENO-C, WENO-M, and WENO-Z schemes



The figures show a zoom in the density of the solution at $t = 0.038$. $N = 200$ points were used. CFL = 0.5.

Figure 30 – Numerical solution of the Gaussian-square-triangle-ellipse linear test by the WENO-Z+, WENO-C, WENO-M, and WENO-Z schemes



The figure shows a zoom in the square wave of the solution at $t = 2$. $N = 200$ points were used. CFL = 0.5.

Gaussian-square-triangle-ellipse linear test. Figure 30 shows a zoom in the square wave of the results of the Gaussian-square-triangle-ellipse problem, with $N = 200$ points. In this test, WENO-M is the least dissipative, with WENO-Z+ and WENO-Z very close to each other, and WENO-C coming behind, in order from the least to the most dissipative.

Other tests. We have also run the Riemann problems of Lax and Sod. The results follow the same trend of GSTE test, that is, from the least to the most dissipative: WENO-M, WENO-Z+, WENO-Z and WENO-C.

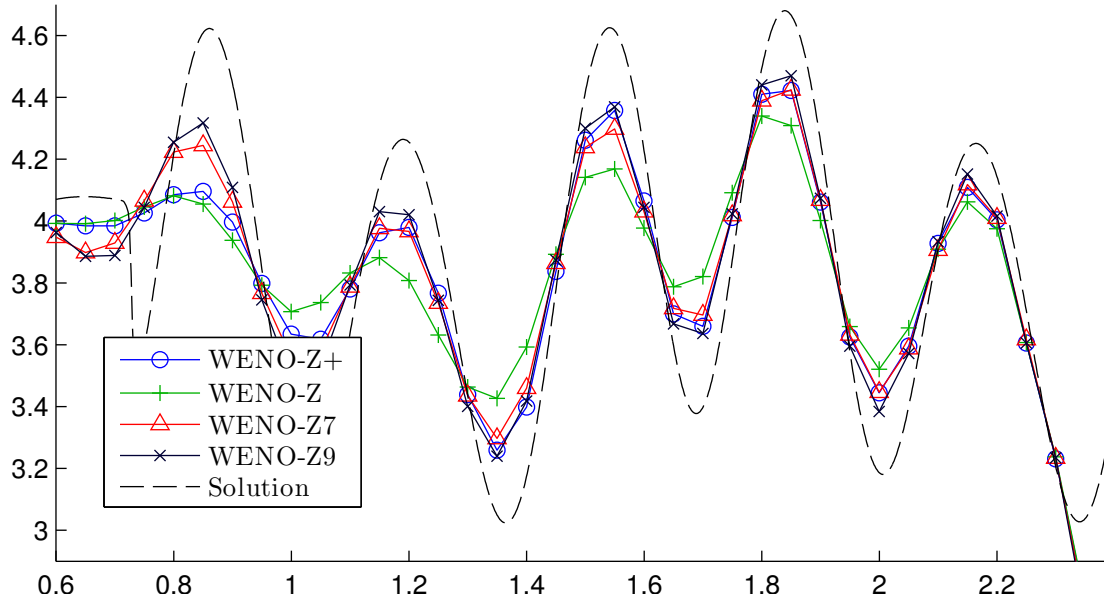
In conclusion, WENO-Z+ really stands out in the shock-entropy tests. In the other tests, WENO-M is less dissipative, however at a much greater cost than WENO-Z+, which comes in second place. The results show that, in problems which do not contain fine structures (such as the ones found in shock-entropy tests), the increased cost of WENO-Z+ may not compensate for its use, since WENO-Z performs fairly close to it in those problems.

8.2.3 Comparison with WENO-Z of different orders

In this section, we will show that the sharpness introduced by the sharpening term η_k^{-1} on the Zico formula makes the results of WENO-Z+ comparable to, or even better than, those of higher-order WENO-Z schemes in shock-entropy problems. As before, all schemes use $p = 2$ and $\varepsilon = 10^{-40}$.

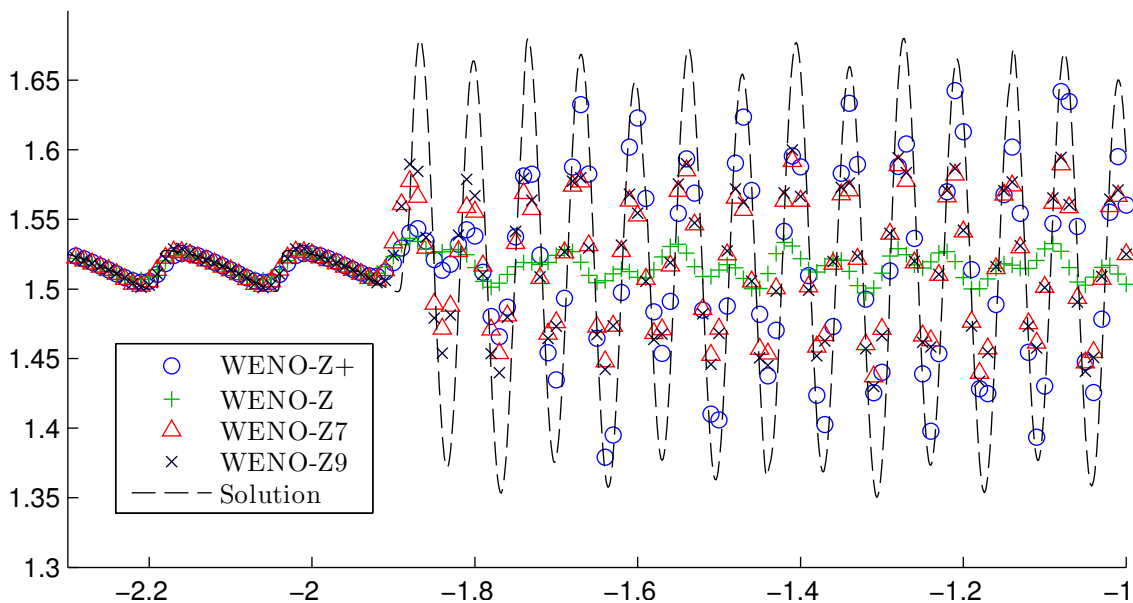
Figure 31 shows the results of the shock-entropy problem of Shu–Osher with $N = 200$ points, and Figure 32 shows the results of the shock-entropy problem of Titarev–Toro with $N = 1000$ points. They show that WENO-Z+ excels in this kind of problem, having at least the resolution power of WENO-Z7 in the Shu–Osher test, and even surpassing WENO-Z9 in the Titarev–Toro test.

Figure 31 – Numerical solution of the shock-entropy problem of Shu–Osher by the WENO-Z+, WENO-Z, WENO-Z7, and WENO-Z9 schemes



The figure show a zoom in the region of high-frequency waves of the density of the solutions at $t = 1.8$. A grid with $N = 200$ points was used. $CFL = 0.5$.

Figure 32 – Numerical solution of the shock-entropy problem of Titarev–Toro by the WENO-Z+, WENO-Z, WENO-Z7, and WENO-Z9 schemes



The figure show a zoom in the region of high-frequency waves of the density of the solutions at $t = 5$. A grid with $N = 1000$ points was used. $CFL = 0.5$.

9 Accuracy of the WENO-Z+ scheme

We now turn to the task of analyzing the accuracy properties of the new WENO-Z+ scheme.

The goal is to find constraints on the parameters of the weights of WENO-Z+ that will assure that the nominal order R is always recovered for smooth solutions, regardless of critical points, that is,

$$\omega_k - d_k = O(\Delta x^{r-1}), \quad (9.1a)$$

$$\omega_{i+\frac{1}{2}}^k - \omega_{i-\frac{1}{2}}^k = O(\Delta x^r), \quad (9.1b)$$

as it is stated in Proposition 2. For simplicity of notation, in this section we use Definition 4 to write, for any term ψ ,

$$\delta_i \psi \triangleq \psi_{i+\frac{1}{2}} - \psi_{i-\frac{1}{2}}.$$

9.1 Properties of β_k

In order to find the constraints on the parameters of the WENO-Z+ formula, we will adopt the same general strategy we introduced in [22] for analyzing the accuracy of the classical WENO and WENO-Z schemes. As such, we use the following properties of the smoothness indicators β_k , which were demonstrated in [22] and whose proofs are included in Appendix B.

Corollary 7. *At a critical point of order n_{cp} (Definition 1), β_k can be decomposed as a sum of a k -invariant (B) and a k -dependent (R_k) components, for $k = 0, \dots, r-1$, namely:*

$$\beta_k = B + R_k,$$

where, if $n_{\text{cp}} < r-1$,

$$\theta(B) = 2(n_{\text{cp}} + 1), \quad \theta(R_k) \geq n_{\text{cp}} + r + 1,$$

and, if $n_{\text{cp}} \geq r-1$,

$$B = 0, \quad \theta(R_k) = 2(n_{\text{cp}} + 1).$$

In particular, $\theta(\beta_k) = 2(n_{\text{cp}} + 1)$, and the upper bounds $\beta_k = O(\Delta x^2)$, $B = O(\Delta x^2)$ and $R_k = O(\Delta x^{r+1})$ hold.

Lemma 9. *Let*

$$\gamma_k \triangleq \frac{R_k}{B + \varepsilon},$$

where B and R_k are given by Corollary 7. If $\varepsilon = \Omega(\Delta x^2)$, then $\gamma_k = O(\Delta x^{r-1})$ and $\delta_i \gamma_k = O(\Delta x^r)$.

9.2 The accuracy constraint

For the analysis of this section, it will be useful to redefine the WENO-Z+ weights so that τ and β_k have distinct accompanying epsilons:

$$\alpha_k \triangleq d_k \left[1 + \left(\frac{\tau + \varepsilon_\tau}{\beta_k + \varepsilon_\beta} \right)^p + \lambda \left(\frac{\beta_k + \varepsilon_\beta}{\tau + \varepsilon_\tau} \right) \right], \quad \omega_k \triangleq \frac{\alpha_k}{\sum_{j=0}^{r-1} \alpha_j}, \quad k = 0, \dots, r-1. \quad (9.2)$$

Let us define

$$\gamma_k \triangleq \frac{R_k}{B + \varepsilon_\beta}, \quad H \triangleq \frac{\tau + \varepsilon_\tau}{B + \varepsilon_\beta}.$$

It should be noted that H (for ‘‘capital eta’’, cf. Eq. (8.2)) is always positive and does not depend on k .

Assumptions. Assume that $p \geq 1$, that $\gamma_k \rightarrow 0$, $H \rightarrow 0$ and $H/\lambda \rightarrow 0$ as $\Delta x \rightarrow 0$, and also that $\lambda = O(1)$ (that is, λ does not grow with Δx as $\Delta x \rightarrow 0$), so the following manipulations are asymptotically valid.

Using Corollary 7, the unnormalized weights (9.2) can be rewritten as

$$\begin{aligned} \alpha_k &= d_k \left[1 + \left(\frac{\tau + \varepsilon_\tau}{B + R_k + \varepsilon_\beta} \right)^p + \lambda \left(\frac{B + R_k + \varepsilon_\beta}{\tau + \varepsilon_\tau} \right) \right] \\ &= d_k \frac{\lambda}{H} \left[\frac{H}{\lambda} + \frac{(\tau + \varepsilon_\tau)^{p+1}}{\lambda(B + \varepsilon_\beta)(B + R_k + \varepsilon_\beta)^p} + (1 + \gamma_k) \right] \\ &= d_k \frac{\lambda}{H} \left[\frac{H}{\lambda} + \frac{(\tau + \varepsilon_\tau)^{p+1}}{\lambda(B + \varepsilon_\beta)^{p+1}(1 + \gamma_k)^p} + 1 + \gamma_k \right] \\ &= d_k \frac{\lambda}{H} \left[\frac{H}{\lambda} + \frac{H^{p+1}}{\lambda} \frac{1}{(1 + \gamma_k)^p} + 1 + \gamma_k \right] \\ &= d_k \frac{\lambda}{H} \left[1 + \frac{H}{\lambda} + \gamma_k + O\left(\frac{H^{p+1}}{\lambda}\right) \right]. \end{aligned}$$

Hence, the normalized weights are given by

$$\begin{aligned} \omega_k &= \frac{d_k \frac{\lambda}{H} \left[1 + \frac{H}{\lambda} + \gamma_k + O\left(\frac{H^{p+1}}{\lambda}\right) \right]}{\sum_{j=0}^{r-1} d_j \frac{\lambda}{H} \left[1 + \frac{H}{\lambda} + \gamma_j + O\left(\frac{H^{p+1}}{\lambda}\right) \right]} = \frac{d_k \left[1 + \frac{H}{\lambda} + \gamma_k + O\left(\frac{H^{p+1}}{\lambda}\right) \right]}{1 + \frac{H}{\lambda} + \sum_{j=0}^{r-1} d_j \gamma_j + O\left(\frac{H^{p+1}}{\lambda}\right)} \\ &= d_k \left[1 + \frac{H}{\lambda} + \gamma_k + O\left(\frac{H^{p+1}}{\lambda}\right) \right] \times \\ &\quad \times \left[1 - \left(\frac{H}{\lambda} + \sum_{j=0}^{r-1} d_j \gamma_j \right) + \left(\frac{H}{\lambda} + \sum_{j=0}^{r-1} d_j \gamma_j \right)^2 + \dots + O\left(\frac{H^{p+1}}{\lambda}\right) \right] \\ &= d_k + d_k \left(\gamma_k - \sum_{j=0}^{r-1} d_j \gamma_j \right) + O(\gamma_k^2) + O\left(\frac{H^2}{\lambda^2}\right) + O\left(\frac{\gamma_k H}{\lambda}\right) + O\left(\frac{H^{p+1}}{\lambda}\right) \\ &= d_k + d_k \left(\gamma_k - \sum_{j=0}^{r-1} d_j \gamma_j \right) + O(\gamma_k^2) + O\left(\frac{H^2}{\lambda^2}\right). \end{aligned} \quad (9.3)$$

The last equality holds because

$$O\left(\frac{H^{p+1}}{\lambda}\right) = O\left(\frac{H^2}{\lambda^2}\right) O(H^{p-1} \lambda) = O\left(\frac{H^2}{\lambda^2}\right) O(1) \text{ (by assumption)} = O\left(\frac{H^2}{\lambda^2}\right).$$

Eq. (9.3) results in

$$\begin{aligned} \omega_k - d_k &= p d_k \left(\gamma_k - \sum_{j=0}^{r-1} d_j \gamma_j \right) + O(\gamma_k^2) + O\left(\frac{H^2}{\lambda^2}\right) = O(\gamma_k) + O\left(\frac{H^2}{\lambda^2}\right), \\ \delta_i \omega_k &= p d_k \left(\delta_i \gamma_k - \sum_{j=0}^{r-1} d_j \delta_i \gamma_j \right) + O(\delta_i \gamma_k^2) + O\left(\frac{\delta_i H^2}{\lambda^2}\right) = O(\delta_i \gamma_k) + O\left(\frac{H^2}{\lambda^2}\right). \end{aligned}$$

The last equality holds because $\theta(\delta_i H) \geq \theta(H)$. Therefore, if we have

$$\begin{aligned} \gamma_k &= O(\Delta x^r), \\ \delta_i \gamma_k &= O(\Delta x^{r-1}), \\ \frac{H^2}{\lambda^2} &= O(\Delta x^r), \end{aligned}$$

conditions (9.1a)–(9.1b) are met.

By Lemma 9, if $\varepsilon_\beta = \Omega(\Delta x^2)$, then $\gamma_k = O(\Delta x^{r-1})$ and $\delta_i \gamma_k = O(\Delta x^r)$. For this reason, let us assume $\varepsilon_\beta = \Omega(\Delta x^2)$. To conclude the analysis, it is sufficient to find a constraint on ε_τ , p and λ so that

$$\theta\left(\frac{H^2}{\lambda^2}\right) \geq r. \quad (9.4)$$

The orders of H and H^2/λ^2 are given by

$$\begin{aligned} \theta(H) &= p [\theta(\tau + \varepsilon_\tau) - \theta(B + \varepsilon_\beta)] = p [\theta(\tau + \varepsilon_\tau) - \theta(\varepsilon_\beta)], \\ \theta\left(\frac{H^2}{\lambda^2}\right) &= 2\theta(H) - 2\theta(\lambda) = 2p [\theta(\tau + \varepsilon_\tau) - \theta(\varepsilon_\beta)] - 2\theta(\lambda). \end{aligned}$$

In the first equality, $\theta(B + \varepsilon_\beta) = \theta(\varepsilon_\beta)$ because $B = O(\Delta x^2)$ by Corollary 7, $\varepsilon_\beta = \Omega(\Delta x^2)$ and both B and ε_β are non-negative. Thus, the condition on the parameters translates to

$$\theta(\tau + \varepsilon_\tau) \geq \frac{r + 2\theta(\lambda)}{2p} + \theta(\varepsilon_\beta). \quad (9.5)$$

Now, there are two cases:

Case 1 ($\theta(\tau)_{opt} \geq \frac{r+2\theta(\lambda)}{2p} + \theta(\varepsilon_\beta)$). The order of $\tau + \varepsilon_\tau$ is the smaller between $\theta(\tau)$ and $\theta(\varepsilon_\tau)$, that is,

$$\theta(\tau + \varepsilon_\tau) = \min\{\theta(\tau), \theta(\varepsilon_\tau)\},$$

and the order of τ is the smallest when $\theta(\tau) = \theta(\tau)_{opt}$ (Section 3.4). Therefore, it is sufficient to choose ε_τ so that

$$\theta(\varepsilon_\tau) \geq \frac{r + 2\theta(\lambda)}{2p} + \theta(\varepsilon_\beta).$$

Case 2 ($\theta(\tau)_{opt} < \frac{r+2\theta(\lambda)}{2p} + \theta(\varepsilon_\beta)$). In the absence of critical points, $\theta(\tau) = \theta(\tau)_{opt}$. In this case, the argument of Case 1 shows that no choice of ε_τ makes relation (9.5) hold.

In sum, we have the following result about the accuracy of the WENO-Z+ scheme:

Proposition 4. *The R th-order WENO-Z+ weights (Eq. (9.2)) with given parameters p and λ satisfy the optimality condition (Condition 3) if*

$$\boxed{\varepsilon_\beta = \Omega(\Delta x^2)} \quad \text{and} \quad \boxed{\theta(\tau)_{opt}, \theta(\varepsilon_\tau) \geq \frac{r + 2\theta(\lambda)}{2p} + \theta(\varepsilon_\beta)}.$$

9.3 The fifth-order WENO-Z+ scheme

For the purpose of illustration, consider the $R = 5$ case, with $p = 1$, $\lambda = \Delta x^{2/3}$ and $\varepsilon_\beta = \Delta x^2$. The choice of $p = 1$ will make it easier to see the accuracy properties of WENO-Z+ in practice. Let us verify which values of ε_τ satisfy the conditions of Proposition 4. We have

$$\frac{r + 2\theta(\lambda)}{2p} + \theta(\varepsilon_\beta) = \frac{3 + 4/3}{2} + 2 = \frac{25}{6}.$$

Since, for order 5, $\theta(\tau)_{opt} = 5 > 25/6$, the condition on ε_τ is

$$\frac{25}{6} \leq \theta(\varepsilon_\tau) < +\infty,$$

that is, ε_τ can be as small as one desires.

9.4 Accuracy tests

In the following, we will test the accuracy of WENO-Z+ with four different sets of parameters, which are described in Table 2.

Profile	λ	p	ε_β	ε_τ	Optimal order?
I	$\Delta x^{2/3}$	1	10^{-40}	10^{-40}	No, ε_β is too small
II	$\Delta x^{2/3}$	1	Δx^2	10^{-40}	Yes
III	$\Delta x^{2/3}$	1	Δx^2	Δx	No, ε_τ is too large
IV	Δx^2	1	Δx^2	10^{-40}	No, λ is too small

Table 2 – Different profiles of WENO-Z+ for accuracy tests

Profile I is the standard set of parameters for the WENO-Z+ (cf. Section 8.2). Since ε_β is negligible, we expect its order of accuracy to be smaller than 5 at some critical points.

Profile II is the same as Profile I, except for ε_β , which is changed to Δx^2 so as to satisfy Proposition 4.

Profile III is an example for showing that ε_τ cannot be too large, otherwise the accuracy degrades. Here, $\theta(\varepsilon_\tau) = 1 \not\geq \frac{r + 2\theta(\lambda)}{2p} + \theta(\varepsilon_\beta) = \frac{25}{6}$, and we cannot apply Proposition 4.

Profile IV is another example, this time for showing that λ cannot be too small. Here,

$$\frac{r + 2\theta(\lambda)}{2p} + \theta(\varepsilon_\beta) = \frac{3 + 4}{2} + 2 = \frac{11}{2} > \theta(\tau)_{opt} = 5$$

and, again, Proposition 4 cannot be applied.

We run the accuracy test (Section 2.5.4) with grid sizes $N = \{20, 40, 60, \dots, 200\}$. The computations were done with double precision.

Figure 33 shows the L^1 order (left column) and error (right column) as functions of N , for the functions $g_0(x)$, $g_1(x)$ and $g_2(x)$ (top, middle, and bottom rows, respectively), where $g_0(x)$ does not contain a critical point, and $g_1(x)$ and $g_2(x)$ contain a single critical point of order 1 and 2, respectively. All profiles achieve the formal order of accuracy in the test with $g_0(x)$, evidencing that WENO-Z+ is indeed a fifth-order scheme regardless of its parameters. However, only Profile II has optimal accuracy for the tests with $g_1(x)$ and $g_2(x)$, which contain critical points. An interesting result is that Profile IV has the smallest errors in this range of grid points, in spite of its order being smaller than 5. The smaller errors of Profile IV can be due the fact that λ is smaller, implying that the sharpening term η_k^{-1} (Eq. (8.2)) has a smaller contribution.

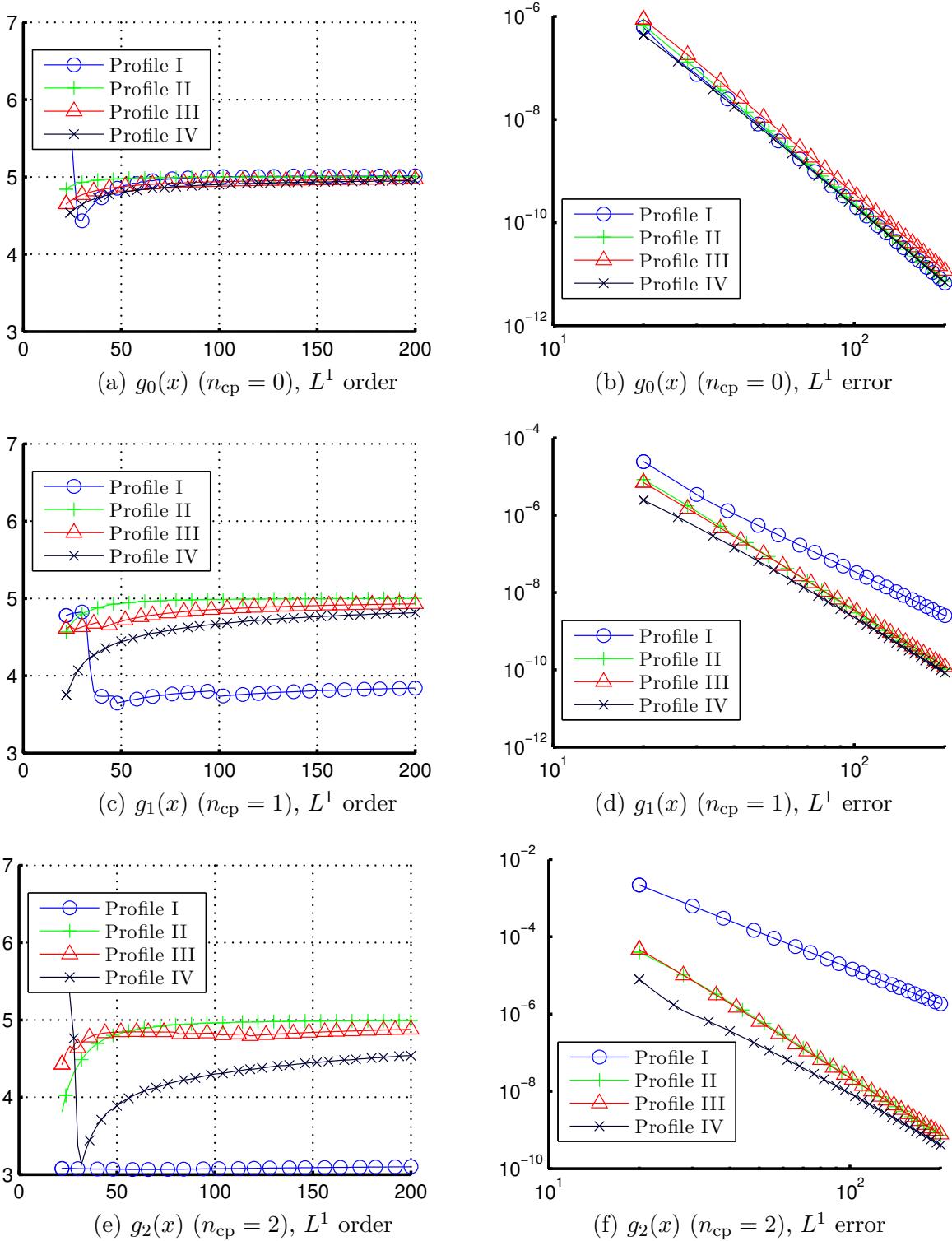
9.5 “Accuracy at critical points” versus “sharpness”

Still considering the profiles in Table 2, we run the Titarev–Toro shock-entropy test (Fig. 34). Interestingly, in the Titarev–Toro test, Profile I, which has the largest errors and smallest orders in Fig. 33, has the second best results overall at the critical points of the high-frequency waves, close to the first place, Profile II. On the other hand, Profile IV, which has the smallest errors in Fig. 33, has the worst results here. It is clear that Profile I performed better than Profiles III and IV in Fig. 34 not because of better accuracy properties at the critical points (which it hasn’t), but because of the sharpening term (cf. Eq. (8.2))

$$\lambda\eta_k^{-1} = \lambda \left(\frac{\beta_k + \varepsilon_\beta}{\tau + \varepsilon_\tau} \right). \quad (9.6)$$

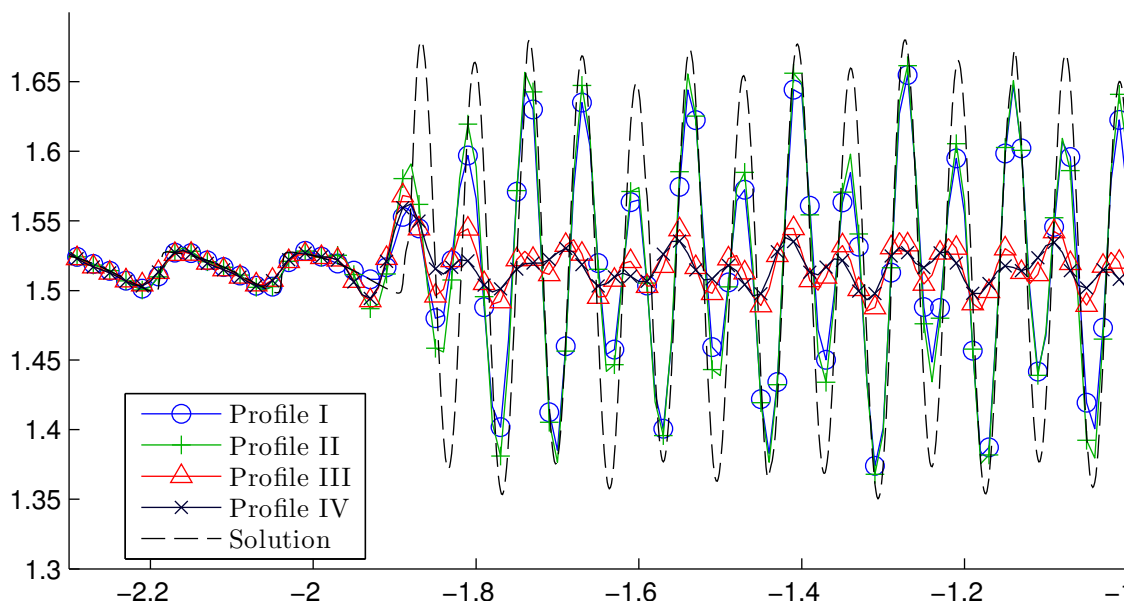
From Eq. 9.6, we can see that the sharpening term gets smaller if λ decreases or ε_τ increases. This is exactly what happens for Profile III (which has a larger ε_τ than Profile I) and Profile IV (smaller λ). Also, although Profile II does have better accuracy at critical points than Profile I, the better results in Fig. 34 may well be entirely due to the fact that Profile II has a larger ε_β than Profile I and therefore, by Eq. (9.6), this results in a larger sharpening term.

Figure 33 – Accuracy tests for the WENO-Z+ scheme with different parameter profiles



The profiles are described in Table 2. The x axis corresponds to different grid sizes $N = [20, 200]$. The error plots are in log-log scale.

Figure 34 – Numerical solution of the shock-entropy problem of Titarev–Toro by the WENO-Z+ scheme with different profiles of parameters



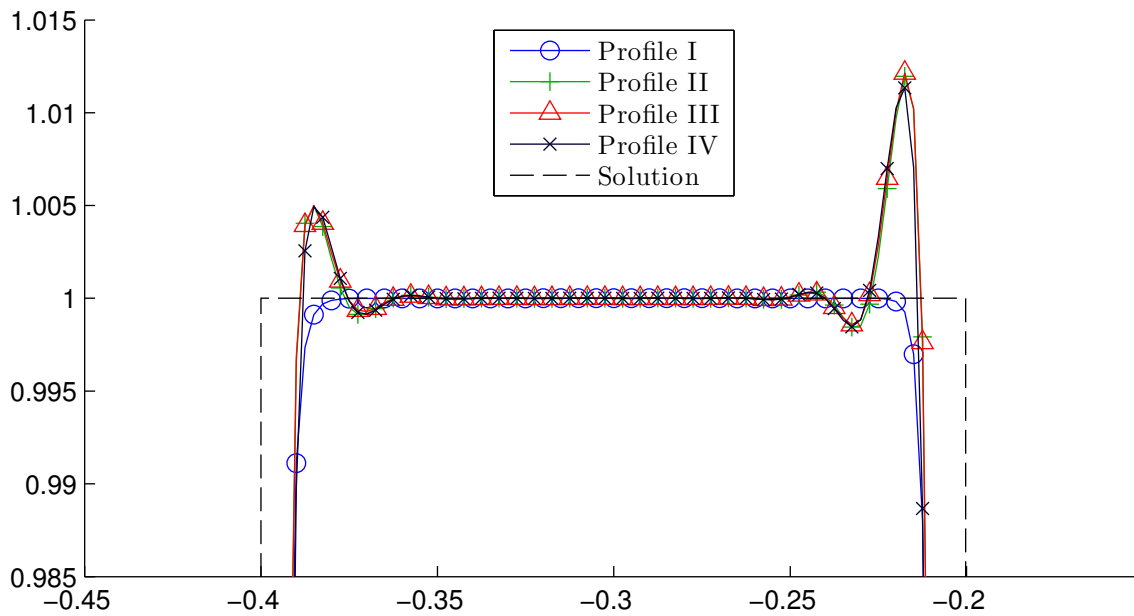
The figure shows a zoom in the region of high-frequency waves of the density of the solutions at $t = 5$. A grid with $N = 1000$ points was used. $CFL = 0.5$. The profiles are listed in Table 2.

9.6 Accuracy and spurious oscillations

Still using the same profiles, we run the Gaussian-square-triangle-ellipse linear test (Fig. 35). It is evident that Profile I is less oscillatory than the others. This is due to the sensitivity parameter ε_β , which assumes the value 10^{-40} for the Profile I and Δx^2 for the other Profiles. As discussed in [22], the larger the value of the sensitivity parameter, the more oscillatory the corresponding WENO schemes are.

So, which profile is most recommended? If the solution of a given problem is known beforehand to be smooth, it may be more advisable to use Profile II (with $\varepsilon_\beta = \Delta x^2$) so as to recover the optimal order (and sharper results) at critical points, since in this case the solution won't suffer with spurious oscillations due to large ε_β . But then again, if the solution is known to be smooth, one should be using a more computationally efficient numerical scheme instead, e.g. spectral methods. The *raison d'être* of WENO schemes is dealing with discontinuous solutions while avoiding spurious oscillations. This is why Profile I is the one we recommend for most cases.

Figure 35 – Numerical solution of the Gaussian-square-triangle-ellipse linear test by the WENO-Z+ scheme with different profiles of parameters



The figure show a zoom on the top of the square wave at $t = 2$. A grid with $N = 800$ points was used. $CFL = 0.5$. The profiles are listed in Table 2.

Conclusions

We introduced the WENO-Z+ scheme, consisting of the fifth-order WENO-Z with the addition of a novel and simple sharpening term that is based on the ratio of its smoothness indicators. This sharpening term increases the resolution of the scheme near critical points of the solution in a controlled way. The new scheme was able to achieve significantly better results than the classical WENO and WENO-Z schemes at tests combining shocks and fine smooth structures like the shock-entropy tests of Shu–Osher and Titarev–Toro. In some tests, it was even able to overcome the results of higher-order WENO-Z schemes, showing much sharper profiles at high-frequency waves.

The accuracy of WENO-Z+ at critical points of the solution was also analyzed and resulted in a condition that the parameter ε has to satisfy in order to achieve the optimal order of convergence. Nevertheless, the use of ε violating this condition still maintain the extra sharpness of WENO-Z+, evidencing that optimal accuracy at critical points is not as relevant to the sharpness of WENO schemes as it is currently thought. The numerical results indicate that the new scheme deserves further investigation with respect to its higher-order versions and the analytical tuning of its set of parameters.

Bibliography

- [1] LAX, P. D. *Hyperbolic systems of conservation laws and the mathematical theory of shock waves*. [S.l.]: SIAM, 1973. ISBN 0898711770, 9780898711776. Cited on page 27.
- [2] LEVEQUE, R. J. *Numerical Methods for Conservation Laws*. [S.l.]: Birkhäuser Verlag, 1992. (Lectures in Mathematics ETH Zürich). ISBN 9783764327231. Cited 3 times on pages 27, 30, and 40.
- [3] TORO, E. F. *Riemann Solvers and Numerical Methods for Fluid Dynamics: A Practical Introduction*. [S.l.]: Springer, 2009. ISBN 9783540498346. Cited 2 times on pages 27 and 53.
- [4] EVANS, L. C. *Partial Differential Equations*. [S.l.]: American Mathematical Society, 2010. (Graduate studies in mathematics). ISBN 9780821849743. Cited on page 27.
- [5] SHU, C.-W. Essentially non-oscillatory and weighted essentially non-oscillatory schemes for hyperbolic conservation laws. *NASA/CR-97-206253 ICASE Report*, n. 97-65, 1997. Cited 8 times on pages 27, 30, 39, 40, 41, 42, 43, and 47.
- [6] BORGES, R. B. de R. *Esquemas Essencialmente Não-Oscilatórios para Leis de Conservação Hiperbólicas*. Dissertação (Mestrado) — Universidade Federal do Rio de Janeiro, Rio de Janeiro, mar. 2006. Cited 10 times on pages 27, 32, 39, 41, 59, 60, 67, 69, 75, and 79.
- [7] WESSELING, P. *Principles of computational fluid dynamics*. [S.l.]: Springer Science & Business, 2009. ISBN 9783642051463. Cited on page 27.
- [8] PIROZZOLI, S. On the spectral properties of shock-capturing schemes. *J. Comput. Phys.*, Elsevier, v. 219, n. 2, p. 489–497, 2006. Cited 3 times on pages 30, 50, and 51.
- [9] SHI, J.; ZHANG, Y.-T.; SHU, C.-W. Resolution of high order WENO schemes for complicated flow structures. *J. Comput. Phys.*, v. 186, n. 2, p. 690–696, 2003. ISSN 0021-9991. Cited on page 30.
- [10] HARTEN, A.; OSHER, S. Uniformly high-order accurate non-oscillatory schemes, I. *SIAM J. Numer. Anal.*, v. 24, n. 2, p. 279–309, 1987. Cited on page 30.
- [11] HARTEN, A.; ENGQUIST, B.; OSHER, S.; CHAKRAVARTHY, S. R. Uniformly high order accurate essentially non-oscillatory schemes, III. *J. Comput. Phys.*, v. 71, n. 2, p. 231–303, 1987. ISSN 0021-9991. Cited 2 times on pages 30 and 59.

- [12] SHU, C.-W.; OSHER, S. Efficient implementation of essentially non-oscillatory shock-capturing schemes. *J. Comput. Phys.*, Elsevier, v. 77, n. 2, p. 439–471, 1988. Cited on page 30.
- [13] SHU, C.-W.; OSHER, S. Efficient implementation of essentially non-oscillatory shock-capturing schemes, II. *J. Comput. Phys.*, v. 83, n. 1, p. 32–78, 1989. ISSN 0021-9991. Cited 5 times on pages 30, 40, 41, 53, and 59.
- [14] LIU, X.-D.; OSHER, S.; CHAN, T. Weighted essentially non-oscillatory schemes. *J. Comput. Phys.*, v. 115, n. 1, p. 200–212, 1994. ISSN 0021-9991. Cited 4 times on pages 32, 59, 63, and 64.
- [15] JIANG, G.-S.; SHU, C.-W. Efficient implementation of weighted ENO schemes. *J. Comput. Phys.*, v. 126, n. 1, p. 202–228, 1996. ISSN 0021-9991. Cited 9 times on pages 32, 46, 47, 51, 59, 60, 63, 64, and 117.
- [16] BORGES, R.; CARMONA, M.; COSTA, B.; DON, W. S. An improved weighted essentially non-oscillatory scheme for hyperbolic conservation laws. *J. Comput. Phys.*, v. 227, n. 6, p. 3191–3211, 2008. ISSN 0021-9991. Cited 11 times on pages 32, 35, 39, 47, 60, 61, 63, 67, 69, 70, and 75.
- [17] CASTRO, M. *Esquemas Essencialmente Não-Oscilatórios de Alta Precisão para Leis de Conservação Hiperbólicas*. Dissertação (Mestrado) — Universidade Federal do Rio de Janeiro, Rio de Janeiro, nov. 2009. Cited 3 times on pages 32, 60, and 69.
- [18] CASTRO, M.; COSTA, B.; DON, W. S. High order weighted essentially non-oscillatory WENO-Z schemes for hyperbolic conservation laws. *J. Comput. Phys.*, v. 230, n. 5, p. 1766–1792, 2011. ISSN 0021-9991. Cited 7 times on pages 32, 60, 61, 65, 68, 69, and 70.
- [19] HENRICK, A. K.; ASLAM, T. D.; POWERS, J. M. Mapped weighted essentially non-oscillatory schemes: Achieving optimal order near critical points. *J. Comput. Phys.*, v. 207, n. 2, p. 542–567, 2005. ISSN 0021-9991. Cited 7 times on pages 35, 39, 47, 55, 63, 65, and 70.
- [20] YAMALEEV, N. K.; CARPENTER, M. H. Third-order energy stable WENO scheme. *J. Comput. Phys.*, v. 228, n. 8, p. 3025–3047, 2009. ISSN 0021-9991. Cited 3 times on pages 35, 70, and 77.
- [21] ARÀNDIGA, F.; BAEZA, A.; BELDA, A. M.; MULET, P. Analysis of WENO schemes for full and global accuracy. *SIAM J. Numer. Anal.*, Society for Industrial and Applied Mathematics, Philadelphia, PA, USA, v. 49, n. 2, p. 893–915, apr 2011. ISSN 0036-1429. Cited 4 times on pages 35, 45, 55, and 70.

- [22] DON, W.-S.; BORGES, R. Accuracy of the weighted essentially non-oscillatory conservative finite difference schemes. *J. Comput. Phys.*, v. 250, p. 347–372, 2013. ISSN 0021-9991. Cited 11 times on pages [35](#), [39](#), [41](#), [55](#), [61](#), [68](#), [70](#), [99](#), [105](#), [117](#), and [121](#).
- [23] GOTTLIEB, S.; SHU, C.-W.; TADMOR, E. Strong stability-preserving high-order time discretization methods. *SIAM review*, SIAM, v. 43, n. 1, p. 89–112, 2001. Cited on page [42](#).
- [24] TITAREV, V. A.; TORO, E. F. ADER: Arbitrary high order godunov approach. *J. Sci. Comput.*, Springer, v. 17, n. 1-4, p. 609–618, 2002. Cited on page [42](#).
- [25] BALSARA, D. S.; SHU, C.-W. Monotonicity preserving weighted essentially non-oscillatory schemes with increasingly high order of accuracy. *J. Comput. Phys.*, v. 160, n. 2, p. 405–452, 2000. ISSN 0021-9991. Cited 6 times on pages [43](#), [45](#), [60](#), [64](#), [77](#), and [117](#).
- [26] GEROLYMOS, G. A.; SÉNÉCHAL, D.; VALLET, I. Very-high-order WENO schemes. *J. Comput. Phys.*, v. 228, n. 23, p. 8481–8524, 2009. ISSN 0021-9991. Cited 5 times on pages [43](#), [45](#), [60](#), [64](#), and [117](#).
- [27] WANG, R.; SPITERI, R. J. Linear instability of the fifth-order WENO method. *SIAM J. Numer. Anal.*, SIAM, v. 45, n. 5, p. 1871–1901, 2007. Cited on page [47](#).
- [28] WOODWARD, P.; COLELLA, P. The numerical simulation of two-dimensional fluid flow with strong shocks. *J. Comput. Phys.*, Elsevier, v. 54, n. 1, p. 115–173, 1984. Cited on page [50](#).
- [29] ZHAO, S.; LARDJANE, N.; FEDIOUN, I. Comparison of improved finite-difference WENO schemes for the implicit large eddy simulation of turbulent non-reacting and reacting high-speed shear flows. *Comput. Fluids*, Elsevier, v. 95, p. 74–87, 2014. Cited 3 times on pages [51](#), [69](#), and [70](#).
- [30] LAX, P. D. Weak solutions of nonlinear hyperbolic equations and their numerical computation. *Comm. Pure Appl. Math.*, Wiley Online Library, v. 7, n. 1, p. 159–193, 1954. Cited on page [53](#).
- [31] SOD, G. A. A survey of several finite difference methods for systems of nonlinear hyperbolic conservation laws. *J. Comput. Phys.*, Elsevier, v. 27, n. 1, p. 1–31, 1978. Cited on page [53](#).
- [32] TITAREV, V. A.; TORO, E. F. Finite-volume WENO schemes for three-dimensional conservation laws. *J. Comput. Phys.*, v. 201, n. 1, p. 238–260, 2004. ISSN 0021-9991. Cited on page [55](#).

-
- [33] SHEN, Y.; ZHA, G. Improvement of the WENO scheme smoothness estimator. *Int. J. Numer. Meth. Fl.*, John Wiley & Sons, Ltd., v. 64, n. 6, p. 653–675, 2009. ISSN 1097-0363. Cited on page [67](#).
- [34] HA, Y.; KIM, C. H.; LEE, Y. J.; YOON, J. An improved weighted essentially non-oscillatory scheme with a new smoothness indicator. *J. Comput. Phys.*, v. 232, n. 1, p. 68–86, 2013. ISSN 0021-9991. Cited 2 times on pages [67](#) and [70](#).
- [35] YAMALEEV, N. K.; CARPENTER, M. H. A systematic methodology for constructing high-order energy stable WENO schemes. *J. Comput. Phys.*, v. 228, n. 11, p. 4248–4272, 2009. ISSN 0021-9991. Cited 2 times on pages [70](#) and [77](#).
- [36] SURESH, A.; HUYNH, H. T. Accurate monotonicity-preserving schemes with Runge–Kutta time stepping. *J. Comput. Phys.*, v. 136, n. 1, p. 83–99, 1997. ISSN 0021-9991. Cited on page [77](#).

APPENDIX A – Constants and expressions used by WENO schemes from order 3 to 9

This appendix contains the expressions of the terms which appears in the formulation of WENO schemes — the substencil approximation $\hat{f}_{i+\frac{1}{2}}^k$ (Chapter 2), ideal weights d_k (Section 2.2), smoothness indicators β_k of Jiang–Shu (Section 3.3), and the global smoothness indicator τ (Section 3.4) — for all relevant k ($k = 0, \dots, r - 1$) and orders $R = 3, 5, 7$, and 9.

A.1 Order 3

Table 3 shows the values of d_k and the expressions of the substencil approximation $\hat{f}_{i+\frac{1}{2}}^k$ and the second-order approximation to $f'(x_i)\Delta x$ in the substencil \mathcal{S}_k , denoted D_1^k .

k	d_k	$\hat{f}_{i+\frac{1}{2}}^k$	D_1^k
0	$\frac{1}{3}$	$\frac{-f_{i-1} + 3f_i}{2}$	$f_i - f_{i-1}$
1	$\frac{2}{3}$	$\frac{f_i + f_{i+1}}{2}$	$f_{i+1} - f_i$

Table 3 – Expressions of d_k , $\hat{f}_{i+\frac{1}{2}}^k$, and D_1^k , for order $R = 3$ and varying k .

β_k can be written in terms of D_1^k , and τ in terms of β_k , as

$$\beta_k = (D_1^k)^2, \quad k = 0, 1,$$

$$\tau = |\beta_0 - \beta_1|.$$

A.2 Order 5

Table 4 shows the values of d_k , and the expressions of the substencil approximation $\hat{f}_{i+\frac{1}{2}}^k$ and the third-order approximations to $f'(x_i)\Delta x$ and $f''(x_i)\Delta x^2$ in the substencil \mathcal{S}_k , denoted D_1^k and D_2^k , respectively.

β_k can be written in terms of D_1^k and D_2^k , and τ in terms of β_k , as

$$\beta_k = (D_1^k)^2 + \frac{13}{12}(D_2^k)^2, \quad k = 0, 1, 2,$$

$$\tau = |\beta_0 - \beta_2|.$$

k	d_k	$\hat{f}_{i+\frac{1}{2}}^k$	D_1^k	D_2^k
0	$\frac{1}{10}$	$\frac{2f_{i-2} - 7f_{i-1} + 11f_i}{6}$	$\frac{f_{i-2} - 4f_{i-1} + 3f_i}{2}$	$f_{i-2} - 2f_{i-1} + f_i$
1	$\frac{3}{5}$	$\frac{-f_{i-1} + 5f_i + 2f_{i+1}}{6}$	$\frac{-f_{i-1} + f_{i+1}}{2}$	$f_{i-1} - 2f_i + f_{i+1}$
2	$\frac{3}{10}$	$\frac{2f_i + 5f_{i+1} - f_{i+2}}{6}$	$\frac{-3f_i + 4f_{i+1} - f_{i+2}}{2}$	$f_i - 2f_{i+1} + f_{i+2}$

Table 4 – Expressions of d_k , $\hat{f}_{i+\frac{1}{2}}^k$, D_1^k , and D_2^k , for order $R = 5$ and varying k .

A.3 Order 7

Table 5 shows the values of d_k , and the expressions of the substencil approximation $\hat{f}_{i+\frac{1}{2}}^k$ and the fourth-order approximations to $f'(x_i)\Delta x$, $f''(x_i)\Delta x^2$, and $f'''(x_i)\Delta x^3$ in the substencil \mathcal{S}_k , denoted D_1^k , D_2^k , and D_3^k , respectively.

β_k can be written in terms of D_1^k , D_2^k and D_3^k , and τ in terms of β_k , as

$$\beta_k = (D_1^k)^2 + \frac{13}{12}(D_2^k)^2 + \frac{781}{720}(D_3^k)^2, \quad k = 0, 1, 2, 3,$$

$$\tau = |\beta_0 + 3\beta_1 - 3\beta_2 - \beta_3|.$$

A.4 Order 9

Finally, Table 6 shows the values of d_k , and the expressions of the substencil approximation $\hat{f}_{i+\frac{1}{2}}^k$ and the fifth-order approximations to $f'(x_i)\Delta x$, $f''(x_i)\Delta x^2$, $f'''(x_i)\Delta x^3$, and $f''''(x_i)\Delta x^4$ in the substencil \mathcal{S}_k , denoted D_1^k , D_2^k , D_3^k , and D_4^k , respectively.

β_k can be written in terms of D_1^k , D_2^k and D_3^k , and τ in terms of β_k , as

$$\beta_k = (D_1^k)^2 + \frac{13}{12}(D_2^k)^2 + \frac{781}{720}(D_3^k)^2 - \frac{1}{360}D_2^k D_4^k + \frac{32803}{30240}(D_4^k)^2, \quad k = 0, 1, 2, 3, 4,$$

$$\tau = |\beta_0 + 2\beta_1 - 6\beta_2 + 2\beta_3 + \beta_4|.$$

k	d_k	$\hat{f}_{i+\frac{1}{2}}^k$	D_1^k	D_2^k	D_3^k
0	$\frac{1}{35}$	$\frac{-3f_{i-3} + 13f_{i-2} - 23f_{i-1} + 25f_i}{12}$	$\frac{-2f_{i-3} + 9f_{i-2} - 18f_{i-1} + 11f_i}{6}$	$-f_{i-3} + 4f_{i-2} - 5f_{i-1} + 2f_i$	$-f_{i-3} + 3f_{i-2} - 3f_{i-1} + f_i$
1	$\frac{12}{35}$	$\frac{f_{i-2} - 5f_{i-1} + 13f_i + 3f_{i+1}}{12}$	$\frac{f_{i-2} - 6f_{i-1} + 3f_i + 2f_{i+1}}{6}$	$f_{i-1} - 2f_i + f_{i+1}$	$-f_{i-2} + 3f_{i-1} - 3f_i + f_{i+1}$
2	$\frac{18}{35}$	$\frac{-f_{i-1} + 7f_i + 7f_{i+1} - f_{i+2}}{12}$	$\frac{-2f_{i-1} - 3f_i + 6f_{i+1} - f_{i+2}}{6}$	$f_{i-1} - 2f_i + f_{i+1}$	$-f_{i-1} + 3f_i - 3f_{i+1} + f_{i+2}$
3	$\frac{4}{35}$	$\frac{3f_i + 13f_{i+1} - 5f_{i+2} + f_{i+3}}{12}$	$\frac{-11f_i + 18f_{i+1} - 9f_{i+2} + 2f_{i+3}}{6}$	$2f_i - 5f_{i+1} + 4f_{i+2} - f_{i+3}$	$-f_i + 3f_{i+1} - 3f_{i+2} + f_{i+3}$

Table 5 – Expressions of d_k , $\hat{f}_{i+\frac{1}{2}}^k$, D_1^k , D_2^k , and D_3^k , for order $R = 7$ and varying k .

k	d_k	$\hat{f}_{i+\frac{1}{2}}^k$	D_1^k	D_2^k
0	$\frac{1}{126}$	$\frac{12f_{i-4} - 63f_{i-3} + 137f_{i-2} - 163f_{i-1} + 137f_i}{60}$	$\frac{3f_{i-4} - 16f_{i-3} + 36f_{i-2} - 48f_{i-1} + 25f_i}{12}$	$\frac{11f_{i-4} - 56f_{i-3} + 114f_{i-2} - 104f_{i-1} + 35f_i}{12}$
1	$\frac{10}{63}$	$\frac{-3f_{i-3} + 17f_{i-2} - 43f_{i-1} + 77f_i + 12f_{i+1}}{60}$	$\frac{-f_{i-3} + 6f_{i-2} - 18f_{i-1} + 10f_i + 3f_{i+1}}{12}$	$\frac{-f_{i-3} + 4f_{i-2} + 6f_{i-1} - 20f_i + 11f_{i+1}}{12}$
2	$\frac{10}{21}$	$\frac{2f_{i-2} - 13f_{i-1} + 47f_i + 27f_{i+1} - 3f_{i+2}}{60}$	$\frac{f_{i-2} - 8f_{i-1} + 8f_{i+1} - f_{i+2}}{12}$	$\frac{-f_{i-2} + 16f_{i-1} - 30f_i + 16f_{i+1} - f_{i+2}}{12}$
3	$\frac{20}{63}$	$\frac{-3f_{i-1} + 27f_i + 47f_{i+1} - 13f_{i+2} + 2f_{i+3}}{60}$	$\frac{-3f_{i-1} - 10f_i + 18f_{i+1} - 6f_{i+2} + f_{i+3}}{12}$	$\frac{11f_{i-1} - 20f_i + 6f_{i+1} + 4f_{i+2} - f_{i+3}}{12}$
4	$\frac{5}{126}$	$\frac{12f_i + 77f_{i+1} - 43f_{i+2} + 17f_{i+3} - 3f_{i+4}}{60}$	$\frac{-25f_i + 48f_{i+1} - 36f_{i+2} + 16f_{i+3} - 3f_{i+4}}{12}$	$\frac{35f_i - 104f_{i+1} + 114f_{i+2} - 56f_{i+3} + 11f_{i+4}}{12}$
k	D_3^k	D_4^k		
0	$\frac{3f_{i-4} - 14f_{i-3} + 24f_{i-2} - 18f_{i-1} + 5f_i}{2}$	$f_{i-4} - 4f_{i-3} + 6f_{i-2} - 4f_{i-1} + f_i$		
1	$\frac{f_{i-3} - 6f_{i-2} + 12f_{i-1} - 10f_i + 3f_{i+1}}{2}$	$f_{i-3} - 4f_{i-2} + 6f_{i-1} - 4f_i + f_{i+1}$		
2	$\frac{-f_{i-2} + 2f_{i-1} - 2f_{i+1} + f_{i+2}}{2}$	$f_{i-2} - 4f_{i-1} + 6f_i - 4f_{i+1} + f_{i+2}$		
3	$\frac{-3f_{i-1} + 10f_i - 12f_{i+1} + 6f_{i+2} - f_{i+3}}{2}$	$f_{i-1} - 4f_i + 6f_{i+1} - 4f_{i+2} + f_{i+3}$		
4	$\frac{-5f_i + 18f_{i+1} - 24f_{i+2} + 14f_{i+3} - 3f_{i+4}}{2}$	$f_i - 4f_{i+1} + 6f_{i+2} - 4f_{i+3} + f_{i+4}$		

Table 6 – Expressions of d_k , $\hat{f}_{i+\frac{1}{2}}^k$, D_1^k , D_2^k , D_3^k , and D_4^k , for order $R = 9$ and varying k .

APPENDIX B – Properties of the smoothness indicator β

Let's recall the definition of the smoothness indicator β (cf. Definition 6):

$$\beta_k = \sum_{l=1}^{r-1} \Delta x^{2l-1} \int_{x_{i-\frac{1}{2}}}^{x_{i+\frac{1}{2}}} \left(\frac{d^l}{dx^l} \hat{f}^k(x) \right)^2 dx, \quad k = 0, \dots, r-1. \quad (\text{B.1})$$

For substencil order $r = 3$, we have seen that β_k can be written in a simpler form, as a sum of powers of finite difference approximations to derivatives of f at x_i ,

$$\begin{aligned} \beta_0 &= \frac{1}{4} (f_{i-2} - 4f_{i-1} + 3f_i)^2 + \frac{13}{12} (f_{i-2} - 2f_{i-1} + f_i)^2, \\ \beta_1 &= \frac{1}{4} (-f_{i-1} + f_{i+1})^2 + \frac{13}{12} (f_{i-1} - 2f_i + f_{i+1})^2, \\ \beta_2 &= \frac{1}{4} (-3f_i + 4f_{i+1} - f_{i+2})^2 + \frac{13}{12} (f_i - 2f_{i+1} + f_{i+2})^2. \end{aligned} \quad (\text{B.2})$$

Notice that these expressions collectively satisfy

$$\beta_k = (f'_i \Delta x + O(\Delta x^3))^2 + \frac{13}{12} (f''_i \Delta x^2 + O(\Delta x^3))^2, \quad k = 0, 1, 2, \quad (\text{B.3})$$

the $O(\Delta x^3)$ terms being different at each substencil \mathcal{S}_k . This allows us to write β_k in the convenient-for-proofs form

$$\begin{aligned} \beta_k &= \left((f'_i)^2 \Delta x^2 + O(\Delta x^4) \right) + \left(\frac{13}{12} (f''_i)^2 \Delta x^4 + O(\Delta x^5) \right) \\ &= \left((f'_i)^2 \Delta x^2 + \frac{13}{12} (f''_i)^2 \Delta x^4 \right) + O(\Delta x^4) = B + R_k. \end{aligned}$$

It is not immediate how, from the definition of β_k , one obtains the more convenient finite differences form (B.2), since Eq. (B.1) involves integrals of squares of derivatives of $\hat{f}^k(x)$ — a polynomial related to $f(x)$, indeed, but distinct from it. Until recently, we had these convenient expressions for $r = 2$ and $r = 3$ only [15], the existing higher-order expressions being rather long and not as useful for accuracy proofs [25, 26]. But in [22], we achieved a result proving the existence of convenient expressions like (B.3) for any suborder r , and we gave such expressions to suborders up to $r = 6$. The result is stated as follows:

Proposition 5. *The smoothness indicators β_k , defined by (B.1), can be written in a bilinear form as*

$$\beta_k = \langle \phi^k, \mathbf{C} \phi^k \rangle = \sum_{m=1}^{r-1} \sum_{n=1}^{r-1} C_{mn} \phi_m^k \phi_n^k, \quad (\text{B.4})$$

where

i) ϕ^k is a $(r - 1)$ vector, whose elements

$$\phi_m^k = \Delta x^{m-1} \int_{x_{i-\frac{1}{2}}}^{x_{i+\frac{1}{2}}} \frac{d^m}{dx^m} \hat{f}^k(x) dx = f_i^{(m)} \Delta x^m + O(\Delta x^r), \quad m = 1, \dots, r-1, \quad (\text{B.5})$$

are the r th-degree polynomial approximation to $f_i^{(m)} \Delta x^m$ in substencil \mathcal{S}_k . The dependence of ϕ^k on k relies on the $O(\Delta x^r)$ terms only.

ii) \mathbf{C} , the smoothness measurement matrix, is a $(r - 1) \times (r - 1)$ constant symmetric positive semidefnite matrix.

For instance, for $r = 4$, Proposition 5 implies that β_k can be written as

$$\begin{aligned} \beta_k &= C_{11}(f_i' \Delta x + O(\Delta x^4))^2 + 2C_{12}(f_i' \Delta x + O(\Delta x^4))(f_i'' \Delta x^2 + O(\Delta x^4)) \\ &\quad + C_{22}(f_i'' \Delta x^2 + O(\Delta x^4))^2 + 2C_{23}(f_i'' \Delta x^2 + O(\Delta x^4))(f_i''' \Delta x^3 + O(\Delta x^4)) \\ &\quad + C_{33}(f_i''' \Delta x^3 + O(\Delta x^4))^2 + 2C_{13}(f_i' \Delta x + O(\Delta x^4))(f_i''' \Delta x^3 + O(\Delta x^4)), \end{aligned}$$

and this allows us to write

$$\begin{aligned} \beta_k &= \left(C_{11}(f_i')^2 \Delta x^2 + 2C_{12}f_i' f_i'' \Delta x^3 + C_{22}(f_i'')^2 \Delta x^4 + 2C_{23}f_i'' f_i''' \Delta x^5 \right. \\ &\quad \left. + C_{33}(f_i''')^2 \Delta x^6 + 2C_{13}f_i' f_i''' \Delta x^4 \right) + O(\Delta x^5) = B + R_k. \end{aligned}$$

The proof of Proposition 5 uses the following lemma about polynomials:

Lemma 6. Let $p(x)$ be a polynomial of degree M and $x_i \in \mathbb{R}$ a given point. There exists a $(M + 1) \times (M + 1)$ constant symmetric matrix \mathbf{A} such that

$$\Delta x \int_{x_i - \Delta x/2}^{x_i + \Delta x/2} (p(x))^2 dx = \langle \mathbf{v}, \mathbf{A} \mathbf{v} \rangle, \quad (\text{B.6})$$

where \mathbf{v} is a vector whose elements are

$$v_m = \Delta x^m \int_{x_i - \Delta x/2}^{x_i + \Delta x/2} \frac{d^m}{dx^m} p(x) dx, \quad m = 0, \dots, M. \quad (\text{B.7})$$

Proof. Without loss of generality, we may assume $x_i = 0$. Consider $p(x)$ a generic polynomial of degree M , namely,

$$p(x) = \sum_{m=0}^M a_m x^m. \quad (\text{B.8})$$

Let \mathbf{a} denote the vector of polynomial coefficients $\{a_m, m = 0, \dots, M\}$ of $p(x)$, and let \mathbf{v} be as stated by Eq. (B.7). By substituting Eq. (B.8) into Eq. (B.7), we notice that v_m is in fact a linear form of \mathbf{a} ,

$$v_m = \sum_{n=0}^M U_{mn} \Delta x^{n+1} a_n, \quad (\text{B.9})$$

or $\mathbf{v} = \mathbf{U}\mathbf{D}\mathbf{a}$ in a matrix-vector form, where the elements of the diagonal matrix \mathbf{D} and of upper triangular matrix \mathbf{U} are

$$D_{mm} = \Delta x^{m+1}, \quad U_{mn} = \begin{cases} \frac{n!}{(n-m+1)!2^{n-m}}, & \text{if } m \leq n, \text{ and } m+n \text{ is even,} \\ 0, & \text{otherwise,} \end{cases} \quad (\text{B.10})$$

respectively. Since the constant matrix \mathbf{U} is an upper triangular matrix with positive diagonal elements, \mathbf{U} is invertible and, hence, $\mathbf{D}\mathbf{a} = \mathbf{U}^{-1}\mathbf{v}$.

Moreover, by substituting Eq. (B.8) into the left-hand side of Eq. (B.6), one has a bilinear form,

$$\Delta x \int_{-\Delta x/2}^{\Delta x/2} (p(x))^2 dx = \sum_{m=0}^M \sum_{n=0}^M B_{mn} \Delta x^{m+n+2} a_m a_n = \langle \mathbf{D}\mathbf{a}, \mathbf{B}\mathbf{D}\mathbf{a} \rangle \triangleq \langle \mathbf{v}, \mathbf{A}\mathbf{v} \rangle, \quad (\text{B.11})$$

where the elements of the constant symmetric matrix \mathbf{B} are

$$B_{mn} = \begin{cases} \frac{1}{2^{m+n}(m+n+1)}, & \text{if } m+n \text{ is even,} \\ 0, & \text{otherwise,} \end{cases} \quad (\text{B.12})$$

and $\mathbf{A} = (\mathbf{U}^{-1})^T \mathbf{B} \mathbf{U}^{-1}$ is a constant symmetric matrix. \square

Now, we are ready to prove the proposition.

Proof of Proposition 5. In the definition of the smoothness indicators β_k (Eq. (B.1)),

$$\beta_k = \sum_{l=1}^{r-1} \Delta x^{2l-1} \int_{x_{i-\frac{1}{2}}}^{x_{i+\frac{1}{2}}} \left(\frac{d^l}{dx^l} \hat{f}^k(x) \right)^2 dx,$$

$\hat{f}^k(x)$ is a polynomial of degree $(r-1)$, and it satisfies

$$\hat{f}^k(x) = h(x) + O(\Delta x^r). \quad (\text{B.13})$$

Therefore, by Lemma 6, there exist $(r-l-1) \times (r-l-1)$ constant symmetric matrices \mathbf{A}^l such that

$$\beta_k = \sum_{l=1}^{r-1} \Delta x^{2l-2} \langle \mathbf{v}^{k,l}, \mathbf{A}^l \mathbf{v}^{k,l} \rangle = \sum_{l=1}^{r-1} \langle \mathbf{u}^{k,l}, \mathbf{A}^l \mathbf{u}^{k,l} \rangle, \quad (\text{B.14})$$

with the elements of vectors $\mathbf{u}^{k,l}$ given by

$$u_m^{k,l} = \Delta x^{l-1} v_m^{k,l} = \Delta x^{m+l-1} \int_{x_{i-\frac{1}{2}}}^{x_{i+\frac{1}{2}}} \frac{d^{m+l}}{dx^{m+l}} \hat{f}^k(x) dx, \quad m = 0, \dots, r-l-1. \quad (\text{B.15})$$

Let's define a new vector $\boldsymbol{\phi}^k$ as

$$\phi_m^k = \Delta x^{m-1} \int_{x_{i-\frac{1}{2}}}^{x_{i+\frac{1}{2}}} \frac{d^m}{dx^m} \hat{f}^k(x) dx, \quad m = 1, \dots, r-1. \quad (\text{B.16})$$

Notice that $u_m^{k,l} = \phi_{m+l}^k$, $m = 0, \dots, r-l-1$; or, in a matrix-vector form,

$$\mathbf{u}^{k,l} = \mathbf{Q}^l \phi^k, \quad \text{with} \quad \mathbf{Q}_{(r-l) \times (r-1)}^l = \begin{bmatrix} \mathbf{0}_{(r-l) \times (l-1)} & \mathbf{I}_{(r-l) \times (r-l)} \end{bmatrix}. \quad (\text{B.17})$$

Substituting Eq. (B.17) into Eq. (B.14) gives

$$\beta_k = \sum_{l=1}^{r-1} \langle \mathbf{Q}^l \phi^k, \mathbf{A}^l \mathbf{Q}^l \phi^k \rangle \triangleq \langle \phi^k, \mathbf{C} \phi^k \rangle, \quad \text{where} \quad \mathbf{C} = \sum_{l=1}^{r-1} (\mathbf{Q}^l)^T \mathbf{A}^l \mathbf{Q}^l. \quad (\text{B.18})$$

Supposing $1 \leq m \leq r-1$ and using Eq. (B.13) and Eq. (B.16), one has

$$\begin{aligned} \phi_m^k &= \Delta x^{m-1} \left. \frac{d^{m-1}}{dx^{m-1}} \hat{f}^k(x) \right|_{x_{i-\frac{1}{2}}}^{x_{i+\frac{1}{2}}} = \Delta x^{m-1} \left(\left. \frac{d^{m-1}}{dx^{m-1}} h(x) \right|_{x_{i-\frac{1}{2}}}^{x_{i+\frac{1}{2}}} + O(\Delta x^{r-m+1}) \right) \\ &= f_i^{(m)} \Delta x^m + O(\Delta x^r), \end{aligned} \quad (\text{B.19})$$

where the $O(\Delta x^r)$ term depends on $\hat{f}^k(x)$ and therefore is different for each k , in general. Finally, by Lemma 6 and Eq. (B.18), \mathbf{C} is a constant symmetric positive semi-definite matrix. \square

Corollary 7. *At a critical point of order n_{cp} (Definition 1), β_k can be decomposed as a sum of a k -invariant (B) and a k -dependent (R_k) components, for $k = 0, \dots, r-1$, namely:*

$$\beta_k = B + R_k,$$

where, if $n_{\text{cp}} < r-1$,

$$\theta(B) = 2(n_{\text{cp}} + 1), \quad \theta(R_k) \geq n_{\text{cp}} + r + 1,$$

and, if $n_{\text{cp}} \geq r-1$,

$$B = 0, \quad \theta(R_k) = 2(n_{\text{cp}} + 1).$$

In particular, $\theta(\beta_k) = 2(n_{\text{cp}} + 1)$, and the upper bounds $\beta_k = O(\Delta x^2)$, $B = O(\Delta x^2)$ and $R_k = O(\Delta x^{r+1})$ hold.

Proof. By Proposition 5, one has

$$\beta_k = \langle \phi^k, \mathbf{C} \phi^k \rangle, \quad \phi_m^k = f_i^{(m)} \Delta x^m + O(\Delta x^r), \quad m = 1, \dots, r-1,$$

where \mathbf{C} is the smoothness measurement matrix. We shall decompose the vector ϕ^k into a sum of its k -invariant and k -dependent components, ϕ^B and ϕ^{R_k} , respectively:

$$\phi_m^B = f_i^{(m)} \Delta x^m, \quad \phi_m^{R_k} = \phi_m^k - \phi_m^B, \quad m = 1, \dots, r-1. \quad (\text{B.20})$$

Since \mathbf{C} is symmetric, one has

$$\beta_k = \langle \phi^B + \phi^{R_k}, \mathbf{C}(\phi^B + \phi^{R_k}) \rangle = \langle \phi^B, \mathbf{C} \phi^B \rangle + 2 \langle \phi^B, \mathbf{C} \phi^{R_k} \rangle + \langle \phi^{R_k}, \mathbf{C} \phi^{R_k} \rangle.$$

Define

$$B \triangleq \langle \phi^B, \mathbf{C}\phi^B \rangle, \quad R_k \triangleq 2 \langle \phi^B, \mathbf{C}\phi^{R_k} \rangle + \langle \phi^{R_k}, \mathbf{C}\phi^{R_k} \rangle. \quad (\text{B.21})$$

By construction, B does not depend on k .

Now, suppose x_i is a critical point of order n_{cp} of $f(x)$. One has

$$\phi_m^B = \begin{cases} f_i^{(m)} \Delta x^m, & \text{if } n_{\text{cp}} < m \\ 0, & \text{if } n_{\text{cp}} \geq m \end{cases}, \quad \phi_m^{R_k} = \begin{cases} O(\Delta x^r), & \text{if } n_{\text{cp}} < r - 1 \\ \Theta(\Delta x^{n_{\text{cp}}+1}), & \text{if } n_{\text{cp}} \geq r - 1 \end{cases},$$

which implies (by Eq. (B.21))

$$B = \begin{cases} \Theta(\Delta x^{2(n_{\text{cp}}+1)}), & \text{if } n_{\text{cp}} < r - 1 \\ 0, & \text{if } n_{\text{cp}} \geq r - 1 \end{cases}, \quad R_k = \begin{cases} O(\Delta x^{r+n_{\text{cp}}+1}), & \text{if } n_{\text{cp}} < r - 1 \\ \Theta(\Delta x^{2(n_{\text{cp}}+1)}), & \text{if } n_{\text{cp}} \geq r - 1 \end{cases}. \quad \square$$

So far, the results in this appendix have only concerned about the $x_{i+\frac{1}{2}}$ -centered version of the smoothness indicator $\beta_k \equiv \beta_{i+\frac{1}{2}}^k$. However, in the analysis of the order of accuracy of the WENO-C and WENO-Z+ schemes, the properties of its $x_{i-\frac{1}{2}}$ -centered counterpart $\beta_{i-\frac{1}{2}}^k$ must also be taken into consideration. Especially, the orders of the centered differences $\delta_i B$ and $\delta_i R_k$, $\theta(\delta_i B)$ and $\theta(\delta_i R_k)$, respectively, play essential roles for proving they satisfy the optimality condition via Proposition 2.

Corollary 8. *The orders of $\delta_i B$ and $\delta_i R_k$ satisfy the inequalities*

$$\theta(\delta_i B) \geq 3, \quad \theta(\delta_i R_k) \geq r + 2.$$

Moreover, at a critical point x_i of $f(x)$ satisfying, $f'(x_i) = 0$, $f''(x_i) \neq 0$ and $f^{(r)}(x_i) \neq 0$, one has exactly

$$\theta(\delta_i B) = 4, \quad \theta(\delta_i R_k) = r + 2.$$

Proof. Now, assume that the only nonzero term in the first row and column of the smoothness measuring matrix is C_{11} , which is equal to 1. This fact, unproven in [22], will be properly demonstrated in a future work. It follows, by Eq. (B.20), that the leading order terms in B and R_k depend only on ϕ_1^k :

$$B = (\phi_1^B)^2 + O(\Delta x^4), \quad R_k = 2\phi_1^B \phi_1^{R_k} + O(\Delta x^{r+2}). \quad (\text{B.22})$$

Recalling from the definitions (B.5) and (B.20),

$$\phi_1^B = f'_i \Delta x, \quad \phi_1^{R_k} = A_r^k f_i^{(r)} \Delta x^r + O(\Delta x^{r+1}).$$

Hence, one has

$$\begin{aligned} \delta_i \phi_1^B &= (f'_i - f'_{i-1}) \Delta x = f''_i \Delta x^2 + O(\Delta x^3), \\ \delta_i \phi_1^{R_k} &= (f_i^{(r)} - f_{i-1}^{(r)}) A_r^k \Delta x^r + O(\Delta x^{r+2}) = A_r^k f_i^{(r+1)} \Delta x^{r+1} + O(\Delta x^{r+2}). \end{aligned}$$

Finally, by Eq. (B.22),

$$\begin{aligned}\delta_i B &= (\phi_1^B)^2 - (\phi_1^B - \delta_i \phi_1^B)^2 + O(\Delta x^5) = f_i' f_i'' \Delta x^3 - (f_i'')^2 \Delta x^4 + O(\Delta x^5), \\ \delta_i R_k &= 2\phi_1^B \phi_1^{R_k} - 2(\phi_1^B - \delta_i \phi_1^B)(\phi_1^{R_k} - \delta_i \phi_1^{R_k}) + O(\Delta x^{r+3}) \\ &= (f_i' f_i^{(r+1)} + f_i'' f_i^{(r)}) 2A_r^k \Delta x^{r+2} + O(\Delta x^{r+3}),\end{aligned}\tag{B.23}$$

Which gives the desired results. \square

Lemma 9. *Let*

$$\gamma_k \triangleq \frac{R_k}{B + \varepsilon},$$

where B and R_k are given by Corollary 7. If $\varepsilon = \Omega(\Delta x^2)$, then $\gamma_k = O(\Delta x^{r-1})$ and $\delta_i \gamma_k = O(\Delta x^r)$.

Proof. Assume $\theta(\varepsilon) \leq 2$. By Corollary 7, we have

$$\gamma_k = \frac{R_k}{B + \varepsilon} = \frac{O(\Delta x^{r+1})}{O(\Delta x^2) + \Omega(\Delta x^2)} = \frac{O(\Delta x^{r+1})}{\Omega(\Delta x^2)} = O(\Delta x^{r-1}),$$

and

$$\delta_i \gamma_k = \frac{R_k}{B + \varepsilon} - \frac{R_k - \delta_i R_k}{B - \delta_i B + \varepsilon} = \frac{(B + \varepsilon)\delta_i R_k - R_k \delta_i B}{(B + \varepsilon)(B + \varepsilon - \delta_i B)}.$$

Using Corollary 8, for any critical point of order n_{cp} one has

$$\begin{aligned}\theta(\delta_i \gamma_k) &= \min\{\theta(\delta_i R_k) + \theta(\varepsilon), \theta(R_k) + \theta(\delta_i B)\} - 2\theta(\varepsilon) \\ &\geq \min\{\theta(\delta_i R_k) - 2, \theta(R_k) + \theta(\delta_i B) - 4\} \geq r.\end{aligned}\tag{B.24}$$

\square

APPENDIX C – Properties of the anti-Zico weights

The purpose of this section is to show that the “anti-Zico” weights of Section 7.2, which violate the ENO property (Condition 3), nevertheless work for smooth solutions. This is done by demonstrating that $\omega_k^{-z} = d_k + O(\Delta x)$ and, therefore, $\omega_k^{-z} \rightarrow d_k$ as $\Delta x \rightarrow 0$.

Proposition 10. *Consider the “anti-Zico” weights ω_k^{-z} , defined as (cf. Eq. (7.9))*

$$\alpha_k^{-z} \triangleq d_k \left[1 + \left(\frac{\beta_k}{\tau + \varepsilon} \right)^p \right], \quad \omega_k^{-z} \triangleq \frac{\alpha_k^{-z}}{\sum_{j=0}^{r-1} \alpha_j^{-z}}, \quad k = 0, \dots, r-1. \quad (\text{C.1})$$

If the solution is smooth and does not contain a critical point of order $n_{\text{cp}} \geq r-1$, and ε is sufficiently small, the weights ω_k^{-z} approach the ideal weights d_k as $\Delta x \rightarrow 0$.

Proof. Let

$$\bar{\beta} \triangleq \sqrt[p]{\sum_{j=0}^{r-1} d_j (\beta_j)^p}.$$

If $\bar{\beta} = 0$ then, by definition (C.1), $\omega_k^{-z} = d_k$ for $k = 0, \dots, r-1$; otherwise, we have

$$\begin{aligned} \omega_k^{-z} - d_k &= \frac{d_k \left[1 + \left(\frac{\beta_k}{\tau + \varepsilon} \right)^p - \sum_{j=0}^{r-1} d_j \left(1 + \left(\frac{\beta_j}{\tau + \varepsilon} \right)^p \right) \right]}{\sum_{j=0}^{r-1} d_j \left(1 + \left(\frac{\beta_j}{\tau + \varepsilon} \right)^p \right)} \\ &= \frac{d_k \left\{ \left(\frac{\beta_k}{\tau + \varepsilon} \right)^p - \left[\sum_{j=0}^{r-1} d_j \left(\frac{\beta_j}{\tau + \varepsilon} \right)^p \right] \right\}}{1 + \sum_{j=0}^{r-1} d_j \left(\frac{\beta_j}{\tau + \varepsilon} \right)^p} \\ &= \frac{d_k \left[\left(\frac{\beta_k}{\tau + \varepsilon} \right)^p - \left(\frac{\bar{\beta}}{\tau + \varepsilon} \right)^p \right]}{1 + \left(\frac{\bar{\beta}}{\tau + \varepsilon} \right)^p} = \frac{d_k \left[\left(\frac{\beta_k}{\bar{\beta}} \right)^p - 1 \right]}{1 + \left(\frac{\tau + \varepsilon}{\bar{\beta}} \right)^p}. \end{aligned}$$

Now, by Corollary 7, for $k = 0, \dots, r-1$ we have $\beta_k = O(\Delta x^2)$ (which implies $\bar{\beta} = O(\Delta x^2)$), and, importantly, β_k can be written as $\beta_k = B + R_k$, where B does not depend on k . Moreover, since the solution is smooth and does not contain a critical point of order

$n_{\text{cp}} \geq r - 1$, and ε is small, we have $\frac{\tau + \varepsilon}{\bar{\beta}} = O(\Delta x)$ and $\frac{R_k}{B} = O(\Delta x)$ at least. Thus,

$$\begin{aligned}
\omega_k^{-z} - d_k &= \frac{d_k \left[\left(\frac{\beta_k}{\bar{\beta}} \right)^p - 1 \right]}{1 + \left(\frac{\tau + \varepsilon}{\bar{\beta}} \right)^p} = \frac{d_k \left[\frac{(\beta_k)^p}{\sum_{j=0}^{r-1} d_j (\beta_j)^p} - 1 \right]}{1 + O(\Delta x^p)} \\
&= d_k \left[\frac{(B + R_k)^p}{\sum_{j=0}^{r-1} d_j (B + R_j)^p} - 1 \right] (1 + O(\Delta x^p)) \\
&= d_k \left[\frac{1 + p \frac{R_k}{B} + O\left(\frac{R_k^2}{B^2}\right)}{\sum_{j=0}^{r-1} d_j \left(1 + p \frac{R_j}{B} + O\left(\frac{R_j^2}{B^2}\right) \right)} - 1 \right] (1 + O(\Delta x^p)) \\
&= d_k \left(\frac{1 + O(\Delta x)}{1 + O(\Delta x)} - 1 \right) (1 + O(\Delta x^p)) \\
&= d_k (1 + O(\Delta x) - 1) (1 + O(\Delta x^p)) = O(\Delta x). \quad \square
\end{aligned}$$

Index

- discontinuous/continuous ratio, 48
- equations
 - Euler equations of compressible flow, 50
 - linear advection, 50
- fifth-order upstream central scheme, 42
- flux (f), 39
- hyperbolic conservation laws, 27, 39
- numerical flux function (h), 41
 - polynomial approximation (\hat{f}), 41, 113
- numerical tests
 - accuracy test, 55
 - ADR analysis, 50
 - blast waves, 50
 - GSTE, 51
 - Riemann problem
 - of Lax, 53
 - of Sod, 53
 - shock-entropy test
 - of Shu–Osher, 53
 - of Titarev–Toro, 55
- order
 - of a critical point (n_{cp}), 21
 - of substencils (r), 43
 - of the scheme (R), 43
- power parameter (p), 63
- sensitivity parameter (ε), 63
- sharpening term, 78, 86
- smoothness indicator, 57
 - global, 67
 - of WENO-Z (τ), 61, 113
 - of Jiang–Shu (β), 59, 113, 117
- steepening term, *see* sharpening term
- suborder, *see* order of substencils
- weights
 - anti-Zico, 82, 123
 - classical, 63
 - ideal (d_k), 45, 113
 - min*, 75, 79
 - nonlinear, 43
 - unnormalized, 49
 - Zico, 67
 - Zico+, 87
- WENO schemes, 43
 - Classical WENO, *see* WENO-C
 - ESWENO, 70
 - Original WENO, 64
 - WENO-C, 64
 - WENO-JS, *see* WENO-C
 - WENO-*min*, 75, 81
 - WENO-MZ, 70
 - WENO-NS, 70
 - WENO-Z, 69
 - WENO-Z+, 90
 - Zico WENO, *see* WENO-Z